

ABSTRACT

Title of dissertation: NEW STATISTICAL METHODS TO
BETTER LEVERAGE EMERGING
HEALTH CARE UTILIZATION DATA

Xu Zhang
Doctor of Philosophy, 2020

Dissertation directed by: Professor Paul J. Smith
Statistics Program
Department of Mathematics
Professor Bruce L. Golden
Robert H. Smith School of Business

Improving the healthcare system is an important task that is always both socially and individually beneficial, and statistics is one of the useful tools that have been applied in pursuit of this goal. However, limitations on current methods and the introduction of new forms of data have created many new challenges and research opportunities. It is therefore crucial to explore and extend statistical methods to better understand and leverage healthcare utilization data, particularly recent and emerging data in new forms. In this dissertation, we develop and apply various innovative statistical methods to address five specific healthcare issues. First, we successfully develop a novel approach to model the length of hospital stay using mixture distributions through an EM algorithm. Second, we extend a two-state continuous time Markov chain to estimate patient readmission risk at a large academic hospital in the U.S. Third, we study changes in accessibility in emergency departments from 2016 to 2018 among 21 hospitals in Maryland Region III. Fourth, we investigate the impact of the global budget payment model on emergency department accessibility. Lastly, we use a multi-state Markov model to explore cascading events during emergency room crowding, also in Region III of Maryland.

NEW STATISTICAL METHODS TO BETTER
LEVERAGE EMERGING HEALTH CARE UTILIZATION DATA

by

Xu Zhang

Dissertation submitted to the Faculty of the Graduate School of the
University of Maryland, College Park in partial fulfillment
of the requirements for the degree of
Doctor of Philosophy
2020

Advisory Committee:
Dr. Paul Smith, Co-Advisor
Dr. Bruce Golden, Co-Advisor
Dr. Abram Kagan
Dr. Ilya Ryzhov
Dr. Frank Alt

© Copyright by
Xu Zhang
2020

Dedication

To my family.

Acknowledgments

I would like to give my sincere thanks to my advisors Professors Paul Smith and Bruce Golden. Also I would like to extend my gratitude to Dr. Sean Barnes for helping with my dissertation research. For the past four years, they turned me from a student whose only skill was taking exams and obtaining high scores to a researcher by teaching me how to discover a scientific problem, evaluate it and develop statistical approaches to investigate it. The help and inspiration from them include far more than knowledge and research. As role models, they showed me almost all the virtue of elegant researchers: solid mathematics background, the enthusiasm of diving into the problem, the ability of communicating with people both inside and outside Statistics and the need to work with people in the research lab. I feel really lucky to have them as my mentors. Everything that I learned from them has been, and will always stay with me and help me for the rest of my life.

I am grateful to my committee members, Drs. Abram Kagan, Ilya Ryzhov, and Frank Alt, for their kind help and constructive advice during these years. I could always gain fresh and new ideas when discussing with them. Also, I would like to take this opportunity to thank all the faculty and friends in our department. I'm grateful to have them around during my study at the University of Maryland.

Last but not least, I would like to give my most sincere thanks to my parents, my two dear sisters and my lovely girlfriend. None of my work could have been done without their support and encouragement, and none of my work would have been so meaningful to me without them.

Table of Contents

Dedication	ii
Acknowledgements	iii
Table of Contents	iv
List of Tables	vi
List of Figures	viii
List of Abbreviations	xi
1 Introduction	1
1.1 Background	1
1.2 Main Contributions	3
2 Lognormal-based Mixture Models for Robust Fitting of Hospital Length of Stay Distributions	6
2.1 Introduction	6
2.2 Methods	9
2.2.1 Lognormal-Exponential Mixture Model	11
2.2.2 Lognormal-Gamma Mixture Model	16
2.2.3 Lognormal-Lognormal Mixture Model	18
2.3 Simulation	19
2.3.1 Simulation for LEMM	20
2.3.2 Simulation for LGMM	21
2.3.3 Simulation for LLMM	23
2.4 Real Data Analysis	24
2.5 Discussion	29
3 A Continuous-time Markov Model for Estimating Readmission Risk for Hospital Inpatients	38
3.1 Introduction	38
3.2 Methods	42
3.2.1 The Continuous-time Markov Model	43
3.2.2 The Estimators	45
3.2.3 Asymptotic Distributions of the Estimators	49

3.3	Simulation	52
3.4	Real Data Analysis	54
3.5	Discussion	63
4	Decreasing Trend of Hospital Emergency Department Access Observed in Maryland Region III from 2016 to 2018	69
4.1	Introduction	69
4.2	Data and Methods	71
4.2.1	Data Source and Management of Emergency Department Resource Availability	71
4.2.2	Study Population	72
4.2.3	Statistical Methods and Data Analysis	72
4.3	Results and Findings	75
4.4	Study Limitations	89
4.5	Conclusion	89
5	Impact of Global Budget Program on Emergency Room Accessibility in Region III of Maryland	91
5.1	Introduction	91
5.2	Statistical Methods	93
5.3	Analysis Results and Findings	95
5.4	Discussion and Conclusions	106
6	Multi-state Markov Model for Cascading Problems in Emergency Rooms in Maryland	109
6.1	Introduction	109
6.2	The Proposed Method Using Multi-state Markov Models	113
6.2.1	The Multi-state Markov Model	115
6.2.2	The Proposed Estimators and Asymptotic Distributions	117
6.2.3	Hypothesis Testing	124
6.3	Simulation	126
6.3.1	The Time-homogeneous Scenario	126
6.3.2	The Time-Heterogeneous Scenario	131
6.3.3	Hypothesis Testing	136
6.4	Real Data Analysis	138
6.5	Discussion	143
6.5.1	Applications in Emergency Room	144
6.5.2	Future Research	145
7	Conclusions	147
	Appendices	149
	Bibliography	156

List of Tables

2.1	Descriptive statistics for observed length of stay (in days) for intensive care unit patients.	25
2.2	Descriptive statistics of observed length of stay (in days) for surgical patients.	26
2.3	Cramer-Von Mises goodness-of-fit test p-values for observed length of stay of intensive care unit patients for Lognormal, IG, Loglogistic, EE, HE, PH, LL, LLW, LEMM, LGMM, and LLMM.	27
2.4	Cramer-Von Mises goodness-of-fit test p-values for observed length of stay of surgical patients for Lognormal, IG, Loglogistic, EE, HE, PH, LL, LLW, LEMM, LGMM, and LLMM.	27
2.5	Parameter estimates for lognormal-based mixture models for different patient populations.	28
2.6	Number of iterations (until convergence) and execution time (R 3.5.1) for estimating parameters for lognormal-based mixture models.	28
3.1	Descriptive statistics for different surgical patient cohorts.	57
3.2	Parameter estimates and goodness-of-fit p-values for different surgical patient cohorts.	57
3.3	MISE for different surgical patient cohorts.	63
3.4	Parameter estimates of different time periods for five surgical patient cohorts.	68
4.1	Descriptive statistics for total alert, including any kind of alert, in each hospital and each year.	76
4.2	Descriptive statistics for red alert in each hospital and each year.	79
4.3	Descriptive statistics for reroute alert in each hospital and each year.	80
4.4	Descriptive statistics for yellow alert in each hospital and each year.	81
4.5	P-values of Kruskal-Wallis tests for alert-free periods.	83
4.6	P-values of Kruskal-Wallis tests for red alert durations.	83
4.7	P-values of Kruskal-Wallis tests for reroute alert durations.	83
4.8	P-values of Kruskal-Wallis tests for yellow alert durations.	83
5.1	Descriptive statistics for alerts-free periods.	96

5.2	Descriptive statistics for duration of red alert.	98
5.3	Descriptive statistics for duration of reroute alert.	99
5.4	Descriptive statistics for duration of yellow alert.	100
5.5	Summary of Kruskal-Wallis test p-values for the difference in outcome probability over time for 2012 and 2013.	103
5.6	Estimated coefficients, standard errors (SE), and P-values obtained from mixed model analysis of log total yellow alert duration on covariates of interest.	105
6.1	Summary of MISE for time-homogeneous scenario.	131
6.2	Summary of MISE for time-inhomogeneous case.	133
6.3	Simulation results for the adjusted model.	137
6.4	Simulation results for the model with varying HR between states. . .	137

List of Figures

2.1	Simulation results for the Lognormal-Exponential Mixture Model. We generated 300 samples from a LEMM with $p = 0.8$, $\mu = 0$, $\sigma = 1$, and $\lambda = 2$	21
2.2	Simulation results for the Lognormal-Gamma mixture model. We generated 300 samples from a LGMM with $p = 0.8$, $\mu = 0$, $\sigma = 1$, $\alpha = 1.5$, and $\beta = 0.5$	22
2.3	Simulation results for the Lognormal-Lognormal Mixture Model. We generated 300 samples from a LLMM with $p = 0.8$, $\mu_1 = 0$, $\sigma_1 = 1$, $\mu_2 = 2$, and $\sigma_2 = 1$	24
2.4	Distributional summary of observed length of stay (in days) in medical and surgical intensive care units.	32
2.5	Length of stay distribution for different sites at ICU, shown with density plots for lognormal-exponential mixture model (LEMM), lognormal-gamma mixture model (LGMM), lognormal-lognormal mixture model (LLMM) and Cramer-Von Mises p-values for goodness of fit tests.	33
2.6	Length of stay distribution for different surgical specialties, shown with density plots for lognormal-exponential mixture model (LEMM), lognormal-gamma mixture model (LGMM), lognormal-lognormal mixture model (LLMM) and Cramer-Von Mises p-values for goodness of fit tests.	34
2.7	True value (dotted line) and the convergence (solid line) of all parameters in lognormal-exponential mixture model (LEMM) in simulation study with vertical lines indicating the number of iterations required to satisfy the convergence threshold ($\epsilon = 10^{-4}$).	35
2.8	True value (dotted line) and the convergence (solid line) of all parameters in lognormal-gamma mixture model (LGMM) in simulation study with vertical lines indicating the number of iterations required to satisfy the convergence threshold ($\epsilon = 10^{-4}$).	36
2.9	True value (dotted line) and the convergence (solid line) of all parameters in lognormal-lognormal mixture model (LLMM) in simulation study with vertical lines indicating the number of iterations required to satisfy the convergence threshold ($\epsilon = 10^{-4}$).	37

3.1	Empirical and estimated readmission risks for patients readmitted 1 time within 72 hours.	55
3.2	Empirical and estimated readmission risks for patients readmitted 2 times within 2 weeks.	56
3.3	Empirical and estimated readmission risks for 57 organ transplant surgery patients.	58
3.4	Empirical and estimated readmission risks for 60 general surgery patients.	59
3.5	Empirical and estimated readmission risks for 65 urology surgery patients.	60
3.6	Empirical and estimated readmission risks for 25 pediatric bronchoscopy surgery patients.	61
3.7	Empirical and estimated readmission risks for all 456 surgical patients.	62
3.8	Probability trajectories for each patient discharged within 30-day time window.	65
3.9	Expected number of readmitted patients over time after a 30-day warmup period, assuming 100 uniformly distributed patient discharges and transition rates λ_{01} and λ_{10} equal to 0.0049 and 0.0035, respectively. We also indicate the average of the long-term number of expected readmitted patients in the second month with the dotted line.	67
4.1	Probability of remaining alert-free over time starting from the end of previous alerts.	85
4.2	Probability of remaining red-alert status starting from the initiation of red alert.	86
4.3	Probability of remaining reroute-alert status starting from the initiation of reroute alert.	87
4.4	Probability of remaining yellow-alert status starting from the initiation of yellow alert.	88
5.1	Hospitals and Counties in Marylands Global Budget Program [122].	95
5.2	Hospitals with significant changes (red) in region III from 2013 to 2015.	102
5.3	Mean duration of yellow alert profile each year by different regions.	103
5.4	Histogram of yellow alert durations (skewed) and QQ-plot of the log duration of yellow alerts (more normal with log scale).	104
5.5	Comparison of fitted model with observed data in region III.	105
5.7	Comparison of fitted model with observed data in Baltimore city.	106
5.6	Comparison of fitted model with observed data in Baltimore county.	106
6.1	Choropleth map for the duration of yellow alerts in Maryland.	111
6.2	Cascading problem observed around November 27, 2018.	112
6.3	A cascading simulation in the region within a month in the time-homogeneous scenario.	128
6.4	The comparison between true and estimated survival curves between states by polynomial approximation in time-homogeneous scenario.	129

6.5	The comparison between true and estimated survival curves between states by Fourier approximation in time-homogeneous scenario.	130
6.6	A cascading simulation in the region within a month in time-inhomogeneous scenario.	133
6.7	The comparison between true and estimated survival curves between states by polynomial approximation in time-inhomogeneous scenario.	134
6.8	The comparison between true and estimated survival curves between states by Fourier approximation in time-inhomogeneous scenario.	135
6.9	Empirical and estimated transition probability from normal to cascading level I within two weeks.	140
6.10	Probability of having a yellow alert at hospital i conditional on hospital j having a yellow alert.	141

List of Abbreviations

AIC	Akaike Information Criterion
ALS	Advanced Life Support
ANOVA	Analysis of Variance
AR1	First-order Autoregressive Process
BIC	Bayesian Information Criterion
BLS	Basic Life Support
CHATS	County/Hospital Alert Tracking System
CMS	Centers for Medicare and Medicaid Services
DLR	Dempster, Laird, and Rubin
GDP	Gross Domestic Product
ED	Emergency Department
EE	Exponential-Exponential Mixture Distribution
EM	Expectation-maximization
ER	Emergency Room
HAIs	Hospital Acquired Infections
HE	Hyperexponential Distribution
ICU	Intensive Care Unit
IG	Inverse Gamma Distribution
IQR	Interquartile Range
IPPS	Inpatient Prospective Payment System
JH	Johns Hopkins Hospital
LEMM	Lognormal-Exponential Mixture Model
LGMM	Lognormal-Gammal Mixture Model
LL	Lognormal-Loglogistic Mixture Distribution
LLMM	Lognormal-Lognormal Mixture Model
LLW	Lognormal-Loglogistic-Weibull Mixture Distribution
LOS	Length of Stay
MIEMSS	Maryland Institute for Emergency Medical Services Systems
MISE	Mean Integrated Squared Error

MLE	Maximum Likelihood Estimation
MRLT	Mean Residual Life Time
PDF	Probability Density Function
PH	Phase-type Distribution
PMF	Probability Mass Function
SE	Standard Error
UMMC	University of Maryland Medical Center

Chapter 1: Introduction

1.1 Background

There has been increasing pressure to eliminate unnecessary healthcare costs in the United States (U.S.) healthcare system, which exceeded \$750 billion in 2011 and represented a third of the total amount Americans spent on healthcare [20]. The major sources of waste in the U.S. healthcare system include inefficiencies in care coordination and delivery, overtreatment, and administrative logistics [20]. It is estimated that if waste reduction strategies were implemented, the total realized savings could have exceeded \$11 trillion dollars for all payers from 2011 through 2019. Such savings could then be redirected to improve patient care and health outcomes [20]. In addition to its obvious connection to high costs, however, hospital inefficiency has also been directly linked to poor patient healthcare outcomes, and efforts to reduce costs through a focus on inefficient spending should also ensure that the results do not adversely affect patient outcomes [103].

A variety of statistical tools have been widely used to address different kinds of healthcare issues [104]. Normal distribution-based methods are frequently used to estimate average healthcare resource use and costs [13, 25, 26, 72, 123]. For instance, the two sample t-test is widely used to identify significant differences in healthcare

efficiency indicators, such as length of hospital stay or healthcare expenditures. For multiple group comparisons, analysis of variance (ANOVA) can be applied. Linear regression is also widely used to explore the relationship between the response variable and covariates of interest. If the assumption of normality is violated, one may need to transform the data by using tools such as Box-Cox transformations before applying the above methods [69]. Additionally, generalized linear models such as logistic regression or Poisson regression can be implemented to binary outcomes (e.g., whether hospitals comply with a certain healthcare policy or not) or to count data (e.g., the number of patients readmitted to hospitals) [17, 23, 24, 98]. Mixture models have been used in the literature to explore positive and skewed data such as length of stay, waiting time in emergency room, or demand for medical care. Mixture models are flexible enough to accommodate such data [11, 42, 146]. In addition to parametric models [68, 97, 112], nonparametric and semi-parametric models are also very useful in many healthcare problems, since they allow for more modeling flexibility and balance between estimation bias and estimation efficiency [36, 46, 60, 93, 111]. Time-to-event data are probably the most common type of data collected in healthcare research, and they are well suited to the use of survival data analysis [18, 48, 49, 113, 145]. Recently, an increasing number of applications have also used Bayesian approaches to analyze healthcare data [84, 92, 94]. When real data are limited or when the proposed statistical methods require validation, Monte Carlo simulation techniques can be used to generate different types of healthcare data [37, 146]. In this dissertation, we build on these foundations to develop and apply various innovative statistical methods to address five specific healthcare issues.

1.2 Main Contributions

The first of these issues is the need to better understand the underlying structure of length of stay distributions, as such an understanding can support operational and clinical decision making in hospitals. This issue is addressed in Chapter 2, where our objective is to develop robust methods to model length of hospital stay. The distribution of length of stay is often skewed and multimodal and the data may thus contain a significant number of outliers. We define several lognormal-based mixture distributions with two components, one to fit the majority of the observations and the other to fit the abnormal observations. This work results in three proposed lognormal-based mixture distributions: one utilizes an exponential distribution as the second component, one utilizes a gamma distribution, and one utilizes a lognormal distribution. We estimate the parameters of each mixture model using the expectation-maximization (EM) algorithm and evaluate the finite-sample performances of our proposed methods using simulation studies. In addition, we apply our proposed method to a dataset collected from multiple studies conducted at the University of Maryland School of Medicine (UMMC) and compare the fit of our mixture models with the fit obtained by other methods.

Research concerning our second healthcare issue, hospital readmission, has mostly focused on regression models including various risk factors that may influence the likelihood of this undesirable outcome. These models are useful in certain settings, but in many cases their performance is still in need of improvement, and the dynamics of how readmission risk changes over time are often ignored. In Chap-

ter 3, our objective is to develop a new method to model readmission risk over time, starting from the point of discharge. We propose a continuous-time Markov chain model and develop both point estimators and interval estimators for readmission risk. We derive the asymptotic distributions of the proposed estimators and validate their performance through simulation studies. We then apply our proposed methods to estimate readmission risk over time using discharge and readmission data for surgical patients.

Our third healthcare issue is facility accessibility in hospital emergency departments (EDs). Accessibility is tracked by the Maryland Institute for Emergency Medical Services Systems (MIEMSS) through its County/Hospital Alert Tracking System (CHATS), which generates alert data for each hospital in the state. The initiation of one type of alert indicates the lack of a certain facility at the emergency department. In Chapter 4, our goal is to identify the trend in ED accessibility changes in Maryland's most populous region, namely, Region III. Since the data are skewed, we use nonparametric tests to evaluate any statistical differences in ED accessibility from 2016 to 2018. We also model the duration of each type of alert and of alert-free periods to understand specific risk changes over time related to ED accessibility.

The fourth issue concerns payment models implemented in the attempt to limit spending growth in healthcare and improve the quality of medical care. In 2014, Maryland revised its all-payer model to establish the global budget payment model in pursuit of these goals, and in Chapter 5, we investigate the impact of this new model on ED accessibility in the state. We use Kruskal-Wallis tests to compare

the durations of alerts collected before and after the new model was implemented in 2014. Furthermore, we develop a linear mixed model to understand the impact of the global budget payment model on ED accessibility in Maryland Region III.

Lastly, we address emergency room crowding. Periodically, the EDs in Maryland Region III experience a high level of crowding that we call a cascading event, in which patients in need of urgent care face reduced ED accessibility. In Chapter 6, we develop a multi-state Markov model to predict the risk of a cascading event over time. We also extend the model to incorporate time-dependent intensities and covariates of interest, which allows for hypothesis testing in more general scenarios. The finite sample performances of the proposed methods are evaluated through simulation studies, then applied to real data collected at Maryland Region III hospitals from 2016 to 2018.

Chapter 2: Lognormal-based Mixture Models for Robust Fitting of Hospital Length of Stay Distributions

2.1 Introduction

Length of stay (LOS) in hospitals serves as an important indicator of the efficiency at which care is being provided, but similar to costs, there are potential benefits and pitfalls involved with reducing LOS. On the one hand, reducing LOS will allow hospitals to better utilize their limited resources such as beds, clinical staff, and medical equipment, ultimately providing more access for patients in need [103]. However, a shorter LOS could be the result of a patient being inappropriately discharged too soon, likely interrupting the recovery and thereby increasing the likelihood of adverse events (e.g., complications, readmissions) and increased costs. On the other hand, a longer LOS is more costly per discharge and blocks access for other patients. In addition, patients who stay longer are susceptible to developing hospital acquired infections (HAIs) [21]. Achieving an optimal length of stay can simultaneously improve patient outcomes and save overall costs.

Length of stay distributions are typically difficult to fit, and often vary significantly across multiple units in a single facility, and across multiple facilities

[12, 63, 89]. In particular, length of stay distributions are often highly skewed and multimodal, and they often contain a significant proportion of outliers [96, 105, 106, 125, 139]. Weissman [139] states that the frequency distributions are usually skewed to the right and include two populations of interest: the “body”, the portion with the majority of the observations, and the “tail”, which captures the behavior of the outliers. Three theoretical distributions that display this body-and-tail behavior include the lognormal, Weibull, and gamma distributions, which have often been used in fitting LOS data [96]. Unfortunately, these individual distributions are not particularly robust, as they do not consistently fit LOS distributions well across multiple patient populations [89]. To address this limitation, several single and mixture distributional models have been proposed, often including these distributions as components, with the lognormal distribution being the most commonly used [12, 58, 63, 73, 115, 119]. These models are useful, but they all suffer from several drawbacks. They are not robust enough to fit LOS in a wide variety of cases. These methods are either computationally complex or have more than two components. These limitations make the estimation of parameters difficult. Additionally, phase-type and related distributions have been leveraged to estimate length of stay. This facilitates approximation of any positive-valued distribution [52, 100, 132]. For example, Marshall et al. (2003) used Bayesian belief networks with Coxian phase-type distributions for modeling length of stay [99]. Tang et al. (2012) also used Coxian phase-type distributions to model length of stay, and they were able to capture the heterogeneity in LOS by selecting an appropriate number of phases and utilizing a regression model for the hazard rates [132]. However, the generality of

the phase-type distributions makes it difficult to estimate all the parameters [99]. In our work, the goal is to fit an assortment of LOS distributions using a mixture model with two components, where robustness and simplicity are the guiding principles. We propose this lognormal-based mixture model where we consider the lognormal distribution to provide information for the majority of observations, since (1) it is widely used and logarithmic LOS roughly appears to be normally distributed, and (2) the lognormal distribution has a robust fitting performance in either single or mixture models [12, 63, 73, 119]. The parameters from the exponential family would have an appealing form when differentiating [45] among distributions with positive support which are most appropriate for modeling LOS. Thus, we suggest three commonly used distributions, specifically, exponential [63], gamma [89], and lognormal [12, 73, 96], as the second component in our mixture models.

In addition to defining the elements of a mixture model, we must also apply a method for estimating the distributional parameters. Maximum likelihood estimation (MLE) is the most frequently used method due to several advantageous statistical properties. However, if no closed-form solution can be found to the optimization problem, the solution to the MLE formulation must be solved numerically via a method such as Newton-Raphson or Fisher Scoring. Rather than apply a numerical method for minimizing the negative log-likelihood function associated with an MLE approach, we prefer to use the expectation-maximization (EM) method, which is an iterative approach to find the ML estimates for parametric probability distributions.

We propose three mixture models for fitting hospital LOS, using the EM algo-

rithm to estimate the mixture model parameters. These are lognormal-exponential, lognormal-gamma, and lognormal-lognormal mixture models. We show that our models are robust for fitting LOS distributions across many hospital settings. The rest of this chapter is organized as follows. In Section 2.2, we present our methodology for estimating the mixture model parameters using the EM algorithm. In Section 2.3, we validate the performance of our parameter estimation approach for each mixture model using simulation. In Section 2.4, we test our mixture models on observed data collected from multiple research studies by researchers at the University of Maryland School of Medicine and their colleagues. Finally, we conclude in Section 2.5 with a discussion of our results and directions for future research.

2.2 Methods

Estimating a parameter θ of a parametric probability distribution is essential in the fitting of any distribution. The most common approach for parameter estimation is maximum likelihood estimation (MLE), for which the objective is to maximize the log-likelihood function given by:

$$l(\theta) = \log L(\theta) = \prod_{i=1}^n f(x_i|\theta)$$

where $\{X_i, \dots, X_n\}$ is an independent and identically distributed (i.i.d.) sample from a population with probability density function (pdf) or probability mass function (pmf) $f(x|\theta)$.

Among all estimation methods, maximum likelihood estimation (MLE) has

excellent performance due to several advantageous properties under regularity conditions [32]:

- consistency: the sequence of MLEs converges in probability to the value being estimated.
- asymptotic normality: the distribution of the normalized MLE tends to the Gaussian distribution as the sample size increases.
- efficiency: the variance of the MLE attains the Cramér-Rao Lower Bound (optimal asymptotic variance) when the sample size tends to infinity.

When direct likelihood maximization is not feasible, the EM algorithm provides an alternative approach. The EM algorithm is particularly useful when applied to incomplete data, such as parameter estimation for mixture distributions. The EM algorithm centers around the idea of replacing a difficult likelihood maximization problem with a sequence of easier maximizations whose limit provides a solution to the original problem. The E step calculates the conditional expectation of the log-likelihood of the complete data given the observed data and current estimated parameters. The M step performs maximum likelihood estimation of parameters, using the estimated log-likelihood calculated in the E step.

The popularity of the EM algorithm was driven by the work of several authors. Sundberg's work provided the foundation for this iterative method, but Dempster, Laird, and Rubin (DLR) introduced the EM algorithm and proved the convergence of EM [45, 129–131]. Wu later corrected the proof of convergence of EM in DLR's

paper [143]. We apply the EM algorithm to estimate the parameters for three lognormal-based distributions in the following subsections.

2.2.1 Lognormal-Exponential Mixture Model

Assume we have n i.i.d. continuous length of stay observations $x_i \in R, i = 1, \dots, n$, drawn from a Lognormal-Exponential Mixture Model (LEMM). Our objective is to estimate the parameter set $\theta = \{p, \mu, \sigma, \lambda\}$ that best fits the observed data. We assume the observations x_i belong to a mixture distribution defined by:

$$X_i = Z_i U_i + (1 - Z_i) V_i$$

where

$$U_i \sim f_1(u_i | \mu, \sigma)$$

$$V_i \sim f_2(v_i | \lambda)$$

$$Z_i \sim f_3(z_i | p)$$

and Z_i is independent of U_i and V_i . We note here that Z_i is a Bernoulli random variable with probability parameter p that determines whether a particular patient's LOS X_i will be drawn from the distribution of U_i with probability p or V_i with probability $1-p$. For any u_i , the probability density function (pdf) for the lognormal

distribution is defined as

$$f_1(u_i|\mu, \sigma) = \frac{1}{\sqrt{2\pi\sigma}} \frac{1}{u_i} \exp\left(-\frac{(\log(u_i) - \mu)^2}{2\sigma^2}\right), \quad \mu \in R, \sigma \in R^+.$$

The pdf for an exponential distribution is:

$$f_2(v_i|\lambda) = \lambda e^{-\lambda v_i}, \quad \lambda \in R^+.$$

The pmf for a Bernoulli distribution is:

$$f_3(z_i|p) = p^{z_i}(1-p)^{(1-z_i)}, \quad p \in [0, 1].$$

The pdf for the LEMM is then defined as:

$$f(x_i|p, \mu, \sigma, \lambda) = pf_1(x_i|\mu, \sigma) + (1-p)f_2(x_i|\lambda).$$

The expectation step (E-step) of the EM algorithm proceeds as follows:

$$\begin{aligned} \epsilon_i^{(m)} &= E(Z_i|X_i, \theta^{(m)}) \\ &= P(Z_i = 1|X_i, \theta^{(m)}) \\ &= \frac{p^{(m)} f_1(x_i|\mu^{(m)}, \sigma^{(m)})}{p^{(m)} f_1(x_i|\mu^{(m)}, \sigma^{(m)}) + (1-p^{(m)}) f_2(x_i|\lambda^{(m)})}. \end{aligned}$$

With the assumption that the samples are i.i.d., we calculate the so-called Q-function

as:

$$\begin{aligned}
Q(\theta|\theta^{(m)}) &= \sum_{i=1}^n \left\{ E(Z_i|X_i, \theta^{(m)}) \log[pf_1(x_i|\mu, \sigma)] \right. \\
&\quad \left. + (1 - E(Z_i|X_i, \theta^{(m)})) \log[(1 - p)f_2(x_i|\lambda)] \right\} \\
&= \sum_{i=1}^n \left\{ \epsilon_i^{(m)} \log[pf_1(x_i|\mu, \sigma)] \right. \\
&\quad \left. + (1 - \epsilon_i^{(m)}) \log[(1 - p)f_2(x_i|\lambda)] \right\} \\
&= \sum_{i=1}^n \left\{ \epsilon_i^{(m)} \left(\log(p) - \log(\sigma) - \log(x_i) - \frac{(\log(x_i) - \mu)^2}{2\sigma^2} \right) \right. \\
&\quad \left. + (1 - \epsilon_i^{(m)}) [\log(1 - p) + \log(\lambda) - \lambda x_i] \right\} + C
\end{aligned}$$

where C does not depend on any of the elements of θ .

The maximization step (M-step) of the EM algorithm determines the next iterate of θ that maximizes the Q-function derived above:

$$\theta^{(m+1)} = \underset{\theta}{\operatorname{argmax}} Q(\theta|\theta^{(m)}).$$

The optimal p , μ , σ , and λ are found by equating the respective partial derivatives to zero, and solving. For p , we have:

$$\frac{\partial Q(\theta|\theta^{(m)})}{\partial p} = \sum_{i=1}^n \left(\frac{\epsilon_i^{(m)}}{p} + \frac{(1 - \epsilon_i^{(m)})}{p - 1} \right) = 0$$

which yields

$$p^{(m+1)} = \frac{1}{n} \sum_{i=1}^n \epsilon_i^{(m)}.$$

For μ and σ , we have:

$$\begin{aligned}\frac{\partial Q(\theta|\theta^{(m)})}{\partial \mu} &= \sum_{i=1}^n \epsilon_i^{(m)} \left(-\frac{1}{2\sigma^2} 2(\log(x_i - \mu)) \right) \\ &= \sum_{i=1}^n \epsilon_i^{(m)} \frac{\log(x_i) - \mu}{\sigma^2} = 0\end{aligned}$$

and

$$\begin{aligned}\frac{\partial Q(\theta|\theta^{(m)})}{\partial \sigma} &= \sum_{i=1}^n \left\{ \epsilon_i^{(m)} \left(-\frac{1}{\sigma} + \sigma^{-3}(\log(x_i) - \mu)^2 \right) \right\} \\ &= \sum_{i=1}^n \left\{ -\frac{\epsilon_i^{(m)}}{\sigma} + \frac{\epsilon_i^{(m)}(\log(x_i) - \mu)^2}{\sigma^3} \right\} = 0\end{aligned}$$

which yields

$$\mu^{m+1} = \frac{\sum_{i=1}^n \epsilon_i^{(m)} \log(x_i)}{\sum_{i=1}^n \epsilon_i^{(m)}}$$

and

$$(\sigma^2)^{(m+1)} = \frac{\sum_{i=1}^n \epsilon_i^{(m)} (\log(x_i) - \mu^{m+1})^2}{\sum_{i=1}^n \epsilon_i^{(m)}}.$$

And finally, for λ , we have:

$$\frac{\partial Q(\theta|\theta^{(m)})}{\partial \lambda} = \sum_{i=1}^n (1 - \epsilon_i^{(m+1)}) \left(\frac{1}{\lambda} - x_i \right) = 0$$

which yields

$$\lambda^{(m+1)} = \frac{\sum_{i=1}^n (1 - \epsilon_i^{(m)})}{\sum_{i=1}^n (1 - \epsilon_i^{(m)}) x_i}.$$

We summarize the process for estimating the parameters p , μ , σ , and λ for LEMM in Algorithm 1.

Algorithm 1. EM algorithm for estimating LEMM parameters

1. Choose initial estimates $\theta^{(0)} = \{p^{(0)} = 0.5, \mu^{(0)} = \bar{x}, \sigma^{(0)} = s, \lambda^{(0)} = 1/\bar{x}\}$ where $\bar{x} = n^{-1}\sum_{i=1}^n x_i$ and $s^2 = (n-1)^{-1}\sum_{i=1}^n (x_i - \bar{x})^2$.

2. E-step: For $i = 1, \dots, n$, compute

$$\epsilon_i^{(m)} = \frac{p^{(m)} f_1(x_i | \mu^{(m)}, \sigma^{(m)})}{p^{(m)} f_1(x_i | \mu^{(m)}, \sigma^{(m)}) + (1 - p^{(m)}) f_2(x_i | \lambda^{(m)})}.$$

3. M-step: Compute new estimates

$$p^{(m+1)} = \frac{1}{n} \sum_{i=1}^n \epsilon_i^{(m)},$$

$$\mu^{(m+1)} = \frac{\sum_{i=1}^n \epsilon_i^{(m)} \log(x_i)}{\sum_{i=1}^n \epsilon_i^{(m)}}, \quad (\sigma^2)^{(m+1)} = \frac{\sum_{i=1}^n \epsilon_i^{(m)} (\log(x_i) - \mu^{m+1})^2}{\sum_{i=1}^n \epsilon_i^{(m)}},$$

$$\lambda^{(m+1)} = \frac{\sum_{i=1}^n (1 - \epsilon_i^{(m)})}{\sum_{i=1}^n (1 - \epsilon_i^{(m)}) x_i}.$$

4. Repeat steps 2 and 3 until $\max_j \left| \frac{\theta_j^{(m+1)} - \theta_j^{(m)}}{\theta_j^{(m)}} \right| < \delta$, where δ is a selected threshold for convergence.
-

2.2.2 Lognormal-Gamma Mixture Model

Similarly, the iterative equations for the five parameters of the LGMM are as follows:

$$\begin{aligned}
 p^{(m+1)} &= \frac{1}{n} \sum_{i=1}^n \epsilon_i^{(m)}, \\
 \mu^{(m+1)} &= \frac{\sum_{i=1}^n \epsilon_i^{(m)} \log(x_i)}{\sum_{i=1}^n \epsilon_i^{(m)}}, \quad (\sigma^2)^{(m+1)} = \frac{\sum_{i=1}^n \epsilon_i^{(m)} (\log(x_i) - \mu^{(m+1)})^2}{\sum_{i=1}^n \epsilon_i^{(m)}}, \\
 \alpha^{(m+1)} &= \psi^{-1} \left\{ \frac{(\log \beta^{(m)}) \sum_{i=1}^n (1 - \epsilon_i^{(m)}) - \sum_{i=1}^n \log x_i (1 - \epsilon_i^{(m)})}{\sum_{i=1}^n (1 - \epsilon_i^{(m)})} \right\}, \\
 \beta^{(m+1)} &= \frac{\sum_{i=1}^n (1 - \epsilon_i^{(m)}) x_i}{\alpha^{(m+1)} \sum_{i=1}^n (1 - \epsilon_i^{(m)})}
 \end{aligned}$$

where $\Gamma(x) = \int_0^\infty z^{x-1} e^{-z} dz$ denotes the gamma function and $\psi(x) = \Gamma'(x)/\Gamma(x)$ denotes the digamma function. The derivation for these iterates is presented in Appendix A.

We summarize the EM algorithm for estimating the parameters p , μ , σ , and λ for the LGMM in Algorithm 2.

Algorithm 2. EM algorithm for estimating LGMM parameters

1. Choose initial estimates $\theta^{(0)} = \{p^{(0)} = 0.5, \mu^{(0)} = \bar{x}, \sigma^{(0)} = s, \alpha^{(0)} = \hat{\alpha}, \beta^{(0)} = \hat{\beta}\}$ where $\bar{x} = \frac{1}{n} \sum_{i=1}^n x_i$, $s^2 = \frac{1}{n-1} \sum_{i=1}^n (x_i - \bar{x})^2$, $\hat{\alpha}$ is MLE for α , and $\hat{\beta}$ is MLE for β .

2. E-step: For $i = 1, \dots, n$, compute

$$\epsilon_i^{(m)} = \frac{p^{(m)} f_1(x_i | \mu^{(m)}, \sigma^{(m)})}{p^{(m)} f_1(x_i | \mu^{(m)}, \sigma^{(m)}) + (1 - p^{(m)}) f_4(x_i | \alpha^{(m)}, \beta^{(m)})}$$

where

$$f_4(x_i | \alpha, \beta) = \frac{1}{\Gamma(\alpha) \beta^\alpha} x_i^{\alpha-1} e^{-\frac{x_i}{\beta}}, \alpha, \beta \in R^+.$$

3. M-step: compute new estimates

$$p^{(m+1)} = \frac{1}{n} \sum_{i=1}^n \epsilon_i^{(m)},$$

$$\mu^{(m+1)} = \frac{\sum_{i=1}^n \epsilon_i^{(m)} \log(x_i)}{\sum_{i=1}^n \epsilon_i^{(m)}}, \quad (\sigma^2)^{(m+1)} = \frac{\sum_{i=1}^n \epsilon_i^{(m)} (\log(x_i) - \mu^{(m+1)})^2}{\sum_{i=1}^n \epsilon_i^{(m)}},$$

$$\alpha^{(m+1)} = \psi^{-1} \left\{ \frac{(\log \beta^{(m)}) \sum_{i=1}^n (1 - \epsilon_i^{(m)}) - \sum_{i=1}^n \log x_i (1 - \epsilon_i^{(m)})}{\sum_{i=1}^n (1 - \epsilon_i^{(m)})} \right\},$$

$$\beta^{(m+1)} = \frac{\sum_{i=1}^n (1 - \epsilon_i^{(m)}) x_i}{\alpha^{(m+1)} \sum_{i=1}^n (1 - \epsilon_i^{(m)})}.$$

4. Repeat steps 2 and 3 until $\max_j \left| \frac{\theta_j^{(m+1)} - \theta_j^{(m)}}{\theta_j^{(m)}} \right| < \delta$, where δ is a selected threshold for convergence.

2.2.3 Lognormal-Lognormal Mixture Model

Last, we present the iterative equations for the five parameters of the LLMM

below:

$$\begin{aligned}
 p^{(m+1)} &= \frac{1}{n} \sum_{i=1}^n \epsilon_i^{(m)}, \\
 \mu_1^{(m+1)} &= \frac{\sum_{i=1}^n \epsilon_i^{(m)} \log(x_i)}{\sum_{i=1}^n \epsilon_i^{(m)}}, \\
 (\sigma_1^2)^{(m+1)} &= \frac{\sum_{i=1}^n \epsilon_i^{(m)} (\log(x_i) - \mu^{m+1})^2}{\sum_{i=1}^n \epsilon_i^{(m)}}, \\
 \mu_2^{(m+1)} &= \frac{\sum_{i=1}^n (1 - \epsilon_i^{(m)}) \log(x_i)}{\sum_{i=1}^n (1 - \epsilon_i^{(m)})}, \\
 (\sigma_2^2)^{(m+1)} &= \frac{\sum_{i=1}^n (1 - \epsilon_i^{(m)}) [\log(x_i) - \mu^{m+1}]^2}{\sum_{i=1}^n (1 - \epsilon_i^{(m)})}.
 \end{aligned}$$

The derivation for these iterates is presented in Appendix B.

We summarize the EM algorithm for estimating the parameters p , μ_1 , σ_1 , μ_2 and σ_2 for the LLMM in Algorithm 3.

Algorithm 3. EM algorithm for estimating LLMM parameters

1. Choose initial estimates $\theta^{(0)} = \{p^{(0)} = 0.5, \mu_1^{(0)} = \bar{x}, \sigma_1^{(0)} = s, \mu_2^{(0)} = \tilde{m}, \sigma_2^{(0)} = IQR\}$ where $\bar{x} = \frac{1}{n} \sum_{i=1}^n x_i$, $s^2 = \frac{1}{n-1} \sum_{i=1}^n (x_i - \bar{x})^2$, \tilde{m} is the median for the sample data, and IQR is the interquartile range for the sample data. For cases in which the same distribution

is used for both mixture components, we must use different initial estimates so that each component is distinct.

2. E-step: For $i = 1, \dots, n$, compute

$$\epsilon_i^{(m)} = \frac{p^{(m)} f_1(x_i | \mu_1^{(m)}, \sigma_1^{(m)})}{p^{(m)} f_1(x_i | \mu_1^{(m)}, \sigma_1^{(m)}) + (1 - p^{(m)}) f_1(x_i | \mu_2^{(m)}, \sigma_2^{(m)})}.$$

3. M-step: compute new estimates

$$p^{(m+1)} = \frac{1}{n} \sum_{i=1}^n \epsilon_i^{(m)},$$

$$\mu_1^{(m+1)} = \frac{\sum_{i=1}^n \epsilon_i^{(m)} \log(x_i)}{\sum_{i=1}^n \epsilon_i^{(m)}}, \quad (\sigma_1^2)^{(m+1)} = \frac{\sum_{i=1}^n \epsilon_i^{(m)} (\log(x_i) - \mu_1^{(m+1)})^2}{\sum_{i=1}^n \epsilon_i^{(m)}},$$

$$\mu_2^{(m+1)} = \frac{\sum_{i=1}^n (1 - \epsilon_i^{(m)}) \log(x_i)}{\sum_{i=1}^n (1 - \epsilon_i^{(m)})}, \quad (\sigma_2^2)^{(m+1)} = \frac{\sum_{i=1}^n (1 - \epsilon_i^{(m)}) (\log(x_i) - \mu_2^{(m+1)})^2}{\sum_{i=1}^n (1 - \epsilon_i^{(m)})}.$$

4. Repeat steps 2 and 3 until $\max_j \left| \frac{\theta_j^{(m+1)} - \theta_j^{(m)}}{\theta_j^{(m)}} \right| < \delta$, where δ is a selected threshold for convergence.

2.3 Simulation

In this section, we validate the performance of each parameter estimation algorithm via simulation. In each scenario, we generate 300 samples from a selected mixture distribution (specifically, LEMM, LGMM, and LLMM) and apply our proposed

algorithms for estimating the associated distributional parameters with $\epsilon = 10^{-4}$. We evaluate the goodness of fit of our estimated distributions using the Cramer-Von Mises test [40].

2.3.1 Simulation for LEMM

The LEMM has four parameters, $\theta = \{p, \mu, \sigma, \lambda\}$. Let's consider the scenario in which the true values of these parameters are:

$$p = 0.8, \quad \mu = 0, \quad \sigma = 1, \quad \lambda = 2.$$

We generate 300 observations from this mixture distribution as follows:

1. Generate 300 observations z_i from the Bernoulli distribution with $p = 0.8$.
2. Generate 300 observations u_i from a lognormal distribution with $\mu = 0$ and $\sigma = 1$.
3. Generate 300 observations v_i from a exponential distribution with $\lambda = 2$.

Then we calculate the observations $x_i = z_i u_i + (1 - z_i) v_i$. We apply Algorithm 1 to the sample data in order to estimate the distributional parameters, arriving at estimates of

$$p = 0.7884, \quad \mu = 0.0043, \quad \sigma = 1.0015, \quad \lambda = 2.0203.$$

after iterations. The resultant p-value of the Cramer-Von Mises goodness-of-fit test

is 0.987, indicating a very close fit of the estimated distribution. In Figure 2.1, we visualize the fitted and true distributions over the observed sample data.

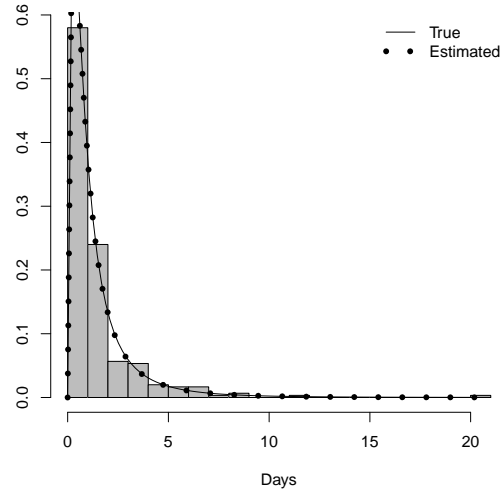


Figure 2.1: Simulation results for the Lognormal-Exponential Mixture Model. We generated 300 samples from a LEMM with $p = 0.8$, $\mu = 0$, $\sigma = 1$, and $\lambda = 2$.

2.3.2 Simulation for LGMM

For the LGMM, we select the following values for the parameters, $\theta = \{p, \mu, \sigma, \alpha, \beta\}$.

$$p = 0.8, \quad \mu = 0, \quad \sigma = 1, \quad \alpha = 1.5, \quad \beta = 0.5.$$

Following a similar process as for Simulation above, we generate 300 observations for the LGMM in the following manner:

1. Generate 300 observations z_i from the Bernoulli distribution with $p = 0.8$.
2. Generate 300 observations u_i from a lognormal distribution with $\mu = 0$ and $\sigma = 1$.

3. Generate 300 observations v_i from a gamma distribution with $\alpha = 1.5$ and $\beta = 0.5$.

After applying Algorithm 2, we estimate the parameters as follows:

$$p = 0.8117, \quad \mu = 0.0110, \quad \sigma = 1.0077, \quad \alpha = 1.4725, \quad \beta = 0.5010.$$

The p-value from the Cramer-Von Mises test is 0.887, validating the fit of the LGMM to the simulated data. In Figure 2.2, we visualize the fitted and true distributions over the observed sample data.

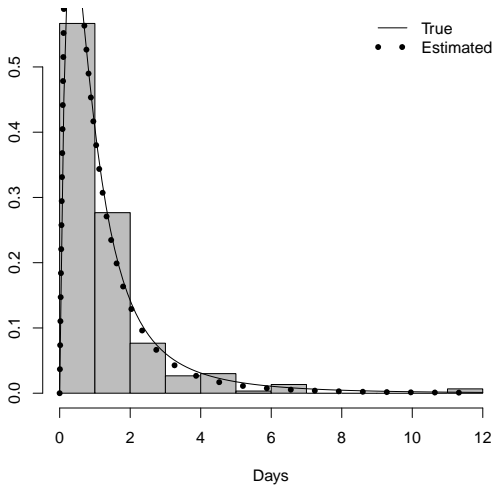


Figure 2.2: Simulation results for the Lognormal-Gamma mixture model. We generated 300 samples from a LGMM with $p = 0.8$, $\mu = 0$, $\sigma = 1$, $\alpha = 1.5$, and $\beta = 0.5$.

2.3.3 Simulation for LLMM

For the LLMM, we select the following values for the parameters $\theta = \{p, \mu_1, \sigma_1, \mu_2, \sigma_2\}$:

$$p = 0.8, \quad \mu_1 = 0, \quad \sigma_1 = 1, \quad \mu_2 = 2, \quad \sigma_2 = 1.$$

We follow a similar process as above to generate 300 observations for the LLMM in the following way:

1. Generate 300 observations z_i from the Bernoulli distribution with $p = 0.8$.
2. Generate 300 observations u_i from a lognormal distribution with $\mu_1 = 0$ and $\sigma_1 = 1$.
3. Generate 300 observations v_i from a lognormal distribution with $\mu_2 = 2$ and $\sigma_2 = 1$.

After applying Algorithm 3, we estimate the parameters as follows:

$$p = 0.7909, \quad \mu_1 = -0.0349, \quad \sigma_1 = 1.0132, \quad \mu_2 = 2.0760, \quad \sigma_2 = 0.9917.$$

The p-value from the Cramer-Von Mises test is 0.991, validating the fit of the LLMM to the simulated data. In Figure 2.3, we visualize the fitted and true distributions over the observed sample data.

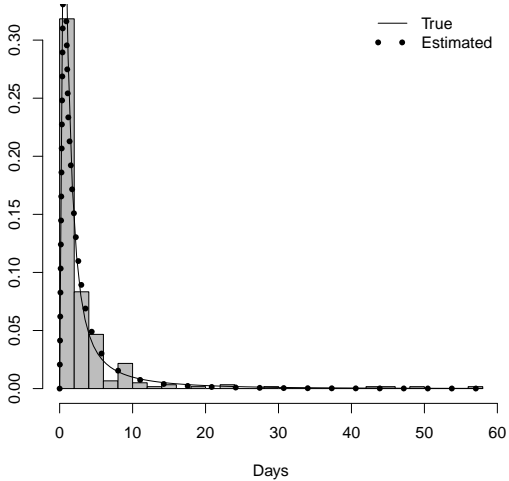


Figure 2.3: Simulation results for the Lognormal-Lognormal Mixture Model. We generated 300 samples from a LLMM with $p = 0.8$, $\mu_1 = 0$, $\sigma_1 = 1$, $\mu_2 = 2$, and $\sigma_2 = 1$.

2.4 Real Data Analysis

In order to test the robustness of our mixture models, we evaluate their performance using two sets of data collected via independent research studies at the University of Maryland School of Medicine. In the first study, researchers from the Department of Epidemiology and Public Health collected data from twenty medical and surgical intensive care units in order to study the impact of universal barrier precautions (i.e., gloves and gowns) on the transmission of multidrug-resistant organisms [62]. In the second study, the hospital provided surgical data during the first half of 2007. We were provided the date and time of the surgery, the dates when the patient was admitted to and discharged from the hospital, and surgical specialty group. Both sets of data contained de-identified length of stay observa-

tions, and, therefore, our studies were exempt from evaluation by the Institutional Review Board.

We summarize the descriptive statistics for each length of stay distribution in Tables 2.1 and 2.2, respectively, for the two sets of data and visualize these distributions for different patient types in Figure 2.4. In the first set of data, the median length of stay ranges from 3 to 5 days, the IQR over different sites varies from 3 to 5 days, and the length of hospital stay ranges widely from 1 to 125 days. In the second data set, the median length of stay ranges from 1 to 7 days, the middle 50% stay at hospital varies from 1 to 10, and all patients stay at hospital from 1 to 75 days. Across all patients admitted for our data sets, more than half stay less than 5 days, most are discharged within a week, and less than 10% stay for more than two weeks. These trends describe strongly right-skewed distributions that are difficult to fit.

Site	Number of patients	Median	Q_1 (1st quantile)	Q_3 (3rd quantile)	Short stay (LOS \leq 5 days)	Discharged in a Week	Discharged after 2 weeks
Site 1	731	5	3	8	442 (60%)	542 (74%)	71 (10%)
Site 2	550	3	2	6	400 (73%)	444 (81%)	25 (5%)
Site 3	564	3	2	5	425 (75%)	477 (85%)	33 (6%)
Site 9	894	4	3	7	611 (68%)	712 (80%)	64 (7%)
Site 11	895	4	3	7	590 (66%)	698 (78%)	80 (9%)
Site 12	731	4	2	7	492 (67%)	566 (77%)	50 (7%)
Site 13	578	3	2	4	484 (84%)	516 (89%)	20 (3%)
Site 14	884	4	3	7	566 (64%)	673 (76%)	66 (7%)
Site 17	568	3	2	6	390 (69%)	451 (79%)	39 (7%)
Site 18	1201	3	2	5	972 (81%)	1079 (90%)	41 (3%)
Site 20	512	3	2	5.25	384 (75%)	434 (85%)	19 (4%)

Table 2.1: Descriptive statistics for observed length of stay (in days) for intensive care unit patients.

In Tables 2.3 and 2.4, we report the p-values for the Cramer-Von Mises

Surgical Specialty	Number of patients	Median	Q_1 (1st quantile)	Q_3 (3rd quantile)	Short stay (LOS \leq 5 days)	Discharged in a Week	Discharged after 2 weeks
Cardiac Surgery	425	7	4	10	133 (31.3%)	224 (52.7%)	48 (11.3%)
Neurosurgery	597	4	2	7	358 (60%)	443 (74.2%)	65 (10.9%)
Organ Transplant	334	6	2	9	147 (44%)	211 (63.2%)	37 (11.1%)
Thoracic Surgery	159	3	1	7	95 (59.7%)	120 (75%)	14 (8.8%)
Vascular Surgery	211	4	2	7	128 (60.7%)	157 (74.4%)	10 (4.7%)
Electroconvulsive Therapy	89	5	1	11	43 (48.3%)	50(56.2%)	14(15.7%)
Gynecology	239	1	1	3	235 (98.3%)	236(98.7%)	2(0.8%)
Pediatric Bronchoscopy	207	1	1	3	164 (79.2%)	170(82.1%)	16(7.7%)
Surgical Oncology	223	4	1	8	126 (56.5%)	156(70%)	15(6.7%)
General Surgery	513	2	1	5	384 (74.9%)	445(86.7%)	20(3.9%)

Table 2.2: Descriptive statistics of observed length of stay (in days) for surgical patients.

test for each fitted distribution. For comparison purposes, we select single or mixture distributions with positive support, including lognormal, inverse gamma (IG), loglogistic, Exponential-Exponential (EE), Hyperexponential (HE), phase-type (PH), Lognormal-Loglogistic mixture (LL), and Lognormal-Loglogistic-Weibull (LLW) mixture distribution. We estimate the parameters for each of these baseline distributions via MLE except for the EE model, for which we estimate the parameters using EM. Our three proposed mixture models perform better than the comparison models, because the p-values of the CVM goodness of fit test are consistently greater than others. Compared with LEMM and LGMM, LLMM performs consistently better across the various ICUs and surgical patient populations. The lognormal distribution has been used extensively as a single distribution to model patient length of stay [12, 63, 73, 119], which may explain why a mixture model only containing lognormal distributions performs better than mixtures of lognormal and other components. Of the baseline methods, the phase-type distribution performed the best across the different LOS distributions. When fitting our 21 surgical groups using the phase-type distribution, only two groups have p-values of the CVM

Model	Site 1	Site 2	Site 3	Site 9	Site 11	Site 12	Site 13	Site 14	Site 17	Site 18	Site 20
Lognormal	0.06	0.021	0.014	0.054	0.106	0.143	< 0.01	0.109	0.2	< 0.01	0.141
IG	0.048	0.013	0.013	0.017	0.089	0.103	< 0.01	0.105	0.033	< 0.01	0.109
Loglogistic	0.2	0.072	0.025	0.084	0.145	0.189	0.018	0.157	0.39	0.015	0.198
EE	< 0.01	< 0.01	< 0.01	< 0.01	< 0.01	< 0.01	< 0.01	< 0.01	< 0.01	< 0.01	< 0.01
HE	< 0.01	< 0.01	< 0.01	< 0.01	< 0.01	< 0.01	< 0.01	< 0.01	< 0.01	< 0.01	< 0.01
PH	0.302	0.005	0.041	0.077	0.162	0.083	0.003	0.192	0.363	0.015	0.194
LL	< 0.01	0.128	0.012	0.13	0.158	0.03	0.018	0.274	0.381	0.016	0.216
LLW	0.045	< 0.01	< 0.01	0.011	< 0.01	< 0.01	< 0.01	0.076	0.042	< 0.01	0.037
LEMM	0.0278	0.12	0.031	0.064	0.152	0.202	0.018	0.217	0.014	0.016	0.221
LGMM	0.06	0.125	0.038	0.063	0.157	0.202	0.018	0.239	0.127	0.016	0.225
LLMM	0.335	0.128	0.034	0.125	0.158	0.206	0.018	0.259	0.381	0.016	0.216

Table 2.3: Cramer-Von Mises goodness-of-fit test p-values for observed length of stay of intensive care unit patients for Lognormal, IG, Loglogistic, EE, HE, PH, LL, LLW, LEMM, LGMM, and LLMM.

Model	Cardiac Surgery	Neurosurgery	Organ Transplant	Thoracic Surgery	Vascular Surgery	Electroconvulsive Therapy	Gynecology	Pediatric Bronchoscopy	Surgical Oncology	General Surgery
Lognormal	< 0.01	0.098	< 0.01	0.013	0.089	0.024	< 0.01	< 0.01	< 0.01	< 0.01
IG	< 0.01	0.109	< 0.01	0.017	0.126	0.011	< 0.01	< 0.01	< 0.01	< 0.01
Loglogistic	< 0.01	0.104	0.024	0.013	0.066	0.028	< 0.01	< 0.01	< 0.01	< 0.01
EE	< 0.01	< 0.01	0.016	0.025	0.014	0.102	< 0.01	< 0.01	< 0.01	< 0.01
HE	< 0.01	< 0.01	0.012	< 0.01	0.013	< 0.01	< 0.01	< 0.01	< 0.01	< 0.01
PH	0.06	0.141	0.149	0.12	0.41	0.142	< 0.01	< 0.01	0.016	0.04
LL	0.016	0.083	< 0.01	0.639	0.374	0.917	< 0.01	< 0.01	0.05	0.06
LLW	< 0.01	< 0.01	< 0.01	0.011	< 0.01	< 0.01	< 0.01	< 0.01	< 0.01	< 0.01
LEMM	0.168	0.134	< 0.01	0.025	0.089	0.141	< 0.01	< 0.01	< 0.01	< 0.01
LGMM	0.057	0.083	0.057	0.259	0.097	0.62	< 0.01	< 0.01	0.056	< 0.01
LLMM	0.098	0.08	0.462	0.649	0.495	0.936	0.43	0.069	0.485	0.058

Table 2.4: Cramer-Von Mises goodness-of-fit test p-values for observed length of stay of surgical patients for Lognormal, IG, Loglogistic, EE, HE, PH, LL, LLW, LEMM, LGMM, and LLMM.

goodness of fit test less than 0.01.

In Figures 2.5 and 2.6, we visualize the histogram of the observed length of stay with the estimated LEMM, LGMM, and LLMM density function. Overall, these models are robust to fit the length of stay data well. Particularly, the LLMM consistently fit the best out of the three lognormal-based mixture models.

We summarize the estimated mixture model parameters for each hospital population. Here, we only present the estimated mixture model parameters for the

Category	LEMM				LGMM					LLMM				
	p	μ	σ	λ	p	μ	σ	α	β	p	μ_1	σ_1	μ_2	σ_2
Site 1	0.754	1.422	0.611	0.05	1	1.698	0.902	1.365	3.031	0.09	3.618	0.175	1.508	0.699
Site 2	0.662	1.108	0.327	0.106	0.663	1.094	0.333	1.473	6.470	0.175	2.609	0.446	1.084	0.427
Site 3	0.686	0.943	0.518	0.112	0.645	0.886	0.485	1.411	6.118	0.098	2.804	0.181	1.061	0.617
Site 9	0.987	1.478	0.631	0.014	0.990	1.481	0.633	1.319	67.17	0.596	1.822	0.704	1.045	0.312
Site 11	0.926	1.389	0.646	0.067	0.898	1.36	0.627	1.437	9.752	0.071	2.779	0.532	1.354	0.625
Site 12	0.923	1.366	0.580	0.061	0.907	1.346	0.566	1.435	10.954	0.209	2.117	0.766	1.268	0.526
Site 13	0.906	0.995	0.463	0.087	0.909	0.988	0.462	1.428	8.377	0.051	2.763	0.467	1.005	0.478
Site 14	0.852	1.535	0.645	0.057	0.811	1.485	0.617	1.439	11.566	0.246	2.532	0.688	1.391	0.581
Site 17	0.032	4.668	0.096	0.190	0.040	4.439	0.458	1.381	3.618	0.032	4.668	0.096	1.385	0.731
Site 20	0.866	1.212	0.597	0.071	0.867	1.197	0.592	1.431	10.255	0.056	3.19	0.269	1.244	0.622
Cardiac Surgery	0.395	1.960	0.281	0.121	0.261	1.916	0.224	1.511	5.448	0.439	1.275	1.176	2.065	0.372
Neurosurgery	0.910	1.325	0.850	0.078	0.699	1.098	0.716	1.430	7.911	0.841	1.640	0.768	0.124	0.091
Organ Transplant	0.999	1.544	0.951	0.115	0.394	1.168	0.928	1.434	5.826	0.835	1.845	0.730	0.018	0.037
Thoracic Surgery	0.305	0.073	0.075	0.138	0.313	0.074	0.076	1.435	5.112	0.678	1.678	0.785	0.075	0.077
Vascular Surgery	1	1.275	0.830	0.101	0.922	1.219	0.802	1.426	6.715	0.062	1.724	0.631	0.396	0.304
Electroconvulsive Therapy	0.315	0.072	0.042	0.091	0.32	0.072	0.043	1.416	7.813	0.642	2.212	0.687	0.085	0.061
Gynecology	0.978	0.577	0.489	0.111	0.979	0.576	0.489	1.402	6.613	0.533	1.018	0.412	0.132	0.058
Pediatric Bronchoscopy	1	0.715	1.008	0.798	1	0.715	1.008	1.279	0.973	0.429	1.589	1.012	0.057	0.028
Surgical Oncology	0.310	0.068	0.047	0.136	0.314	0.068	0.047	1.389	5.31	0.673	1.77	0.707	0.069	0.049
General Surgery	0.448	0.38	0.32	0.174	0.429	0.341	0.192	1.398	4.047	0.740	1.283	0.724	0.12	0.093

Table 2.5: Parameter estimates for lognormal-based mixture models for different patient populations.

Category	LEMM				LGMM					LLMM				
	p	μ	σ	λ	p	μ	σ	α	β	p	μ_1	σ_1	μ_2	σ_2
Number of iterations	203	157	92	434	385	218	161	23	349	14	44	409	312	56
Execution time	0.2 seconds				0.25 seconds					0.27 seconds				

Table 2.6: Number of iterations (until convergence) and execution time (R 3.5.1) for estimating parameters for lognormal-based mixture models.

LEMM, the LGMM, and the LLMM in Table 2.5.

We present the convergence of all parameters in the lognormal-exponential mixture model (LEMM), the lognormal-gamma mixture model (LGMM), and the lognormal-lognormal mixture model (LLMM) in simulation study. In the Figure 2.7 through 2.9 and Table 2.6 below, we demonstrate that our convergence criteria are satisfied in all cases in less than 500 iterations.

2.5 Discussion

Length of stay is an important criterion of hospital utilization [35, 101, 116]. Appropriate modeling of hospital LOS can help decision-makers evaluate the efficiency of the care they provide and compare their performance with distributions for similar patient populations. However, the distribution of length of stay is usually right-skewed with more than one mode and it includes outliers [96, 105, 106, 125, 139]. These particular features make model fitting more complicated for length of stay. In the existing literature, different combinations of mixture distributions have been proposed to model the length of stay, having both pros and cons.

We have developed a robust method for fitting LOS distributions using lognormal-based mixture models, with the assumption that most distributions are fit well with two appropriately defined components. Our data analyses using real-world data demonstrate lognormal is an effective component. We employed the EM algorithm to estimate the parameters of each mixture model, because closed-form solutions could not be produced via MLE. We demonstrated that our mixture models performed consistently well for a variety of LOS distributions, including for ICU settings across multiple sites and for different classes of surgical patients at the same site. With two components in our mixture models, we also validated that our three algorithms are easier to implement. Our hope is that better estimation of these distributions can support improved operational and clinical decision-making in hospitals, ultimately leading to improved outcomes for patients and more efficient delivery of care by providers.

In general, mathematical modeling has far-reaching implications that could help hospitals more efficiently allocate their limited resources. We believe there are many practical applications that could benefit from the use of parametric models such as the lognormal-based mixture models that we have proposed. While parametric LOS distributions have been used in a predictive manner [57], they have been used much more often to support simulation modeling at the hospital level [15, 50, 55, 59, 71, 80, 102, 110]. Oftentimes, these models rely on accurate distributions of LOS in order to properly simulate patient flow within a hospital, providing an advantage over methods that rely on deterministic estimates of LOS which often result in underestimating bed capacity requirements [61]. In particular, simulation provides a useful method for informing bed planning and capacity management. For example, Costa et al. (2003) and Torabipour et al. (2016) each developed models that relied on parametric distributions of LOS to simulate patient flow through various hospital units, and they used these models to support bed capacity planning [39, 134]. Likewise, Zhu (2012) used simulation to determine an appropriate level of ICU bed capacity [148]. Additionally, simulation models based on historical LOS distributions have been used to improve the scheduling of surgical patients or forecasting emergency department crowding in hospitals [4, 51, 70, 120]. For all of these studies, the authors relied on parametric distributions, such as lognormal etc., for LOS, which our methods consistently outperform in terms of fit. The use of our models in such studies may improve the accuracy of the simulated outcomes, and thus, impact the subsequent prescriptive policies.

It would be interesting to extend our analysis in two ways. The first extension

would involve removing the assumption that the distribution of length of stay is a mixture with no more than two components. The parameters for such a mixture model would be more complex to estimate, but would be more flexible in capturing the behavior of more than two components. This type of model may be appropriate for more heterogeneous patient populations, such as those observed in general or surgical hospital units or the emergency department. The challenge associated with this approach would be to develop a method for optimizing the number of mixture model components, taking into consideration the quality of fit and the complexity of the model. The second extension involves developing mixture models with components other than exponential-family distributions, which is a more difficult estimation problem. These problems are beyond the scope of this chapter and will be interesting topics for future research.

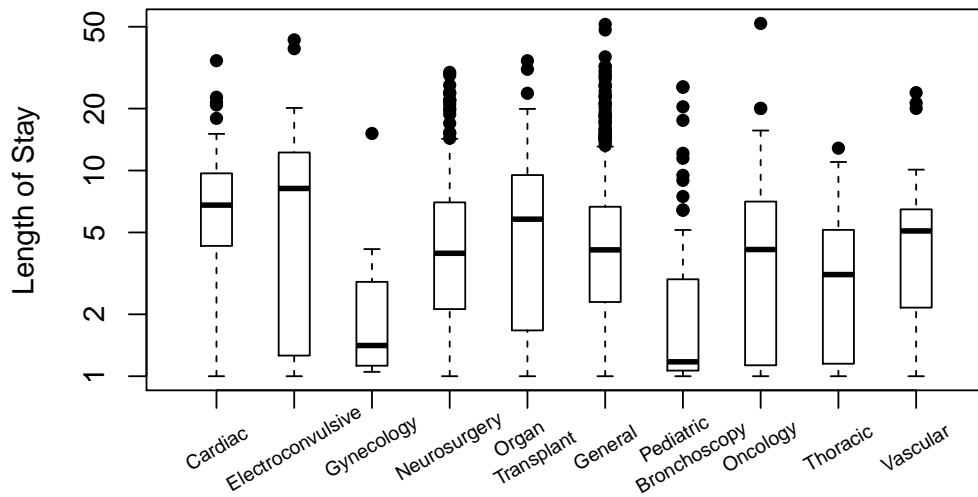
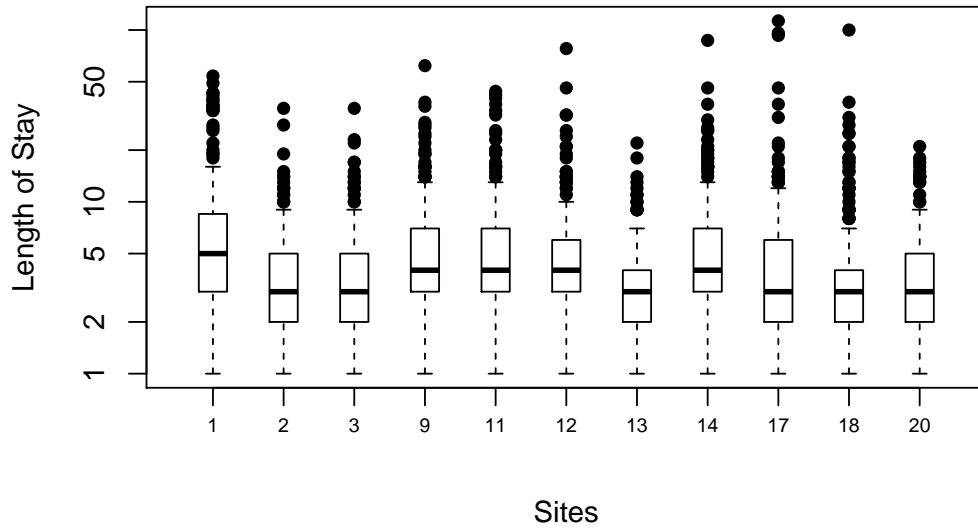


Figure 2.4: Distributional summary of observed length of stay (in days) in medical and surgical intensive care units.

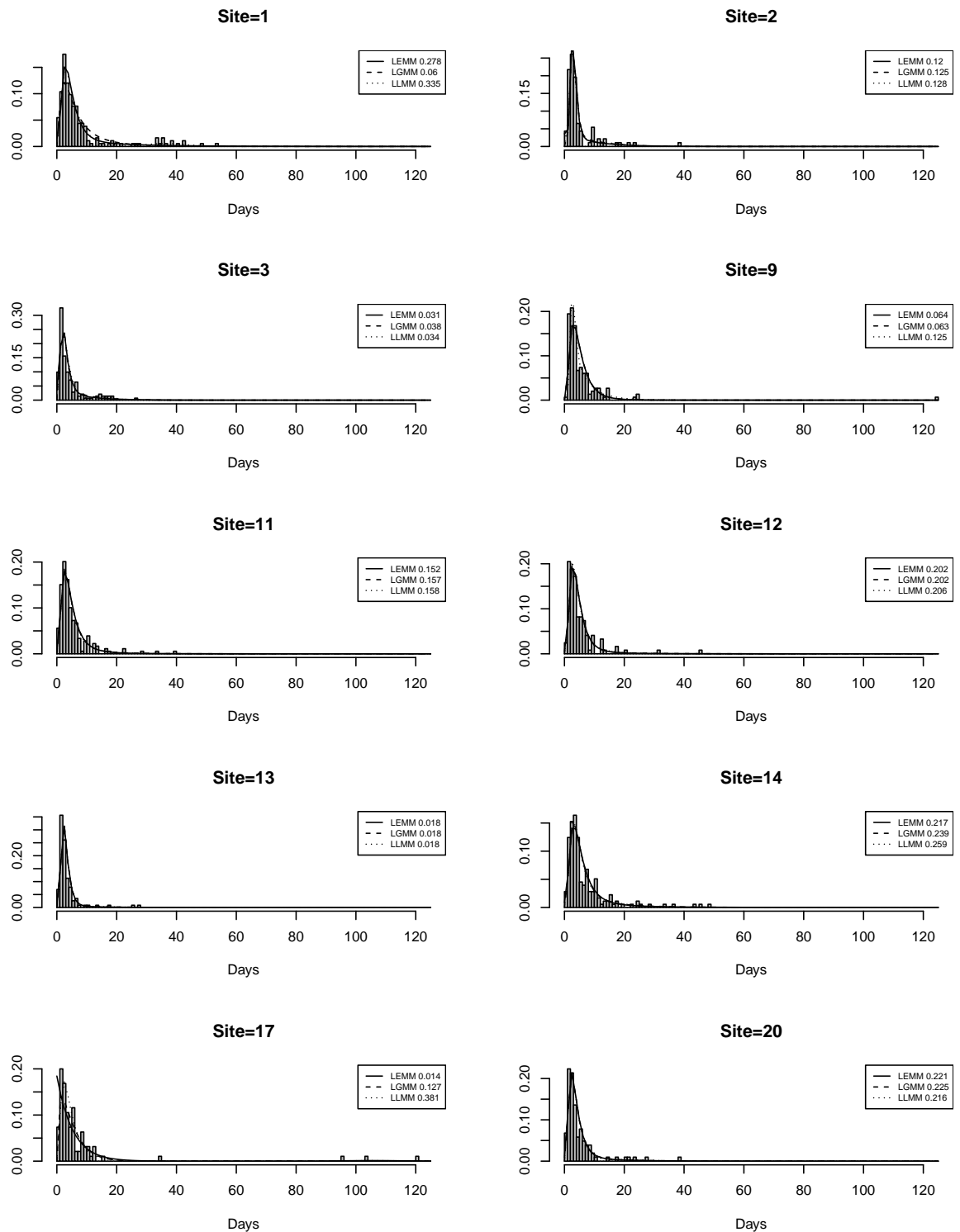


Figure 2.5: Length of stay distribution for different sites at ICU, shown with density plots for lognormal-exponential mixture model (LEMM), lognormal-gamma mixture model (LGMM), lognormal-lognormal mixture model (LLMM) and Cramer-Von Mises p-values for goodness of fit tests.

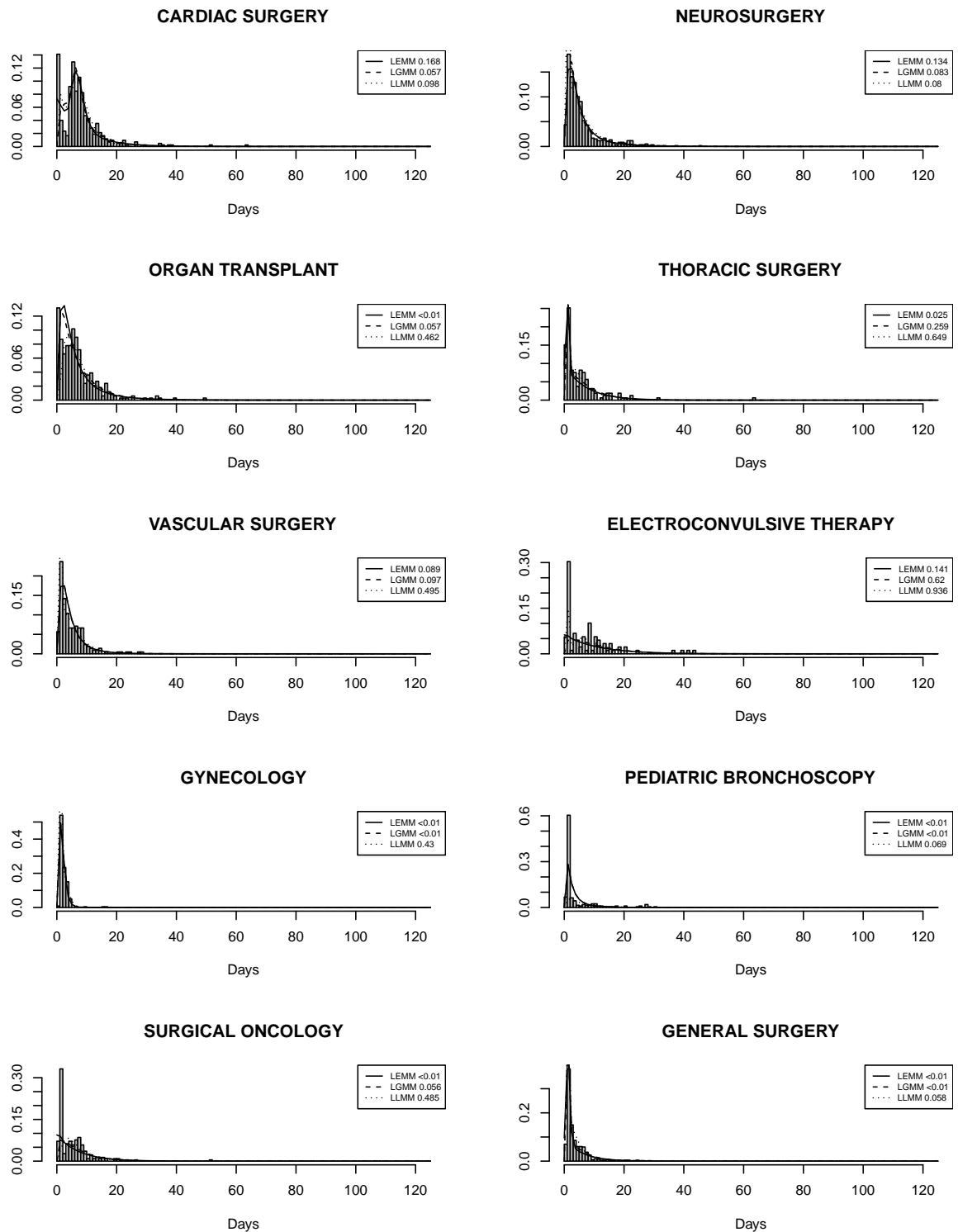


Figure 2.6: Length of stay distribution for different surgical specialties, shown with density plots for lognormal-exponential mixture model (LEMM), lognormal-gamma mixture model (LGMM), lognormal-lognormal mixture model (LLMM) and Cramer-Von Mises p-values for goodness of fit tests.

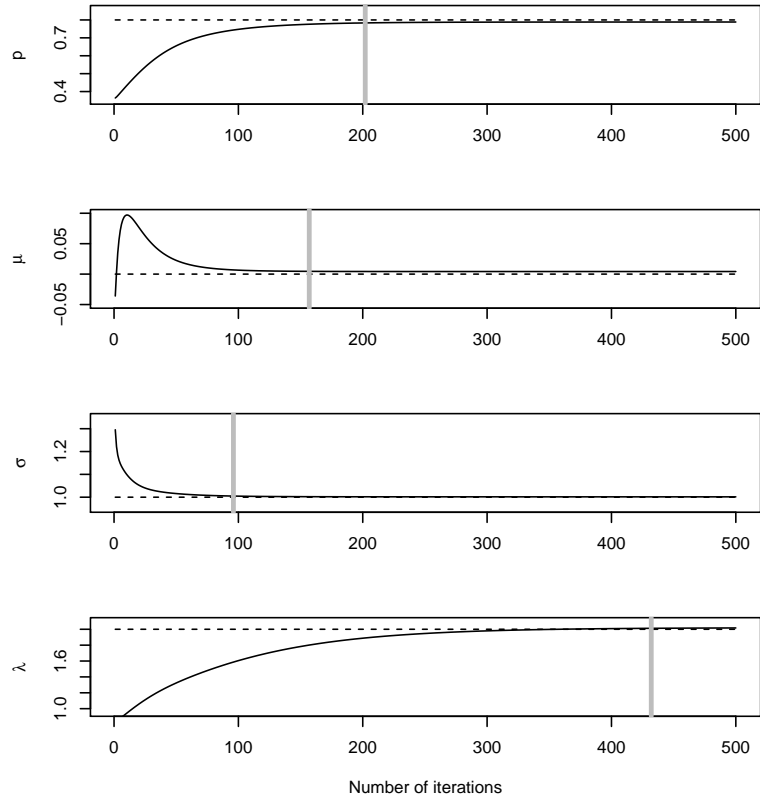


Figure 2.7: True value (dotted line) and the convergence (solid line) of all parameters in lognormal-exponential mixture model (LEMM) in simulation study with vertical lines indicating the number of iterations required to satisfy the convergence threshold ($\epsilon = 10^{-4}$).

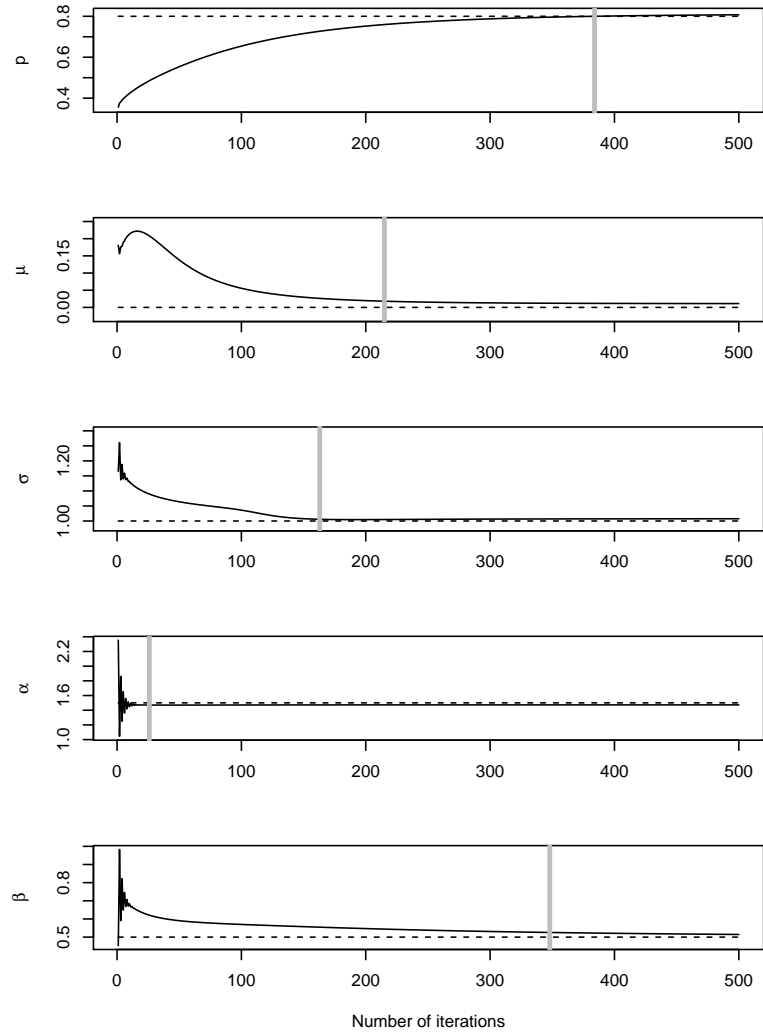


Figure 2.8: True value (dotted line) and the convergence (solid line) of all parameters in lognormal-gamma mixture model (LGMM) in simulation study with vertical lines indicating the number of iterations required to satisfy the convergence threshold ($\epsilon = 10^{-4}$).

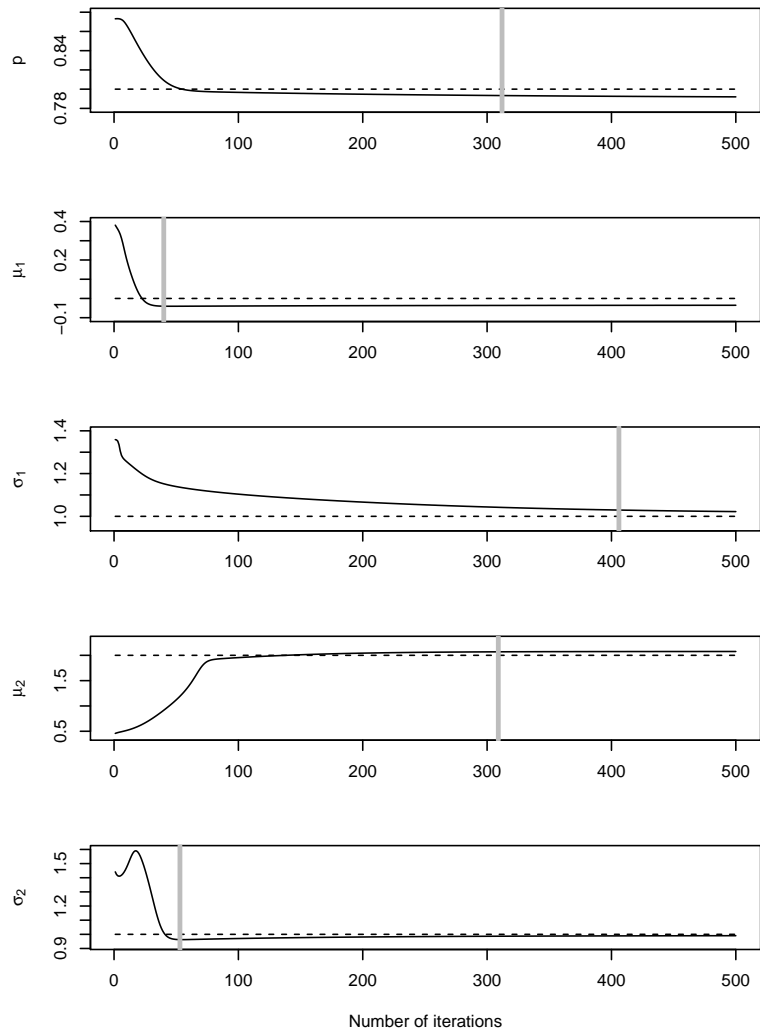


Figure 2.9: True value (dotted line) and the convergence (solid line) of all parameters in lornormal-lognormal mixture model (LLMM) in simulation study with vertical lines indicating the number of iterations required to satisfy the convergence threshold ($\epsilon = 10^{-4}$).

Chapter 3: A Continuous-time Markov Model for Estimating Readmission Risk for Hospital Inpatients

3.1 Introduction

Estimating hospital readmission risk can support clinical and operational decision making in hospitals. On the clinical side, medical staff can incorporate knowledge of the readmission risk into their plan of care for patients. For example, patients with a low risk of readmission could be evaluated further for the possibility of early discharge, whereas patients with a high risk of readmission could be retained for further evaluation and treatment. With respect to operations, hospital beds are a critical resource that must be managed efficiently. On one hand, patients being discharged early frees up beds for incoming patients [7, 44]; but on the other hand, patients who are discharged inappropriately could experience adverse outcomes in the future, including not only readmission but increased morbidity and mortality [22, 41, 75, 95]. In addition, understanding how readmission risk varies over time can help hospitals to better plan their capacity for other limited resources such as medical equipment and clinical staff.

In addition to the clinical and operational considerations, readmissions also

have a significant financial impact on hospitals. Readmission rates have been used as a key indicator for hospital performance, as indicated by recent efforts by the U.S. Centers for Medicare and Medicaid Services (CMS) to disincentivize hospitals by lowering reimbursement rates for readmitted patients [81, 91, 127]. Since 2012, CMS has reduced Medicare payments for Inpatient Prospective Payment System (IPPS) hospitals with high 30-day readmission rates in an effort to promote high-quality and patient-centered care. This change has motivated hospitals to think more holistically about how to make better clinical decisions for admitted patients, which in turn will likely drive better operational and financial outcomes.

Since the enforcement of CMS reimbursement penalties, modeling readmission risk has been an area of focus for research in the healthcare space. Early studies apply traditional statistical methods such as linear, generalized linear, or nonlinear regression models to estimate the readmission risk for a patient [30, 64, 81, 87, 136, 147]. Generalized additive models have also been applied to the readmission risk estimation problem, which relax the linearity assumption from traditional regression models [31]. Supervised machine learning models have been applied to this problem as well, including support vector machines and random forests [79]. Most recently, deep learning has been leveraged to estimate readmission risk, which offers additional prospects for incorporating rich predictor data. For example, Jamei et al. used Google’s TensorFlow library to build an artificial neural network model to predict the risk of 30-day hospital readmission using data from more than 300,000 hospital stays,[78] and Xie et al. employed the trajectory-based deep learning methods for predicting the readmission risk to capture various illness trajectories and account

for the patient heterogeneity using data from 18 million patients [79, 144].

These models may be useful in specific settings (e.g., unit type, patient cohort), but their performance may be limited for clinical purposes. For example, in a systematic review, Kansagara et al. tested 26 regression models for readmission risk, and found that most models perform poorly for individual patients [81]. The aforementioned statistical and machine learning techniques rely on a broad range of information to train them, which may not be accessible or even (digitally) available in every hospital setting. In addition to the data requirements, the development, evaluation, and implementation of these models requires a certain level of expertise and resources that may also not be available.

In addition, most of the aforementioned models do not incorporate the effect of time since discharge on readmission risk. Hospital readmissions usually occur shortly after a patient is discharged, and the likelihood declines over time. Approximately one third of readmissions occur within a month of discharge, half of them within 90 days, and 80% within a year [10, 19, 34, 38, 67, 128, 149]. There are various conventions for defining the most relevant time window to consider when evaluating readmissions, such as within 1, 2, 4, or 12 months of the time of discharge [8, 9, 29, 43, 56, 83, 138, 141]; however, most preventable readmissions have been reported to occur within one month of discharge [9, 56, 91]. Therefore, we focus on the 30-day readmission window, which is consistent with the CMS reimbursement penalty definition.

In this study, our goal is to estimate the risk of readmission for patients over time. Specifically, we select surgical patients since they involve more resources from

hospitals such as nurses, bed planning, and more post-operative care. Readmission after surgery happens frequently and is associated with high cost [140]. Surgical complications and respiratory failures result in most of the readmissions or mortality in a surgical clinic [14, 137]. In addition to biomedical applications [33], Markov chains also have been used to model readmission in a variety of hospital settings, such as estimating the probability of this outcome for hospital patients with chronic obstructive pulmonary disease or respiratory failure, or patients in geriatric settings [16, 133]. Our work is not limited to scenarios where patient-specific data is required, and could be employed anywhere that the time of patient discharge and readmission is available. We propose a two-state continuous-time Markov chain model with a constant transition rate, which we use to compute point and interval estimators for the readmission probability as a function of the time since the patient is discharged [66]. Our version of the readmission problem has several challenging characteristics. First, we have a limited amount of information on which to base our estimations for readmission risk. In contrast with many of the previous models, we do not have access to electronic medical record data that would likely contain many significant predictors of readmission risk. We only have information on the times of discharge and readmission, along with some basic information that we can use to group the patients into cohorts (e.g., surgical specialty). The second challenge is that we need to develop an appropriate link between readmission probability and time. Moreover, we need to be able to develop asymptotic distributions in order to compute the interval estimators. To address these limitations, we utilize techniques from stochastic processes and survival analysis to develop our models for readmission

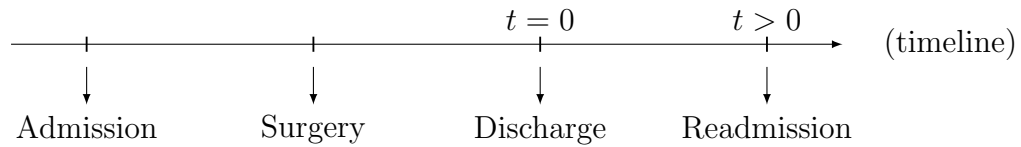
risk. The stochastic processes will be utilized to link readmission probabilities with time. Meanwhile, we use survival analysis to gain information from the time until the occurrence of events of interest, that is, discharge or readmission, assuming the constant transition rate.

The remaining sections of this chapter are organized as follows. In Section 3.2, we formulate our problem and describe the data we use in this study. We describe our methodology for estimating readmission probabilities using the two-state continuous-time Markov chain. In Section 3.3, we validate the performance of our estimation approach for different hospital readmission scenarios using simulation studies. In Section 3.4, we test the performance of our estimation approach using real data collected by researchers at the University of Maryland Medical Center. Finally, we conclude with a discussion of our results and future research directions in Section 3.5. In this final section, we also illustrate how hospitals could aggregate these dynamic estimations for individual patients into an overall estimate of expected readmissions within a 30-day time window.

3.2 Methods

In this section, we introduce the two-state continuous-time Markov chain to formulate our model for patient discharge and readmission. We then estimate our readmission probabilities using maximum likelihood estimation (MLE). Finally, we present asymptotic distributions and interval estimation for the readmission probability.

A significant portion of hospitals' revenues and profits come from surgical volume [7]. Tsai et al. found that almost one in seven surgical patients is readmitted to the hospital within 30 days [135]. Our study population consists of surgical patients admitted to the University of Maryland Medical Center between January 1, 2007 and June 1, 2007. The dataset contains the surgical specialty group that performed the surgery, the dates when the patient was initially admitted to and discharged from the hospital, and the dates when the patient was readmitted, as illustrated in the diagram below:



We want to analyze how readmission risk changes as a function of time once a patient has been discharged after surgery at a large, academic medical center. After a patient is initially discharged, the patient will remain in one of two hospital states: discharge or readmission.

Thus, we denote our probabilities of interest as follows:

$$P_{00}(t) = \Pr\{\text{Patient remains discharged at time } t \text{ after being discharged}\}$$

$$P_{01}(t) = \Pr\{\text{Patient is readmitted at time } t \text{ after being discharged}\}$$

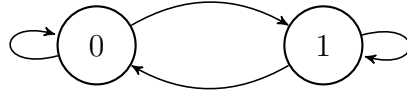
Our goal is to estimate these two probabilities. We propose the following methods to achieve these estimators.

3.2.1 The Continuous-time Markov Model

We define the state of a patient at time $t \in R^+$ as :

$$\zeta_t = \begin{cases} 0 & \text{if the patient is discharged at time } t \\ 1 & \text{if the patient has been readmitted and is still in the hospital at time } t. \end{cases}$$

We model the evolution of the patient state as a stochastic process using a continuous-time Markov chain with a constant transition rate. We illustrate the two-state, continuous-time Markov chain in the diagram below:



After a patient is initially discharged at time $t = 0$, the patient remains discharged unless he or she is readmitted at some future time t . If readmitted, patients remain in state 1 until they are discharged, at which point they transition back to state 0.

We seek to estimate two probability functions:

1. Probability of remaining discharged at time t after being discharged.

$$P_{00}(0, t) = \Pr(\zeta_t = 0 | \zeta_0 = 0) = P_{00}(t)$$

2. Probability of being readmitted at time t after being discharged.

$$P_{01}(0, t) = \Pr(\zeta_t = 1 | \zeta_0 = 0) = P_{01}(t)$$

We note that for patients who are readmitted multiple times, we simply model

the probability of remaining discharged or being readmitted since their most recent discharge.

3.2.2 The Estimators

We use the Kolmogorov backward equations [90] to model the rate of change of our readmission probabilities over time, which are appropriate for modeling continuous-time Markov processes. This approach yields the following system of ordinary differential equations:

$$\frac{dP_{00}(t)}{dt} = \lambda_{00}P_{00}(t) + \lambda_{10}P_{01}(t)$$

and

$$\frac{dP_{01}(t)}{dt} = \lambda_{01}P_{00}(t) + \lambda_{11}P_{01}(t)$$

where λ_{ij} is the transition rate from state i to state j and $i, j = 0$ or 1 .

The system of equations are equivalent to the following matrix form

$$\frac{d}{dt}P\vec{(t)} = AP\vec{(t)}$$

where

$$P\vec{(t)} = \begin{pmatrix} P_{00}(t) \\ P_{01}(t) \end{pmatrix}$$

and

$$A = \begin{pmatrix} \lambda_{00} & \lambda_{10} \\ \lambda_{01} & \lambda_{11} \end{pmatrix}.$$

The solution to the system is

$$P(\vec{t}) = e^{At}P(\vec{0})$$

where

$$P(\vec{0}) = \begin{pmatrix} P_{00}(0) \\ P_{01}(0) \end{pmatrix} = \begin{pmatrix} 1 \\ 0 \end{pmatrix}.$$

Let λ_1 and λ_2 be two distinct eigenvalues of A . To obtain the closed-form of $P(\vec{t})$,

we decompose the matrix A as

$$A = Q\Lambda Q^{-1}$$

where Λ is the diagonal matrix whose diagonal elements are the eigenvalues of A , and Q is the square matrix whose columns are the corresponding eigenvectors.

Specifically,

$$\Lambda = \begin{pmatrix} \lambda_1 & 0 \\ 0 & \lambda_2 \end{pmatrix}$$

where

$$\lambda_1 = \frac{1}{2}(\lambda_{00} + \lambda_{11} + \sqrt{(\lambda_{00} - \lambda_{11})^2 + 4\lambda_{01}\lambda_{10}}),$$

$$\lambda_2 = \frac{1}{2}(\lambda_{00} + \lambda_{11} - \sqrt{(\lambda_{00} - \lambda_{11})^2 + 4\lambda_{01}\lambda_{10}}).$$

and

$$Q = \begin{pmatrix} \lambda_{10} & \lambda_{10} \\ \lambda_1 + \lambda_{01} & \lambda_2 + \lambda_{01} \end{pmatrix}.$$

Here, we see that the two eigenvectors are linearly independent, so we can perform eigendecomposition for the coefficient matrix A above as follows:

$$\begin{aligned} P(\vec{t}) &= e^{At}P(\vec{0}) = \sum_{k=0}^{+\infty} (At)^k \frac{1}{k!} P(\vec{0}) \\ &= \sum_{k=0}^{+\infty} Q \Lambda^k Q^{-1} \frac{t^k}{k!} P(\vec{0}) = Q \left(\sum_{k=0}^{+\infty} \Lambda^k \frac{t^k}{k!} \right) Q^{-1} P(\vec{0}) \\ &= Q \begin{pmatrix} e^{\lambda_1 t} & 0 \\ 0 & e^{\lambda_2 t} \end{pmatrix} Q^{-1} P(\vec{0}). \end{aligned}$$

After we compute the matrix multiplication, we have

$$P_{00}(t) = \frac{e^{\lambda_1 t}(\lambda_2 + \lambda_{01}) - e^{\lambda_2 t}(\lambda_1 + \lambda_{01})}{\lambda_2 - \lambda_1}$$

and

$$P_{01}(t) = \frac{(e^{\lambda_1 t} - e^{\lambda_2 t})(\lambda_1 + \lambda_{01})(\lambda_2 + \lambda_{01})}{\lambda_{10}(\lambda_2 - \lambda_1)}.$$

The matrix A is the generator matrix for our Markov chain model; therefore the row sums are equal to zero. Thus, we have $\lambda_1 = 0$ and $\lambda_2 = -\lambda_{01} - \lambda_{10}$, and the following equations are achieved.

Solving the equations [117] yields

$$P_{00}(t) = \frac{-\lambda_{10} - \lambda_{01}e^{\lambda_2 t}}{\lambda_2}$$

and

$$P_{01}(t) = \frac{-\lambda_{01} + \lambda_{01}e^{\lambda_2 t}}{\lambda_2}$$

where $\lambda_2 = -\lambda_{01} - \lambda_{10}$.

The stationary distributions of the continuous-time Markov chain model are

$$\lim_{t \rightarrow \infty} P_{00}(t) = \frac{\lambda_{10}}{\lambda_{01} + \lambda_{10}}$$

and

$$\lim_{t \rightarrow \infty} P_{01}(t) = \frac{\lambda_{01}}{\lambda_{01} + \lambda_{10}}.$$

These limits and can also be viewed as limits of both readmission probabilities.

Hence, the two estimators are

$$\widehat{P_{00}}(t) = P_{00}(t, \hat{\theta}) = \frac{-\hat{\lambda}_{10} - \hat{\lambda}_{01}e^{\lambda_2(\hat{\theta})t}}{\lambda_2(\hat{\theta})}$$

and

$$\widehat{P_{01}}(t) = P_{01}(t, \hat{\theta}) = \frac{-\hat{\lambda}_{01} + \hat{\lambda}_{01}e^{\lambda_2(\hat{\theta})t}}{\lambda_2(\hat{\theta})},$$

where $\theta = \{\lambda_{01}, \lambda_{10}\}$ and $\hat{\lambda}_{ij}$ is the MLE of λ_{ij} , where $i, j = 0$ or 1 .

3.2.3 Asymptotic Distributions of the Estimators

In addition to the point estimates derived in the previous subsection, we would like to have some guarantee of capturing the probabilities of interest using an interval estimator. In order to succeed at interval estimation, we need to derive the asymptotic distributions of the estimators below. We begin with the asymptotic distribution for $P_{01}(t, \hat{\theta})$. The distribution for $P_{00}(t, \hat{\theta})$ follows in a similar fashion.

Theorem 3.1. *The asymptotic distribution for $P_{01}(t, \hat{\theta})$ is*

$$\sqrt{n}(P_{01}(t, \hat{\theta}) - P_{01}(t, \theta)) \xrightarrow{\mathcal{D}} \mathcal{N}(0, a_1^2 \lambda_{01}^2 + b_1^2 \lambda_{10}^2)$$

where

$$a_1 = \frac{\lambda_{10} - (\lambda_{10} + \lambda_{01} \lambda_2 t) e^{-\lambda_2 t}}{\lambda_2^2}$$

and

$$b_1 = \frac{-\lambda_{01} + \lambda_{01}(1 - \lambda_2 t) e^{-\lambda_2 t}}{\lambda_2^2}.$$

Proof. Let's first expand $P_{01}(t, \hat{\theta})$ using a first-order Taylor series around $\hat{\theta} = \theta$, giving

$$\begin{aligned} P_{01}(t, \hat{\theta}) &= P_{01}(t, \theta) + \frac{\partial P_{01}(t, \theta)}{\partial \lambda_{01}} (\hat{\lambda}_{01} - \lambda_{01}) \\ &\quad + \frac{\partial P_{01}(t, \theta)}{\partial \lambda_{10}} (\hat{\lambda}_{10} - \lambda_{10}) + r(n) \end{aligned}$$

where $r(n) = o((\hat{\lambda}_{01} - \lambda_{01}) + (\hat{\lambda}_{10} - \lambda_{10}))$. Since each $\hat{\lambda}_{ij}$ is the MLE of λ_{ij} , where

$i, j = 0$ or 1 , we have the following asymptotic distribution for λ_{ij} :

$$\sqrt{n}(\hat{\lambda}_{ij} - \lambda_{ij}) \xrightarrow{\mathcal{D}} \mathcal{N}(0, \sigma_{ij}^2)$$

where $\sigma_{ij}^2 = \lambda_{ij}^2$, where $i, j = 0$ or 1 .

Since $\hat{\lambda}_{ij} \xrightarrow{\mathcal{P}} \lambda_{ij}$, it follows that $r(n) \xrightarrow{\mathcal{P}} 0$. By applying Slutsky's Theorem to

$$\sqrt{n}(P_{01}(t, \hat{\theta}) - P_{01}(t, \theta)) = a_1 \sqrt{n}(\hat{\lambda}_{01} - \lambda_{01}) + b_1 \sqrt{n}(\hat{\lambda}_{10} - \lambda_{10})$$

where

$$a_1 = \frac{\partial P_{01}(t, \theta)}{\partial \lambda_{01}} \quad \text{and} \quad b_1 = \frac{\partial P_{01}(t, \theta)}{\partial \lambda_{10}},$$

the results now follow. □

By using Theorem 1, we have a general method to construct the approximate $1 - \alpha$ confidence interval for $P_{01}(t, \theta)$.

Let's define $\sigma_1^2(\theta) = a_1^2 \lambda_{01}^2 + b_1^2 \lambda_{10}^2$. Since $\hat{\theta}$ is the MLE for θ , we have

$$\sigma_1(\hat{\theta}) \xrightarrow{\mathcal{D}} \sigma_1(\theta).$$

Thus, we have

$$\frac{\sigma_1(\theta)/\sqrt{n}}{\sigma_1(\hat{\theta})/\sqrt{n}} \xrightarrow{\mathcal{P}} 1.$$

On the other hand, we have

$$\frac{P_{01}(t, \hat{\theta}) - P_{01}(t, \theta)}{\sigma_1(\theta)/\sqrt{n}} \xrightarrow{\mathcal{D}} \mathcal{N}(0, 1).$$

By applying Slutsky's Theorem, it yields

$$\frac{P_{01}(t, \hat{\theta}) - P_{01}(t, \theta)}{\sigma_1(\hat{\theta})/\sqrt{n}} \xrightarrow{\mathcal{D}} \mathcal{N}(0, 1),$$

giving the approximate $1 - \alpha$ confidence interval

$$P_{01}(t, \hat{\theta}) - z_{\alpha/2} \frac{\sigma_1(\hat{\theta})}{\sqrt{n}} \leq P_{01}(t, \theta) \leq P_{01}(t, \hat{\theta}) + z_{\alpha/2} \frac{\sigma_1(\hat{\theta})}{\sqrt{n}}.$$

Theorem 3.2. *The asymptotic distribution for $P_{00}(t, \hat{\theta})$ is*

$$\sqrt{n}(P_{00}(t, \hat{\theta}) - P_{00}(t, \theta)) \xrightarrow{\mathcal{D}} \mathcal{N}(0, a_2^2 \lambda_{01}^2 + b_2^2 \lambda_{10}^2)$$

where

$$a_2 = \frac{-\lambda_{10} + (\lambda_{10} + \lambda_{01} \lambda_2 t) e^{\lambda_2 t}}{\lambda_2^2} \quad \text{and} \quad b_2 = \frac{\lambda_{01} + \lambda_{01} (\lambda_2 t - 1) e^{\lambda_2 t}}{\lambda_2^2}.$$

Proof. The proof of Theorem 2 is almost identical to that of Theorem 1. □

Similarly, we have the approximate $1 - \alpha$ confidence interval for $P_{00}(t, \theta)$

$$P_{00}(t, \hat{\theta}) - z_{\alpha/2} \frac{\sigma_2(\hat{\theta})}{\sqrt{n}} \leq P_{00}(t, \theta) \leq P_{00}(t, \hat{\theta}) + z_{\alpha/2} \frac{\sigma_2(\hat{\theta})}{\sqrt{n}}$$

where

$$\sigma_2^2(\theta) = a_2^2 \lambda_{01}^2 + b_2^2 \lambda_{10}^2.$$

3.3 Simulation

In this section, we validate the performance of our estimation via simulation in order to demonstrate the flexibility of our method. In each scenario, we generate 500 readmitted patients and compare our estimators with the empirical readmission probability. Here, we consider three scenarios to validate our methods, assuming $\lambda_{01} = 0.01$ and $\lambda_{10} = 0.05$.

In scenario A, we simulate 500 trajectories for patients who are readmitted once within 72 hours of discharge. First, we generate 500 interevent times between the initial discharge and the impending readmission by sampling from the exponential distribution with $\lambda_{01} = 0.01$. Then, we generate 500 length of stay observations for the readmitted patients by sampling from an exponential distribution with $\lambda_{10} = 0.05$.

In scenario B, we simulate 500 trajectories for patients who are readmitted twice within 2 weeks of discharge. In order to conduct this experiment, we simply repeat the two steps from scenario A to simulate multiple discharges and readmissions.

For each scenario, we compute the empirical risk as the proportion of patients

who are in state 0 or 1 at time t :

$$\widetilde{P_{0j}(t)} = \frac{\# \text{ of patients in state } j \text{ at time } t}{500}$$

where $j = 0$ or 1 .

Last, we compare $\widetilde{P_{0j}(t)}$ with $\widehat{P_{0j}(t)}$ where $j = 0$ or 1 in each scenario, since $\forall t > 0, \widetilde{P_{0j}(t)} - \widehat{P_{0j}(t)} \xrightarrow{\mathcal{P}} 0$. We provide more details about the relationship between $\widetilde{P_{0j}(t)}$ and $\widehat{P_{0j}(t)}$ below. Here, $\widehat{P_{00}(t)}$ and $\widehat{P_{01}(t)}$ are defined in section 3.2.2 above.

Here, we prove Theorem 3.3 below.

Theorem 3.3. $\forall t > 0, \widetilde{P_{0j}(t)} - \widehat{P_{0j}(t)} \xrightarrow{\mathcal{P}} 0$.

Proof. To ease the notation, denote $\widetilde{P_{0j}(t)}$ as $\widetilde{P_n(t)}$, $\widehat{P_{0j}(t)}$ as $\widehat{P_n(t)}$, where n represents the sample size, and let $P(t)$ be the true transition probability.

First, since $\forall t > 0, \widetilde{P_n(t)} \xrightarrow{\mathcal{P}} P(t)$, it follows that $\forall \delta > 0, \forall \epsilon > 0, \exists N_1 > 0$, s.t. when $n > N_1, Pr(|\widetilde{P_n(t)} - P(t)| > \delta/2) < \epsilon/2$.

Then, since $\forall t > 0, \widehat{P_n(t)} \xrightarrow{\mathcal{P}} P(t)$, it follows that $\forall \delta > 0, \forall \epsilon > 0, \exists N_2 > 0$, s.t. when $n > N_2, Pr(|\widehat{P_n(t)} - P(t)| > \delta/2) < \epsilon/2$.

Therefore, $\forall \delta > 0, \forall \epsilon > 0$, let $N = \max(N_1, N_2) + 1$. Then,

$$\begin{aligned} Pr(|\widehat{P_n} - P| > \delta) &\leq Pr(|\widetilde{P_n(t)} - P(t)| + |\widehat{P_n(t)} - P(t)| > \delta) \\ &\leq Pr(|\widetilde{P_n(t)} - P(t)| > \delta/2 \cup |\widehat{P_n(t)} - P(t)| > \delta/2) \\ &\leq Pr(|\widetilde{P_n(t)} - P(t)| > \delta/2) + Pr(|\widehat{P_n(t)} - P(t)| > \delta/2) \\ &< \epsilon, \quad \forall n > N. \end{aligned}$$

□

Also, it's easy to observe that $\widetilde{P}_n(t)$ follows a binomial distribution for a given t .

In addition to the comparison, we also implement 5-fold cross-validation to assess the method. We split the data into 5 roughly equal-sized parts. For each part, we train the model on the 4 parts of the data, and calculate the mean integrated squared error (MISE), defined below, using the remaining part.

$$MISE = \mathbb{E} \int_0^t (\widetilde{P}_{0j}(t) - \widehat{P}_{0j}^k(t))^2 dt = \frac{1}{5} \sum_{k=1}^5 \int_0^t (\widetilde{P}_{0j}(t) - \widehat{P}_{0j}^k(t))^2 dt$$

where $\widehat{P}_{0j}^k(t)$ is the estimator calculated by the data without the k th part.

In Figure 3.1, and 3.2, we visualize the comparison of our estimators with the empirical risks. The MISE is 4.35, validating the fit of the method to the simulated data. As we can see for each figure, the empirical risk is approximately centered on the estimated readmission risk and mostly contained within the estimated interval limits. The method is robust for patients with single and multiple readmissions.

3.4 Real Data Analysis

In this section, we evaluate our methods using real data collected for a previous study conducted by researchers at the University of Maryland School of Medicine [7]. We apply our methods on data collected for four cohorts of surgical patients, including organ transplant surgery, general surgery, urology surgery, and pediatric

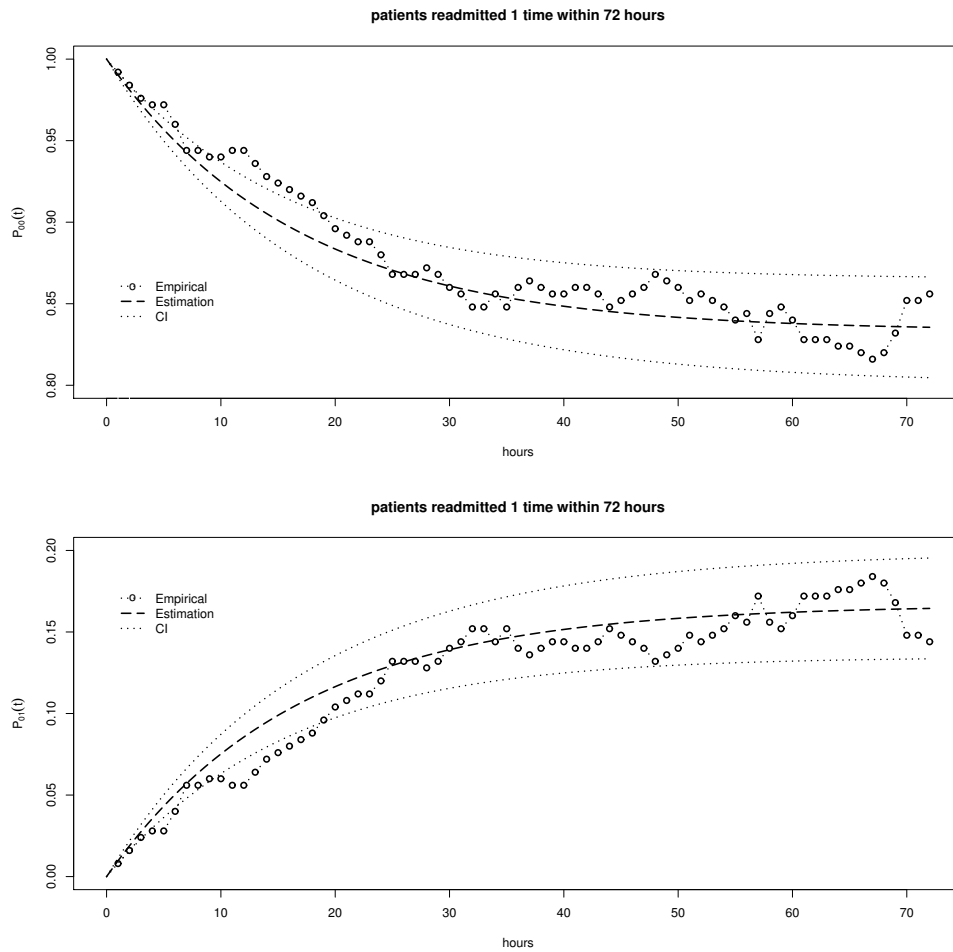


Figure 3.1: Empirical and estimated readmission risks for patients readmitted 1 time within 72 hours.

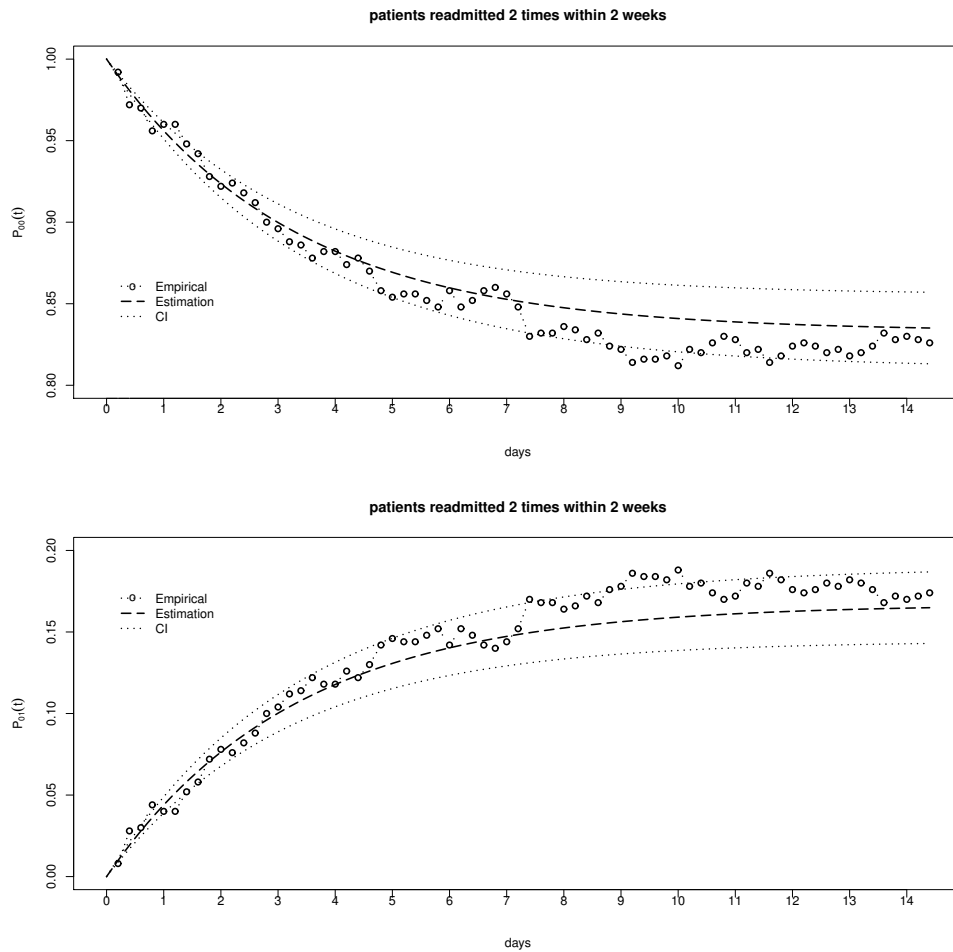


Figure 3.2: Empirical and estimated readmission risks for patients readmitted 2 times within 2 weeks.

brochoscopy. In addition to these four groups, we also analyze all surgical patients, because these patients are occupying critical bed resources longer than others. We show that our method is useful to estimate readmission probabilities across multiple surgical patient cohorts.

In Table 3.1, we summarize the descriptive statistics for each group of patients, including the number of patients and their average stay at the hospital and average time between admission and readmission. The average stay at the hospital ranges from 283 to 429 hours, while average time between admission and readmission ranges from 204 to 450 hours. In Table 3.2, we report the estimates for our two parameters λ_{01} and λ_{10} , and the p-values for the Cramer-Von Mises test [40] for each fitted distribution. As shown in the table, the p-values for each surgical cohort are not statistically significant ($p > 0.05$), thus validating our assumptions about the exponential distribution of times between states and the constant transition rate.

	Organ Transplant	General Surgery	Urology	Pediatric Bronchoscopy	All surgical patients
Number of Patients	57	60	65	25	456
Average length of stay in hospital (hours)	305	283	307	286	370
Average time between hospital stays (hours)	290	204	253	450	222

Table 3.1: Descriptive statistics for different surgical patient cohorts.

	Organ Transplant	General Surgery	Urology	Pediatric Bronchoscopy	Stay over 48 hours
$\hat{\lambda}_{01}$	0.0034	0.0049	0.0039	0.0022	0.0045
P-value ($\hat{\lambda}_{01}$)	0.058	0.1232	0.1510	0.1574	0.0364
$\hat{\lambda}_{10}$	0.0033	0.0035	0.0033	0.0035	0.0027
P-value ($\hat{\lambda}_{10}$)	0.059	0.1438	0.0827	0.0977	0.0143

Table 3.2: Parameter estimates and goodness-of-fit p-values for different surgical patient cohorts.

In Figures 3.3 through 3.7, we visualize our point and interval estimators of readmission risks compared to empirical estimators. As we can see in Figure 3.3,

the curves of the estimation of $P_{00}(t)$ and $P_{01}(t)$ oscillate around the curves of the empirical estimation over time and these curves are contained in the interval estimator nearly all the time. We observe similar patterns for the scenarios visualized in Figures 3.3 through 3.7.

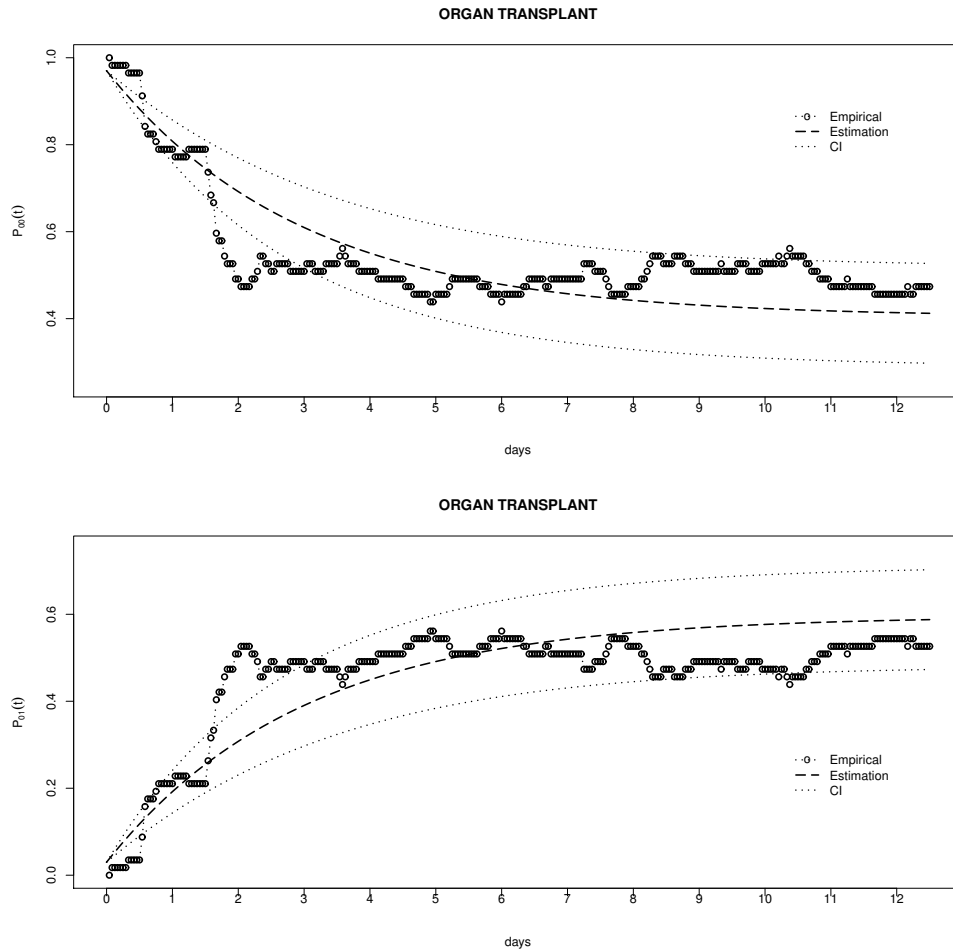


Figure 3.3: Empirical and estimated readmission risks for 57 organ transplant surgery patients.

Due to the sample size consideration, we implement 2-fold cross-validation for all surgical patients. We show the trajectories for p_{01} using different training and test sets in Figure 3.7. Additionally, we also summarize the MISE results for different

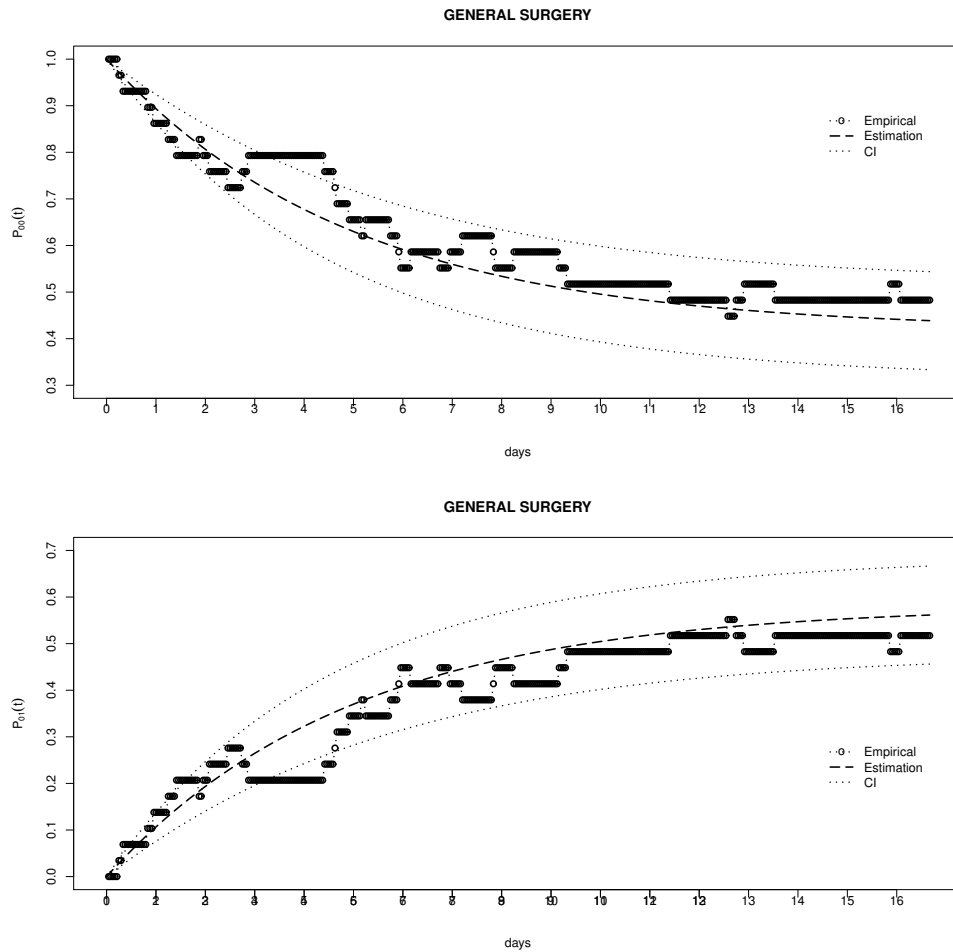


Figure 3.4: Empirical and estimated readmission risks for 60 general surgery patients.

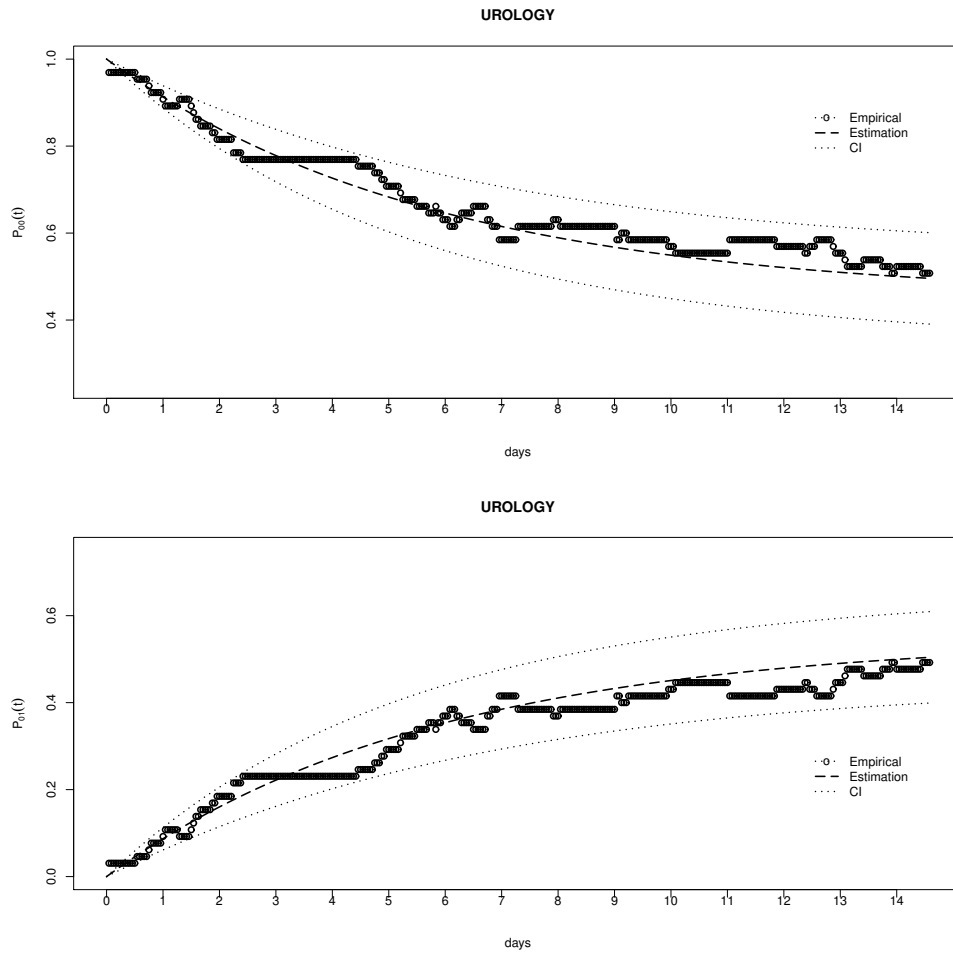


Figure 3.5: Empirical and estimated readmission risks for 65 urology surgery patients.

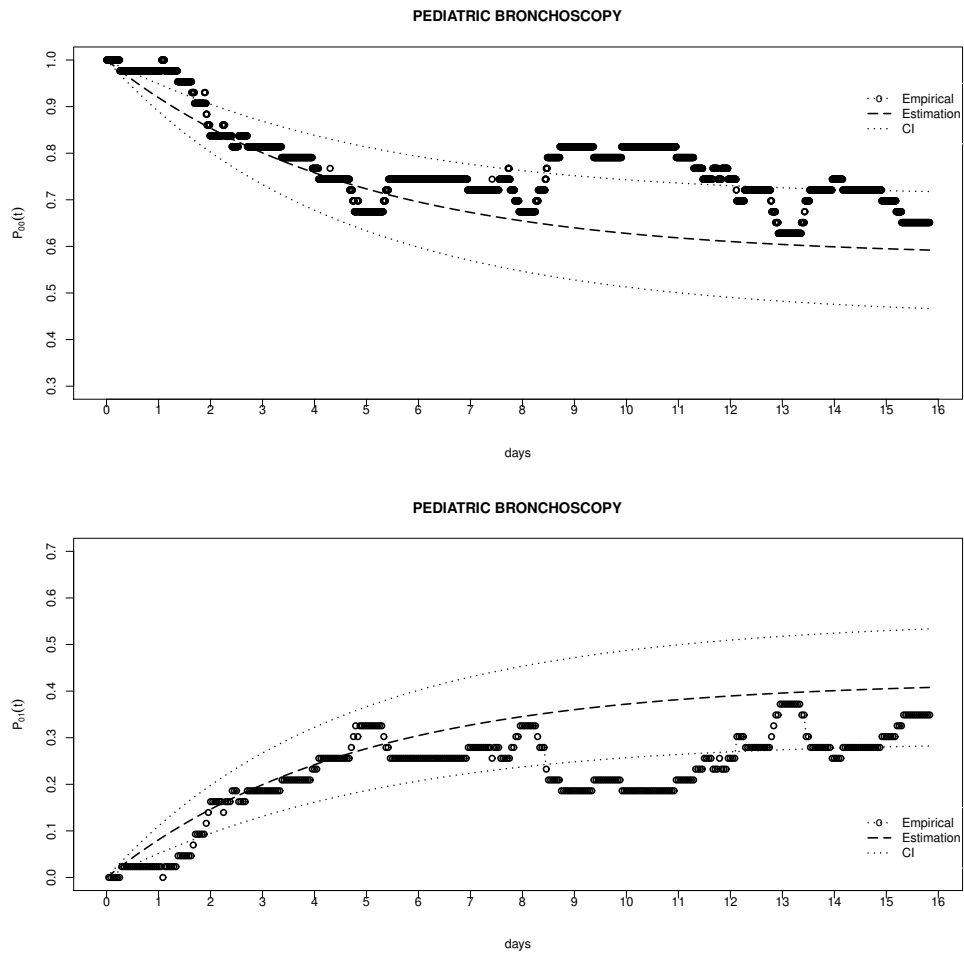


Figure 3.6: Empirical and estimated readmission risks for 25 pediatric bronchoscopy surgery patients.

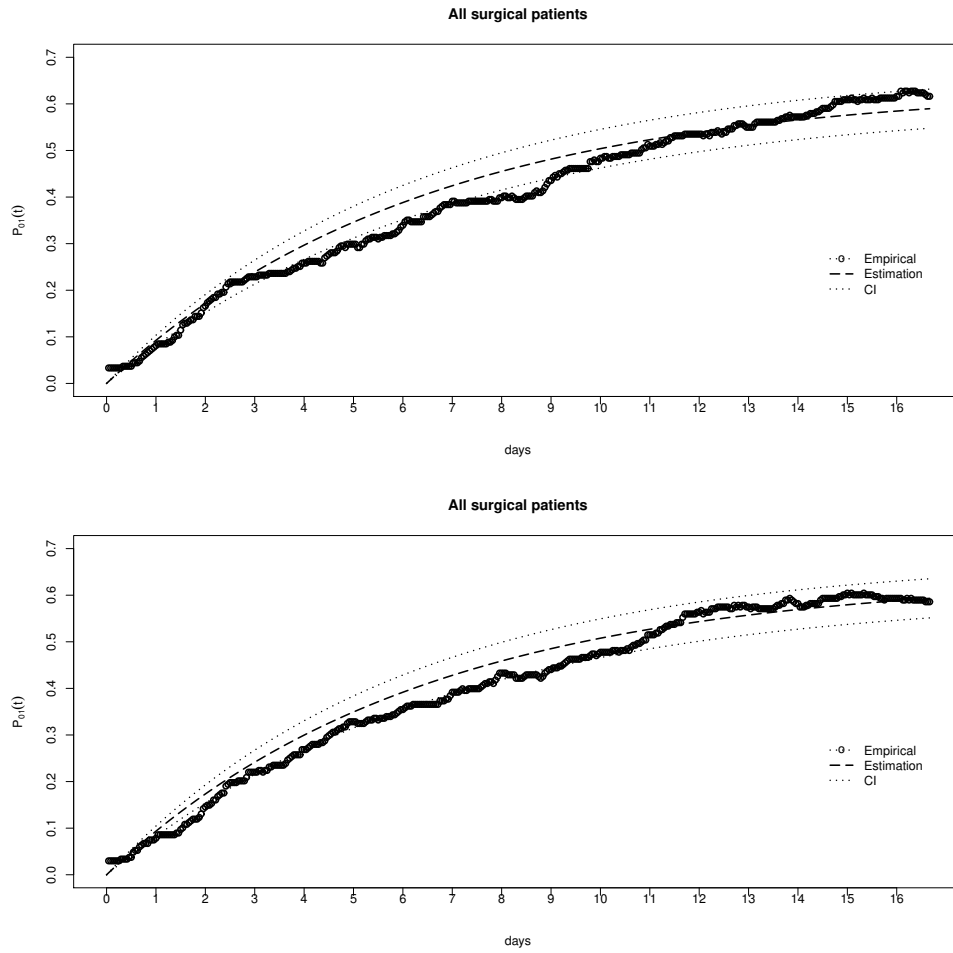


Figure 3.7: Empirical and estimated readmission risks for all 456 surgical patients.

surgical group patients in Table 3.3; this validates the good fit for the transition probabilities.

	Organ Transplant	General Surgery	Urology	Pediatric Bronchoscopy	All surgical patients
MISE	9.77	11.02	6.09	3.58	9.43

Table 3.3: MISE for different surgical patient cohorts.

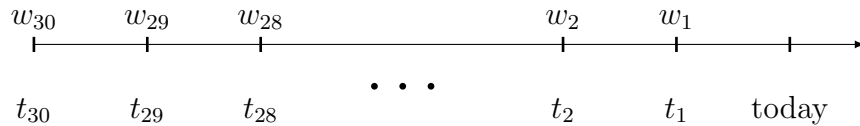
3.5 Discussion

Appropriate modeling of readmission risks can help hospitals make efficient decisions with respect to clinical and operational objectives. However, the performance of individual prediction models for readmission risk has had limited impact to date. In this chapter, we provide a consistent approach that hospitals can use to estimate readmission risks based on limited information. Our approach makes it useful for hospitals to evaluate clinical outcomes or plan for future operations. Our method does not rely on complex data sources that vary from hospital to hospital, but rather the method is easy to implement in a variety of settings as long as discharge and readmission times for patients are accessible. We believe that this study will benefit both high- and low-resource settings to support decision-making for hospitals, particularly for short- and long-term bed planning. For the former, our method could be used as a simple approach prior to the development and implementation of sufficiently accurate individual prediction models. For the latter, our method could provide much needed decision support where the availability of digitized data and analytical expertise are often limited [53].

We model hospital readmission risks using a two-state continuous-time Markov

chain with constant transition rate. Starting from the Kolmogorov backward equations, we developed point and interval estimators for the probability of readmission as a function of time. We demonstrated that our methods to estimate readmission risk performed well for both simulated and real scenarios and that our two-state and constant transition rate assumptions were validated by the latter analysis.

This study could be applied to healthcare practice in the following ways. First, we could use our estimators to monitor the readmission risk trajectory for patients over time. Second, our methods could be used to evaluate the quality of care provided by a particular hospital, by examining both the post-discharge behavior of readmission probability (e.g., does it rise slowly or sharply) as well as the steady-state risk. Third, we could use our model to monitor the expected number of readmitted patients over time, based on the patients that have been recently discharged. For example, we estimate that the expected number of readmitted patients among patients who have been discharged within the previous 30 days is $\sum_{i=1}^{30} w_i P_{01}(t_i)$, where w_i is the number of patients discharged i days ago and t_i is the time period between today and the time when w_i patients were discharged. We illustrate the timeline in the diagram below:



From the continuous-time point of view, if the i^{th} patient is discharged at time t_i , where $i \in \mathbb{Z}^+$ and we assume there are $N_t - n_t + 1$ patients discharged within the previous 30 days, then we observe the following timeline:

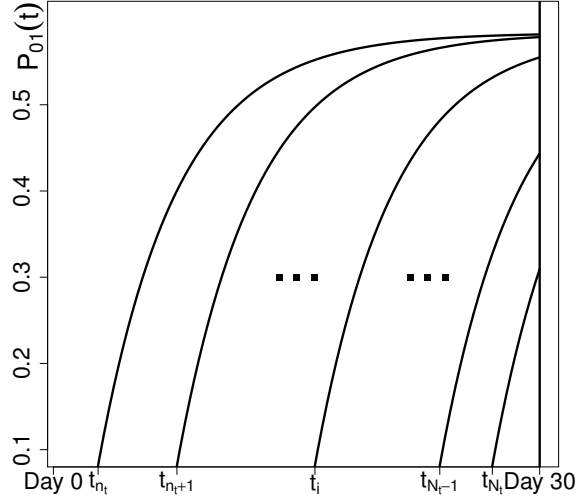
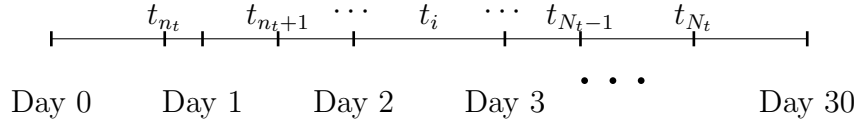


Figure 3.8: Probability trajectories for each patient discharged within 30-day time window.



We visualize the readmission probability trajectories for each patient over a 30-day time window in Figure 3.8.

Let's define $X_i(t) = 1$ if the i^{th} patient will be readmitted at time t , otherwise, $X_i(t) = 0$, namely:

$$X_i(t) = \begin{cases} 1, & \text{with probability } P_{01}(t - t_i), \\ 0, & \text{with probability } 1 - P_{01}(t - t_i), \end{cases}$$

and let $X(t)$ denote the total number of patients who were discharged within the

previous 30 days and readmitted at time t . Then it follows that

$$X(t) = \sum_{i=n_t}^{N_t} X_i$$

and

$$\mathbb{E} X(t) = \sum_{i=n_t}^{N_t} \mathbb{E} X_i(t) = \sum_{i=n_t}^{N_t} P_{01}(t - t_i) \text{ for all } t,$$

where $\forall t, N_t \in Z^+, n_t \in Z^+, t_{N_t} \leq t < t_{N_t+1}, |t - t_{n_t}| \leq 30$ (days) and $|t - t_{n_t-1}| > 30$ (days). Using these definitions, we are able to estimate the expected number of patients readmitted at time t . We demonstrate this idea in a simple simulation, which we visualize in Figure 3.9. In this scenario, we stochastically generate 100 discharge times uniformly throughout the two-month time period, and aggregate the readmission probabilities for patients discharged within the previous 30 days using $\mathbb{E} X(t)$. We observe that the expected number of readmitted patients increases as the time since discharge increases for the included patients (i.e., those discharged within the most 30 days) and as new patients are discharged, and decreases as any included patients are readmitted or as the time since discharge for included patients moves beyond the 30-day window. We assume that each discharged patient will be readmitted with probability of $\lambda_{01}/(\lambda_{01} + \lambda_{10})$, and generate their time until readmission from an exponential distribution with λ_{01} . We also indicate the average value of this time series, which hospitals could use as an estimate for the expected number of readmissions. We can calculate this average estimate by $\frac{1}{t_b - t_a} \sum_{i=1}^{n_t} \int_{t_a}^{t_b} P_{01}(t - t_i) dt$ if we are interested in a specific time period $[t_a, t_b]$. This steady-state value in Fig-

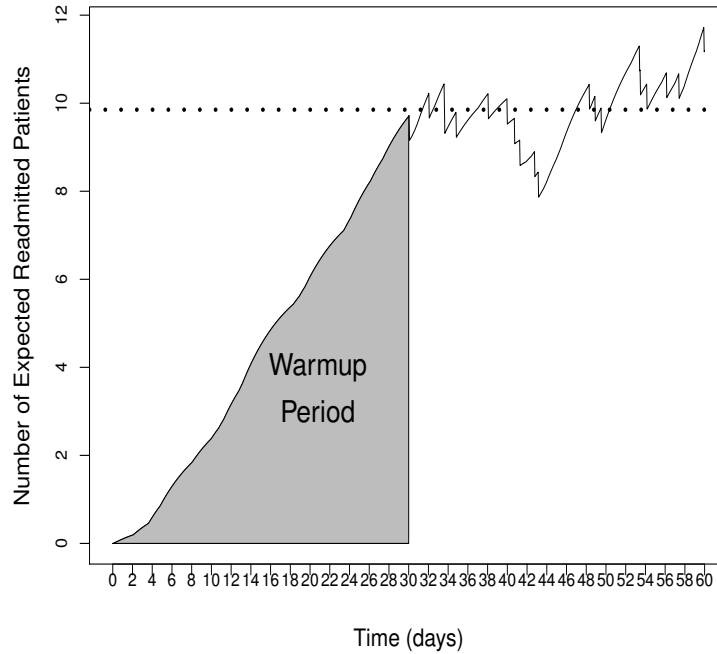


Figure 3.9: Expected number of readmitted patients over time after a 30-day warmup period, assuming 100 uniformly distributed patient discharges and transition rates λ_{01} and λ_{10} equal to 0.0049 and 0.0035, respectively. We also indicate the average of the long-term number of expected readmitted patients in the second month with the dotted line.

Figure 3.9 is approximately 10 patients for the second month. This type of information would be useful for hospitals so that they could anticipate arrivals for readmitted patients and factor this information into their bed management policies.

In future work, our methodology could be extended in the following ways. First, it would involve developing time-dependent transition rates. Although we validate this assumption for surgical cohorts in our sample, it may not work for other patient cohorts. Second, we choose the patient group selected from 2007. It will be beneficial to have recent data analyzed so the model could be updated. The third extension would involve removing the two-state assumption. In Table 3.4, we

estimate the time until readmission and length of stay parameters for patients who are readmitted twice in our surgical cohort samples. The similarity between the first and second sets of estimates supports our use of the two-state and Markovian assumption; therefore, relaxation of this assumption would likely have minimal impact on our results. However, development of such an approach may prove beneficial for other patient samples. These problems are beyond the scope of this chapter and will be interesting topics for future research.

	Organ Transplant	General Surgery	Urology	Pediatric Bronchoscopy	All surgical patients
$\hat{\lambda}_{01}^1$ ^a	0.0035	0.0055	0.0036	0.0027	0.0029
$\hat{\lambda}_{10}^1$ ^b	0.0034	0.0031	0.0032	0.0025	0.0021
$\hat{\lambda}_{01}^2$ ^c	0.0027	0.0041	0.0039	0.002	0.0037
$\hat{\lambda}_{10}^2$ ^d	0.0031	0.0042	0.0035	0.0036	0.0029

^a Time to first readmission after initial discharge

^b Time to second discharge after first readmission

^c Time to second readmission after second discharge

^d Time to third discharge after second readmission

Table 3.4: Parameter estimates of different time periods for five surgical patient cohorts.

Chapter 4: Decreasing Trend of Hospital Emergency Department Access Observed in Maryland Region III from 2016 to 2018

4.1 Introduction

Hospital emergency department (ED) services play an important role in the healthcare system for critically ill patients and urgent unplanned conditions. Thus, efforts to improve the efficiency of ED services are critical [82, 88]. Access to ED services is one important indicator of the efficiency at which a hospital is operating, which not only includes the ED but also inpatient services [6, 27, 118]. In this study, we utilize data collected in Maryland Region III on the frequency and duration of ED alert status to study such accessibility changes over the past three years.

In the literature, several studies have analyzed changes in ED utilization, but it usually contains broader regions such as the whole nation and typically investigated a relatively older time period [28, 47, 121]. To our best knowledge, none of the studies specifically evaluated such a critical health care issue in Maryland locally. In this chapter, we try to fill this gap and focus on analyzing the accessibility and efficiency of ED services in Maryland for the most recent (and complete) three years (2016-2018), specifically, in Region III. Region III in Maryland contains five counties

(Anne Arundel, Baltimore, Carroll, Harford, and Howard) and Baltimore city, and is the most populous region in the state. In this study, we enrolled 21 hospitals in this region, including Anne Arundel Medical Center, Baltimore Washington Medical Center, Bon Secours Hospital, Carroll Hospital Center, Franklin Square Hospital, Good Samaritan Hospital, Greater Baltimore Medical Center, Harbor Hospital, Harford Memorial Hospital, Howard County General Hospital, Johns Hopkins Hospital (JH), Johns Hopkins Bayview Hospital (JH Bayview), Mercy Medical Center, Northwest Hospital Center, Sinai Hospital, Saint Agnes Hospital (St. Agnes), Saint Josephs Hospital (St. Joseph), Union Memorial Hospital, University of Maryland Medical Center (UMMC), University of Maryland Medical Center Midtown (Midtown), and Upper Chesapeake Medical Center [1]. We develop statistical tools to estimate and examine the changes in ED accessibility over time using data collected by the state of Maryland on the alert status of each hospital’s ED. By analyzing the frequency and duration of yellow, red, and reroute alerts, we provide an assessment of the overall trends related to ED accessibility in Region III hospitals from 2016 to 2018.

The remaining sections of this chapter are organized as follows. In Section 4.2, we formulate our problem and describe the data we use in this study. We describe our methods for comparing changes in the duration of alerts for the last three years. In Section 4.3, we present the descriptive statistics for the duration of alerts, significant changes over the three years, and the patterns of those significant changes. In Section 4.4, we discuss several future research directions. Finally, we conclude with a discussion of our results in Section 4.5.

4.2 Data and Methods

4.2.1 Data Source and Management of Emergency Department Resource Availability

Provided by the Maryland Institute for Emergency Medical Services Systems (MIEMSS), the County/Hospital Alert Tracking System (CHATS) generates real-time and historical data about the timing (i.e., start and end date and time) of yellow, red, and reroute alerts for each hospital in the state [2]. The system is updated every 60 seconds and enables the EDs to provide notice to surrounding hospitals and EMS providers about their operational status and thus control incoming patient demand. The event of high ED utilization or unavailability of monitored beds may result in a hospital activating an alert status. Specifically, a yellow alert is initiated when the ED is experiencing a high level of crowding such that patients with urgent needs (e.g., emergency severity index level 2 and 3 patients) are not being managed safely. In such cases, the ED will temporarily request that no new patients in need of urgent medical care can be received, and they should go to other EDs around. When the hospital does not have any available electrocardiogram-monitored beds, the ED will activate its red alert status. Reroute alerts are activated when an Advanced Life Support (ALS)/Basic Life Support (BLS) unit is being held in the ED of a hospital because of the lack of an available bed.

4.2.2 Study Population

We specifically focus on the data collected from 21 EDs in Maryland Region III in 2016, 2017, and 2018 in the database. The Region III area in Maryland includes Baltimore City and Anne Arundel, Baltimore, Carroll, Harford, and Howard counties.

4.2.3 Statistical Methods and Data Analysis

In order to investigate the changes in the levels of access for the 21 EDs over the last three years, we study trends related to the frequency and duration of each type of alert. We calculate descriptive statistics for the time between alerts and the duration of alerts for each of the 21 hospital EDs. Kruskal-Wallis test [85] is used to check for any significant statistical differences in these measures over the most recent (and complete) three years. We tried the exponential, Weibull, and log-logistic distributions to model the durations of these alerts, and validated the distribution fitting using the Cramer-von Mises test to identify the most appropriate model fitting.

Specifically, for each hospital, we analyze the duration of time between alerts, for example, the duration of yellow, red, and reroute alerts. We are also interested in each hospital's alert-free period, which represents the hospital ED's high efficiency and accessibility. We define the alert-free period as the time from the end of any alert to the beginning of the next alert, which we illustrate in the diagram below:

yellow respectively. Then our alert-free period denoted by U will be $\min(X, Y, Z)$. We fit X , Y , and Z using exponential and Weibull distributions and compare the fits using criteria of Akaike information criterion (AIC) and Bayesian information criterion (BIC) [3, 124]. To estimate parameters in the models of X , Y , and Z , we need to write the log likelihood function as:

$$\log L = \sum_{j=1}^n \sum_{i=1}^3 \log [f_i(t_j)]^{\delta_i(t_j)} [S_i(t_j)]^{1-\delta_i(t_j)}$$

where the alert status indicator is defined as

$$\delta_i(t_j) = \begin{cases} 1 & \text{if alert } i \text{ occurs at time } t_j \\ 0 & \text{otherwise,} \end{cases}$$

n is the number of alert-free periods, and $f_i(t_j)$ and $S_i(t_j)$ are density and survival functions for X , Y , and Z . Here the index i is from 1 to 3 representing Red, ReRoute, and Yellow Alerts. We estimate parameters in exponential and Weibull distributions by maximizing this log likelihood function. When assuming exponential, the estimated parameters are $\lambda_i = \frac{\sum_{j=1}^{n_h} \delta_i(t_j)}{\sum_{j=1}^{n_h} t_j}$. When using Weibull, we maximize the log likelihood function numerically. Modeling of U becomes a competing risk model among the events of red, reroute, and yellow alert signals.

4.3 Results and Findings

In Tables 4.1, 4.2, 4.3, and 4.4, we present descriptive statistics including the number of alerts, total hospital-wise alert duration, and median and interquartile range (IQR) for the alert-free periods, Red Alert duration, ReRoute Alert duration, and Yellow Alert duration, respectively for all 21 hospitals in Maryland Region III from 2016 to 2018.

As shown in Table 4.1, the total number of alerts ranges from 57 (Harford Hospital) to 352 (Baltimore Washington) in 2016, from 28 (Harford Hospital) to 415 (St. Agnes) in 2017, and from 94 (Harford Hospital) to 480 (St. Agnes) in 2018. From 2016 to 2018, the number of alerts strictly increased in eight hospitals (Bon Secours, Howard, John Hopkins, JH Bayview, Sinai, St. Agnes, St. Joseph, and Upper Chesapeake), while two hospitals (Good Samaritan and Greater Baltimore) are observed to have decreased total number of alerts from year to year. The median duration of alert-free periods ranges from 11.33 hours (Baltimore Washington) to 69.11 hours (Carroll Hospital) in 2016, from 10.57 hours (St. Agnes) to 137 hours (Harford Hospital) in 2017, and from 8.21 hours (St. Agnes) to 47 hours (Harford Hospital) in 2018. The median duration of alert-free periods becomes shorter and shorter from 2016 to 2018 for seven hospitals (Bon Secours, Carroll, Good Samaritan, Howard, Sinai, St. Agnes, and UMMC). Only Union Memorial Hospital is observed with an increased median alert-free duration year by year from 2016 to 2018.

The number of red alerts ranges from 1 (Mercy Medical) to 105 (Union memorial) in 2016, from 2 (Baltimore Washington) to 115 (St. Agnes) in 2017, and from

Hospitals	Variables	Year 2016	Year 2017	Year 2018	P-values
Anne Arundel	Total Number of Alerts	287	223	281	0.0091
	Hours of Alert-free Period*	12.68 (25.99)	19.1 (40.35)	12.65 (29.68)	
Baltimore Washington	Total Number of Alerts	352	284	363	0.4353
	Hours of Alert-free Period*	11.33 (22.13)	13.27 (30.42)	10.98 (20.8)	
Bon Secours	Total Number of Alerts	86	96	191	< 0.0001
	Hours of Alert-free Period*	50.82 (136.58)	35.81 (128.13)	18.03 (41.08)	
Carroll Hospital	Total Number of Alerts	74	117	95	< 0.0001
	Hours of Alert-free Period*	693.11 (93.31)	28.62 (59.42)	21.07 (36.4)	
Franklin Square	Total Number of Alerts	281	81	180	< 0.0001
	Hours of Alert-free Period*	13.32 (9.28)	37.32 (114.37)	21.79 (36.4)	
Good Samaritan	Total Number of Alerts	206	172	152	0.0605
	Hours of Alert-free Period*	17.91 (29.45)	18.58 (47.33)	23.4 (48.06)	
Greater Baltimore	Total Number of Alerts	182	173	155	0.9635
	Hours of Alert-free Period*	21.78 (42.12)	21.38 (37.23)	23.23 (48.7)	
Harbor Hospital	Total Number of Alerts	247	184	298	0.0085
	Hours of Alert-free Period*	16.42 (35.37)	18.13 (65.28)	13.83 (26.11)	
Harford Hospital	Total Number of Alerts	57	28	94	0.0042
	Hours of Alert-free Period*	44.12 (109.82)	137 (353.14)	47 (116.6)	
Howard County	Total Number of Alerts	93	109	141	0.175
	Hours of Alert-free Period*	43.08 (86.38)	41.85 (80)	34.3 (59.32)	
Johns Hopkins	Total Number of Alerts	181	202	211	0.0002
	Hours of Alert-free Period*	16.85 (32.4)	15.3 (24.9)	12.62 (16.78)	
JH Bayview	Total Number of Alerts	320	336	344	0.2454
	Hours of Alert-free Period*	11.76 (14.68)	13.82 (13.68)	13.13 (12.75)	
Mercy Medical	Total Number of Alerts	210	193	207	0.8712
	Hours of Alert-free Period*	20.06 (32.18)	20.48 (33.77)	19.45 (32.13)	
Midtown	Total Number of Alerts	248	220	405	0.1761
	Hours of Alert-free Period*	13.49 (32.07)	19.05 (32.02)	8.35 (13.07)	
Northwest	Total Number of Alerts	175	153	163	0.8569
	Hours of Alert-free Period*	22.37 (53.89)	23.85 (53.97)	22.4 (56.93)	
Sinai Hospital	Total Number of Alerts	289	302	344	< 0.0001
	Hours of Alert-free Period*	15.18 (21.42)	14.92 (18.71)	9.13 (14.71)	
St. Agnes	Total Number of Alerts	301	415	480	< 0.0001
	Hours of Alert-free Period*	14.9 (25.88)	10.57 (14.075)	8.21 (12.14)	
St. Joseph	Total Number of Alerts	185	262	249	0.1853
	Hours of Alert-free Period*	18.62 (35.7)	15.39 (26.38)	16.57 (28.22)	
UMMC	Total Number of Alerts	289	364	353	< 0.0001
	Hours of Alert-free Period*	15.5 (17.53)	13.15 (13.3)	10.37 (10.95)	
Union Memorial	Total Number of Alerts	227	189	193	0.1324
	Hours of Alert-free Period*	15.38 (30.37)	20.5 (40.92)	21.02 (38)	
Upper Chesapeake	Total Number of Alerts	165	167	247	0.0005
	Hours of Alert-free Period*	25.55 (58.85)	37.25 (59.5)	17.75 (30.44)	

* reports the corresponding median hours of all alert-free periods, in parentheses are the interquartile ranges (IQRs).

Table 4.1: Descriptive statistics for total alert, including any kind of alert, in each hospital and each year.

1 (Franklin square) to 150 (Sinai Hospital) in 2018. In particular, Howard County hospital had no red alerts in 2017 and Mercy Medical had no red alerts in 2017 and 2018. Among the 21 hospitals in Maryland Region III, only Mercy Medical hospital and Union Memorial hospital had decreased total durations of red alerts from 2016 to 2018. Most of the other hospitals experienced some increased trend of the total durations of red alerts, and 10 hospitals (Carroll, Good Samaritan, Greater Baltimore, Johns Hopkins, Midtown, Northwest, Sinai, St. Agnes, St. Joseph, and UMMC) had strictly increasing total red-alert durations year by year, which indicates that over the years, the hospital's total red-alert duration becomes longer and longer. For the past three years, five hospitals (Franklin Square, Harbor, Harford, Howard, and Mercy Medical) had a fairly small amount of red alerts. However, eight hospitals (Greater Baltimore, John Hopkins, JH Bayview, Midtown, Sinai, St. Agnes, UMMC, and Union Memorial) experienced a relatively large number of red alerts. With regard to the median duration of red alerts, it ranges from 0.22 hours (Mercy Medical) to 20.06 hours (Good Samaritan) in 2016, from 2.51 hours (Baltimore Washington) to 21.49 hours (John Hopkins) in 2017, and from 2.36 hours (Franklin Square) to 31.72 hours (Carroll Hospital) in 2018. From 2016 to 2018, four hospitals (Bon Secours, Northwest, UMMC, and Upper Chesapeake) were observed to have longer and longer median durations of red alerts over the years and only two hospitals (Greater Baltimore and St. Agnes) did a great job to control their red alert durations well, such that the median durations of red alerts becomes shorter over the three years, however not statistically significant.

In Table 4.3, the number of reroute alerts ranges from 4 (Union Memorial)

to 289 (Baltimore Washington) in 2016, from 1 (Carroll) to 236 (St. Agnes) in 2017, and from 11 (Union Memorial) to 295 (Baltimore Washington) in 2018. Six hospitals (Bon Secours, Howard, Northwest, Sinai, St. Joseph and Union Memorial) have the number of reroute alerts increasing and only Midtown was having a smaller and smaller number of reroute alerts across the last three years. We notice that the median duration of reroute alert for most hospitals oscillates around one hour.

In Table 4.4, the number of yellow alert ranges from 35 (Bon Secours and Harford) to 273 (Franklin Square) in 2016, from 14 (Bon Secours and Harford) to 280 (JH Bayview) in 2017, and from 66 (Harford) to 313 (Midtown) in 2018. We notice that at five hospitals (John Hopkins, Sinai, St. Agnes, UMMC, and Upper Chesapeake) both the number of alerts and the total alert durations have increased over the years, while two hospitals (Good Samaritan and Northwest) have a decreasing trend. We further compare the duration of each yellow alert from year to year. The median duration of yellow alerts ranges from 3.05 hours (Sinai) to 12.71 hours (John Hopkins) in 2016, from 2.44 hours (Harford) to 11.96 hours (John Hopkins) in 2017, and from 3.19 hours (Franklin Square) to 14.98 hours (John Hopkins) in 2018. The median duration of yellow alerts for five hospitals (Carroll, Midtown, Northwest, Sinai, and UMMC) were statistically significantly increasing over the three years, while at two hospitals (Greater Baltimore and Union Memorial) they were significantly decreasing.

Hospitals	Variables	Year 2016	Year 2017	Year 2018	P-values
Anne Arundel	Total Number of Alerts	21	12	23	0.2355
	Total Alert Duration	214.1	80.4	224.13	
	Hours of Each Alert*	7.52 (10.11)	4.87 (3.55)	7.23 (9.46)	
Baltimore Washington	Total Number of Alerts	7	2	34	0.0201
	Total Alert Duration	34.14	5.02	313.35	
	Hours of Each Alert*	4.48 (3.3)	2.51 (1.42)	7.35 (7.23)	
Bon Secours	Total Number of Alerts	17	4	14	0.0502
	Total Alert Duration	120.97	36.55	365.51	
	Hours of Each Alert*	5.06 (5.16)	8.01 (6.16)	10.93 (7.81)	
Carrol Hospital	Total Number of Alerts	8	30	68	0.0022
	Total Alert Duration	121.45	518.22	2736.6	
	Hours of Each Alert*	9.43 (8.91)	13.43 (14.68)	31.72 (46.53)	
Franklin Square	Total Number of Alerts	2	3	1	0.3041
	Total Alert Duration	15.95	33.8	2.36	
	Hours of Each Alert*	7.98 (0.085)	8.31 (8.71)	2.36 (0)	
Good Samaritan	Total Number of Alerts	37	56	56	0.1882
	Total Alert Duration	939.15	1111.42	1337.11	
	Hours of Each Alert*	20.06 (19.47)	15.51 (17.44)	17.34 (14.48)	
Greater Baltimore	Total Number of Alerts	53	52	65	0.2912
	Total Alert Duration	939.15	1111.42	1337.11	
	Hours of Each Alert*	12.16 (14.02)	10.89 (11.07)	9.9 (13.25)	
Harbor Hospital	Total Number of Alerts	2	2	11	0.1762
	Total Alert Duration	37.72	9.06	80.35	
	Hours of Each Alert*	18.86 (8.76)	4.53 (0.84)	7.89 (5.87)	
Harford Hospital	Total Number of Alerts	3	2	7	0.2106
	Total Alert Duration	48.53	5.85	83.17	
	Hours of Each Alert*	12.82 (13.53)	2.93 (1.95)	6.44 (1.35)	
Howard County	Total Number of Alerts	2	0	7	0.5582
	Total Alert Duration	11.31	0	39.13	
	Hours of Each Alert*	5.66 (0.62)	NA	4.81 (5.12)	
Johns Hopkins	Total Number of Alerts	48	58	95	0.0557
	Total Alert Duration	1047.27	1396.87	1934.54	
	Hours of Each Alert*	18.16 (12.48)	21.49 (18.29)	14.85 (16.63)	
JH Bayview	Total Number of Alerts	55	47	57	0.5313
	Total Alert Duration	373.81	260.81	385.07	
	Hours of Each Alert*	4.85 (6.47)	4.15 (4.89)	5.69 (5.38)	
Mercy Medical	Total Number of Alerts	1	0	0	NA
	Total Alert Duration	0.22	0	0	
	Hours of Each Alert*	0.22 (0)	NA	NA	
Midtown	Total Number of Alerts	85	81	167	0.3127
	Total Alert Duration	883.04	1049.08	2178.46	
	Hours of Each Alert*	7.44 (10.99)	9.61 (13.24)	8.66 (11.325)	
Northwest	Total Number of Alerts	6	15	26	0.3686
	Total Alert Duration	77.72	209.39	516.65	
	Hours of Each Alert*	9.24 (6.26)	15.04 (11.54)	15.5 (17.99)	
Sinai Hospital	Total Number of Alerts	61	73	150	0.0665
	Total Alert Duration	699.76	1317.99	2256.48	
	Hours of Each Alert*	8.27 (10.55)	12.16 (16.9)	10.44 (11.98)	
St. Agnes	Total Number of Alerts	67	115	148	0.157
	Total Alert Duration	886.3	1555.83	1598.37	
	Hours of Each Alert*	11.61	10.68 (10.82)	9.83 (7.25)	
St. Joseph	Total Number of Alerts	26	23	48	0.5014
	Total Alert Duration	255.7	289.24	475.32	
	Hours of Each Alert*	7.29 (5.93)	10.75 (11.84)	7.75 (8.67)	
UMMC	Total Number of Alerts	53	89	113	0.5382
	Total Alert Duration	341.77	577.44	777.13	
	Hours of Each Alert*	4.72 (4.59)	5.55 (5.33)	5.98 (5.44)	
Union Memorial	Total Number of Alerts	105	106	75	0.5938
	Total Alert Duration	1921.74	1507.97	1049.85	
	Hours of Each Alert*	11.63 (11.91)	11.32 (13.31)	11.96 (11.57)	
Upper Chesapeake	Total Number of Alerts	18	5	21	0.5415
	Total Alert Duration	346	93.57	407.79	
	Hours of Each Alert*	11.62 (8.83)	11.88 (11.49)	16.45 (9.54)	

* reports the corresponding median hours of all alert durations, in parentheses are the interquartile ranges (IQRs).

Table 4.2: Descriptive statistics for red alert in each hospital and each year.

Hospitals	Variables	Year 2016	Year 2017	Year 2018	P-values
Anne Arundel	Total Number of Alerts	254	214	287	0.0061
	Total Alert Duration	375.92	309.57	551.11	
	Hours of Each Alert*	1.32 (1.12)	1.31 (1.26)	1.57 (1.75)	
Baltimore Washington	Total Number of Alerts	289	216	295	0.1696
	Total Alert Duration	425.39	281.04	414.11	
	Hours of Each Alert*	1.3 (1.08)	1.18 (0.94)	1.21 (1.09)	
Bon Secours	Total Number of Alerts	51	88	118	0.0223
	Total Alert Duration	52.36	100.05	160.99	
	Hours of Each Alert*	0.83 (0.52)	0.89 (0.72)	1.15 (0.97)	
Carrol Hospital	Total Number of Alerts	NA	1	NA	NA
	Total Alert Duration	0	1.6	0	
	Hours of Each Alert*	NA	1.6 (0)	NA	
Franklin Square	Total Number of Alerts	74	44	63	0.285
	Total Alert Duration	82.6	43.55	71.06	
	Hours of Each Alert*	1.03 (0.64)	0.81 (0.73)	1.03 (0.72)	
Good Samaritan	Total Number of Alerts	27	23	34	0.2008
	Total Alert Duration	30.2	24.72	40.33	
	Hours of Each Alert*	0.61 (0.83)	1.04 (0.59)	1.01 (0.79)	
Greater Baltimore	Total Number of Alerts	16	15	24	0.5369
	Total Alert Duration	30.2	24.72	40.33	
	Hours of Each Alert*	0.81 (0.36)	0.97 (1.11)	1 (0.68)	
Harbor Hospital	Total Number of Alerts	179	150	249	0.0051
	Total Alert Duration	196.14	174.22	329.26	
	Hours of Each Alert*	0.96 (0.81)	0.95 (0.82)	1.11 (0.9)	
Harford Hospital	Total Number of Alerts	29	20	59	0.6458
	Total Alert Duration	28.01	18.43	50.8	
	Hours of Each Alert*	0.95 (0.65)	0.72 (0.87)	0.63 (0.88)	
Howard County	Total Number of Alerts	8	18	62	0.0172
	Total Alert Duration	11.94	26.6	127.13	
	Hours of Each Alert*	1.08 (1.48)	0.99 (1.06)	1.66 (1.32)	
Johns Hopkins	Total Number of Alerts	36	55	40	0.6008
	Total Alert Duration	46.66	66.77	56.68	
	Hours of Each Alert*	1.06 (1.09)	1.06 (0.65)	1.17 (1.14)	
JH Bayview	Total Number of Alerts	147	133	145	0.7447
	Total Alert Duration	174.01	159.29	167.19	
	Hours of Each Alert*	1 (0.76)	1.03 (0.74)	1.04 (0.71)	
Mercy Medical	Total Number of Alerts	45	54	50	0.5658
	Total Alert Duration	62.02	74.72	65.02	
	Hours of Each Alert*	0.78 (1.08)	0.94 (1.21)	0.86 (0.84)	
Midtown	Total Number of Alerts	86	80	75	0.4453
	Total Alert Duration	93.63	101.84	78.44	
	Hours of Each Alert*	0.85 (0.74)	0.97 (0.99)	0.92 (0.65)	
Northwest	Total Number of Alerts	43	47	67	0.253
	Total Alert Duration	41.15	48.56	78.22	
	Hours of Each Alert*	0.86 (0.68)	0.93 (0.68)	1.07 (0.79)	
Sinai Hospital	Total Number of Alerts	45	62	65	0.0001
	Total Alert Duration	27.14	69.4	78.58	
	Hours of Each Alert*	0.52 (0.53)	0.98 (0.83)	0.82 (0.94)	
St. Agnes	Total Number of Alerts	176	236	182	0.0406
	Total Alert Duration	191.92	277.58	222.81	
	Hours of Each Alert*	0.93 (0.625)	1.05 (0.77)	1.11 (0.88)	
St. Joseph	Total Number of Alerts	66	73	100	0.705
	Total Alert Duration	67.6	82.05	116.45	
	Hours of Each Alert*	0.95 (0.66)	0.97 (0.74)	0.92 (0.85)	
UMMC	Total Number of Alerts	100	170	151	0.0041
	Total Alert Duration	131.27	197.62	271.94	
	Hours of Each Alert*	0.94 (0.68)	0.93 (0.79)	1.18 (1.13)	
Union Memorial	Total Number of Alerts	4	5	11	0.1512
	Total Alert Duration	4.17	3.79	20.8	
	Hours of Each Alert*	0.58 (1.57)	0.44 (0.51)	1.34 (0.99)	
Upper Chesapeake	Total Number of Alerts	143	119	213	0.006
	Total Alert Duration	129.16	128.92	236.6	
	Hours of Each Alert*	0.67 (0.65)	0.9 (0.89)	0.97 (0.93)	

* reports the corresponding median hours of all alert durations, in parentheses are the interquartile ranges (IQRs).

Table 4.3: Descriptive statistics for reroute alert in each hospital and each year.

Hospitals	Variables	Year 2016	Year 2017	Year 2018	P-values
Anne Arundel	Total Number of Alerts	155	43	82	0.2953
	Total Alert Duration	1588.46	338.06	712	
	Hours of Each Alert*	6.89 (8.795)	5.49 (5.68)	6.89 (6.54)	
Baltimore Washington	Total Number of Alerts	144	117	146	0.0605
	Total Alert Duration	947.6	647.82	961.92	
	Hours of Each Alert*	5.84 (4.86)	4.55 (4.13)	5.92 (4.6)	
Bon Secours	Total Number of Alerts	35	14	97	0.9825
	Total Alert Duration	149.36	64.23	425.85	
	Hours of Each Alert*	3.86 (2.54)	5.09 (5.06)	3.92 (3.08)	
Carrol Hospital	Total Number of Alerts	73	111	102	< 0.0001
	Total Alert Duration	570.86	1200.06	1593.07	
	Hours of Each Alert*	6.68 (5.19)	9.94 (7.66)	11.16 (12.3)	
Franklin Square	Total Number of Alerts	273	56	162	0.0001
	Total Alert Duration	3945.31	309.41	822.74	
	Hours of Each Alert*	10.54 (10.02)	2.47 (6.49)	3.19 (3.05)	
Good Samaritan	Total Number of Alerts	185	140	110	0.2008
	Total Alert Duration	1496.42	1111.46	946.89	
	Hours of Each Alert*	6.32 (5.38)	6.09 (6.13)	7.96 (6.9)	
Greater Baltimore	Total Number of Alerts	167	136	96	0.0013
	Total Alert Duration	1496.42	1111.46	946.89	
	Hours of Each Alert*	7.64 (7.55)	7.48 (7.59)	5.63 (4.25)	
Harbor Hospital	Total Number of Alerts	155	71	128	0.2311
	Total Alert Duration	685.29	291.04	610.19	
	Hours of Each Alert*	3.67 (3.58)	3.27 (3.58)	4.14 (4.08)	
Harford Hospital	Total Number of Alerts	35	14	66	0.0002
	Total Alert Duration	128.37	40.06	357.23	
	Hours of Each Alert*	3.07 (2.46)	2.44 (2.39)	5.04 (4.17)	
Howard County	Total Number of Alerts	90	102	104	< 0.0001
	Total Alert Duration	851.4	512.87	558.94	
	Hours of Each Alert*	7.89 (7.12)	3.58 (4.64)	3.82 (3.72)	
Johns Hopkins	Total Number of Alerts	176	188	199	0.0085
	Total Alert Duration	2938.75	3022.04	4231.27	
	Hours of Each Alert*	12.71 (10.63)	11.96 (12.34)	14.98 (20.46)	
JH Bayview	Total Number of Alerts	270	280	269	0.0506
	Total Alert Duration	2872	2328.71	2488.66	
	Hours of Each Alert*	9.03 (10.04)	7.16 (7.35)	8.1 (7.85)	
Mercy Medical	Total Number of Alerts	186	166	179	0.0172
	Total Alert Duration	1221.96	967.93	1440.2	
	Hours of Each Alert*	5.32 (5.41)	4.66 (5.25)	6.27 (6.49)	
Midtown	Total Number of Alerts	145	106	313	< 0.0001
	Total Alert Duration	636.59	574.31	2087.34	
	Hours of Each Alert*	3.23 (3.71)	4.69 (5.54)	5.36 (5.99)	
Northwest	Total Number of Alerts	148	127	103	0.0428
	Total Alert Duration	746.87	729.03	718.73	
	Hours of Each Alert*	4.37 (5.44)	4.71 (4.11)	5.62 (6.62)	
Sinai Hospital	Total Number of Alerts	238	253	295	< 0.0001
	Total Alert Duration	1162.11	1324.14	2315.62	
	Hours of Each Alert*	3.05 (4.97)	3.25 (3.53)	5.5 (6.99)	
St. Agnes	Total Number of Alerts	188	284	385	0.0136
	Total Alert Duration	1026.79	1354.1	2176.41	
	Hours of Each Alert*	4.69 (4.36)	4.06 (4.23)	4.74 (4.63)	
St. Joseph	Total Number of Alerts	148	218	187	0.0015
	Total Alert Duration	1473.93	1647.4	1492.87	
	Hours of Each Alert*	7.85 (8.49)	5.89 (6.98)	6.09 (6.49)	
UMMC	Total Number of Alerts	220	229	254	< 0.0001
	Total Alert Duration	2032.88	2216.97	3388.78	
	Hours of Each Alert*	8.25 (7.61)	9.12 (6.95)	11.78 (7.44)	
Union Memorial	Total Number of Alerts	190	138	157	0.0199
	Total Alert Duration	1470.35	952.13	886.9	
	Hours of Each Alert*	5.33 (5.95)	5.03 (4.79)	4.28 (5.05)	
Upper Chesapeake	Total Number of Alerts	77	100	156	< 0.0001
	Total Alert Duration	515.8	649.02	1476.82	
	Hours of Each Alert*	5.74 (5.88)	5.24 (5.12)	8.02 (6.98)	

* reports the corresponding median hours of all alert durations, in parentheses are the interquartile ranges (IQRs).

Table 4.4: Descriptive statistics for yellow alert in each hospital and each year.

Although we have observed some significant overall change trends over the three years in Tables 4.1-4.4, we further employed Kruskal-Wallis test in order to evaluate any statistically significant differences between any two years. We chose Kruskal-Wallis test, such a nonparametric test, instead of traditional methods such as t-tests with normality assumptions, because our preliminary exploration shows that the empirical distributions of alert-free period or any alert duration are all skewed. We summarize the pair-wise comparison test results for those hospitals that have any significant differences in Table 4.5 for alert-free period, Table 4.6 for red alert duration, Table 4.7 for reroute alert duration, and Table 4.8 for yellow alert duration. P-values smaller than 0.05 reject the null hypothesis and suggest that the changes are significantly different. In Table 4.5, we observe that the alert-free period in 10 hospitals (Bon Secours, Carroll, Franklin Square, Harbor, Harford, Johns Hopkins, Mercy Medical, Sinai, St. Agnes, UMMC, and Upper Chesapeake) are statistically significant from year to year. For red alert duration (Table 4.5), only one hospital (Carroll) has significant changes from year 2018 compared to either 2016, or 2017. For reroute alert durations, four hospitals (Harbor, Sinai, UMMC, Upper Chesapeake) have significant changes from year to year, and for yellow alert durations, 11 hospitals (Carroll, Franklin Square, Greater Baltimore, Harford, Howard County, Johns Hopkins, Midtown, Sinai, St. Joseph, UMMC, and Upper Chesapeake) significantly changed from year to year over the last three years.

In addition, we analyzed the time to alert, and duration of each type of alert, using time-to-event analysis, and visualized the estimated survival functions of each metric in Figures 4.1 to 4.4 for each hospital. For the alert-free periods, the survival

Hospitals	2016 v.s. 2017	2016 v.s. 2018	2017 v.s. 2018
Bon Secours	0.1588	< 0.0001	0.0075
Carrol Hospital	0.0002	< 0.0001	0.1275
Franklin Square	< 0.0001	< 0.0001	0.0024
Harbor Hospital	0.1566	0.0611	0.0032
Harford Hospital	0.0057	0.0129	0.0011
Johns Hopkins	0.0949	< 0.0001	0.0198
Sinai Hospital	0.1435	< 0.0001	< 0.0001
St. Agnes	< 0.0001	< 0.0001	0.0021
UMMC	0.0011	0.0259	< 0.0001
Upper Chesapeake	0.9362	0.0018	0.0007

Table 4.5: P-values of Kruskal-Wallis tests for alert-free periods.

Hospitals	2016 v.s. 2017	2016 v.s. 2018	2017 v.s. 2018
Carroll Hospital	0.3612	0.0303	0.0023

Table 4.6: P-values of Kruskal-Wallis tests for red alert durations.

Hospitals	2016 v.s. 2017	2016 v.s. 2018	2017 v.s. 2018
Harbor Hospital	0.5693	0.0024	0.0243
Sinai Hospital	< 0.0001	0.0041	0.1215
UMMC	0.6789	0.0053	0.0043
Upper Chesapeake	0.0222	0.0019	0.6647

Table 4.7: P-values of Kruskal-Wallis tests for reroute alert durations.

Hospitals	2016 v.s. 2017	2016 v.s. 2018	2017 v.s. 2018
Carroll Hospital	0.0005	< 0.0001	0.1083
Franklin Square	< 0.0001	< 0.0001	0.0092
Greater Baltimore	0.2465	0.0002	0.0167
Harford Hospital	0.1062	0.0031	0.0009
Howard County	< 0.0001	< 0.0001	0.5364
Johns Hopkins	0.1419	0.0959	0.0025
Midtown	0.2334	< 0.0001	0.0056
Sinai Hospital	0.5314	< 0.0001	< 0.0001
St. Joseph	0.0004	0.0068	0.3713
UMMC	0.2523	< 0.0001	< 0.0001
Upper Chesapeake	0.9567	0.0014	0.0002

Table 4.8: P-values of Kruskal-Wallis tests for yellow alert durations.

curves represent the probability of remaining alert-free over time starting from the end of previous alerts. For the duration time of red, reroute, and yellow alerts, the survival curves allow us to compare the probability of remaining on experiencing a given type of alert over time starting from the alert initiation.

Figure 4.1 illustrates the probabilities of remaining alert-free during the next 5 days starting from the end of previous alerts for Bon Secours, Carroll Hospital, Franklin Square, Harbor, Harford, Johns Hopkins, Sinai, St. Agnes, UMMC, and Upper Chesapeake. Among those 10 hospitals, we notice that six hospitals (Bon Secours, Carroll, Johns Hopkins, Sinai, St. Agnes, and Upper Chesapeake) have similar patterns. These six hospitals have the lowest survival curves in 2018, followed by 2017, and then 2016, which means that the risk of experiencing alerts was increasing over years from 2016 to 2018 in those hospitals. Among the other four hospitals, Midtown doesn't have much changes at all over the three years. But for Franklin Square hospital, Year 2016 experienced the lowest probability of remaining alert free, followed by 2018, while 2017 had the best alert-free experiences. For Harbor and Harford hospitals, we also observed the lowest probability of being alert free in the last year 2018, but followed by 2016, and then 2017.

For red alert, our previous results in Table 4.6 show that only one hospital (Carroll) has significant differences in red-alert durations. We examined the probability of remaining the red-alert status once it starts in Carroll hospital for 2016, 2017, and 2018 respectively in Figure 4.2. Obviously, this probability is always higher in 2018 compared to 2017 and 2016, while 2016 has the lowest probability of remaining to be red-alert status.

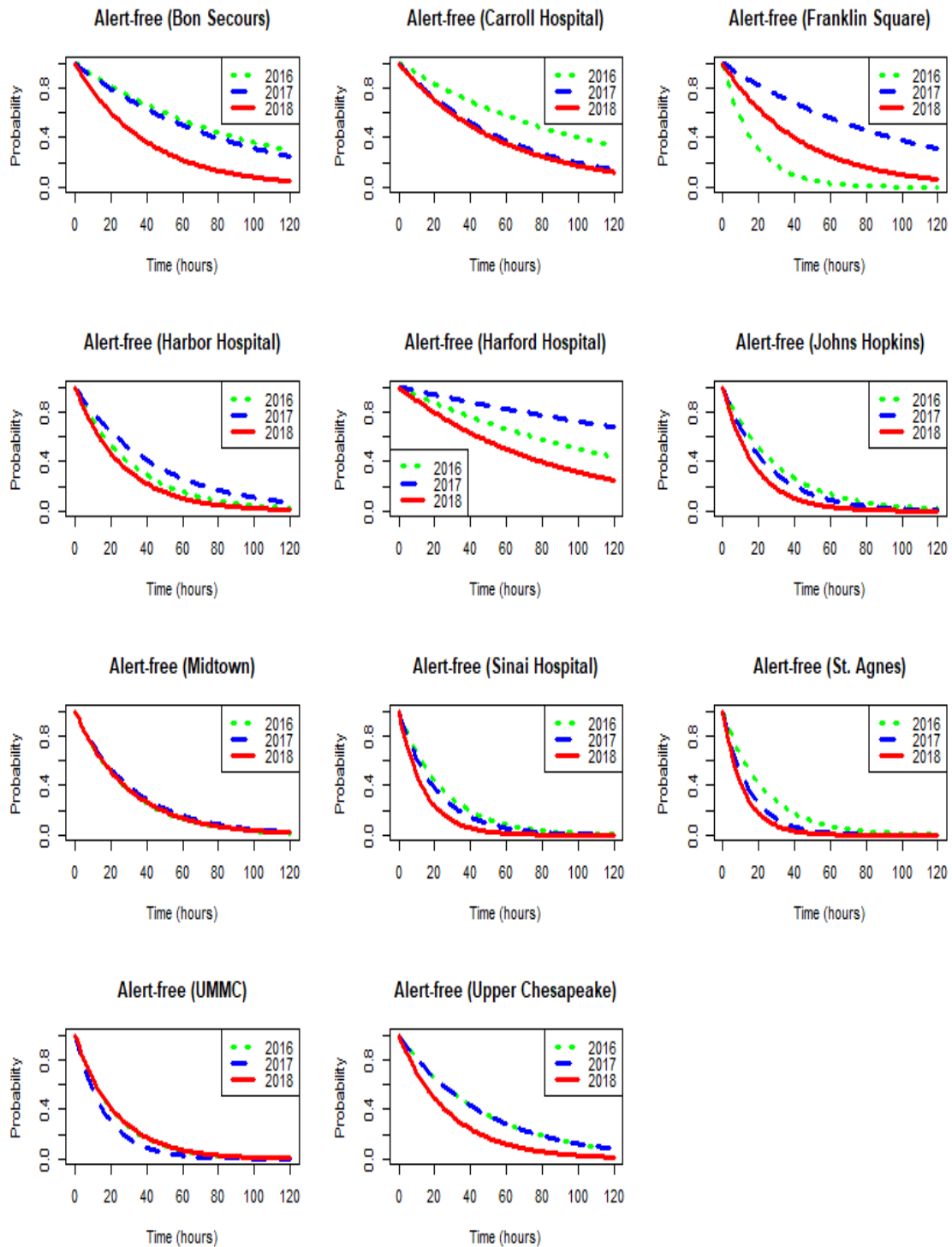


Figure 4.1: Probability of remaining alert-free over time starting from the end of previous alerts.

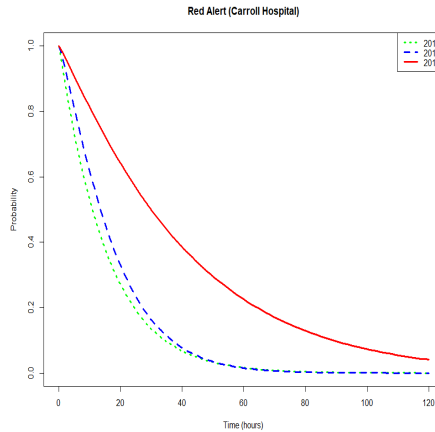


Figure 4.2: Probability of remaining red-alert status starting from the initiation of red alert.

We also model the reroute alert durations and yellow alert durations for those hospitals which demonstrate significant differences in the pair-wise year comparisons using Kruskal-Wallis tests. In Figure 4.3, the probabilities of remaining reroute alert status are very similar for Years 2016 and 2017, but become much higher in 2018, for Harbor Hospital and UMMC. But for Sinai Hospital and Upper Chesapeake Hospital, the probability of remaining to be reroute alert is the lowest for 2016, and becomes higher later on in years 2017 and 2018, but the later two years have the probability curves crossed over. For yellow alerts in Figure 4.4, seven hospitals (Carroll, Harford, Johns Hopkins, Midtown, Sinai, UMMC, Upper Chesapeake) have the highest probabilities of remaining to be yellow-alert status once the yellow alert starts in 2018, which indicates a more serious ED crowding problem in 2018. Among these seven hospitals, Sinai, UMMC and Upper Chesapeake have similar risk of remaining yellow-alert status over time in 2016 and 2017, while Midtown and Carroll observe the risk to be higher from 2016 to 2017, and Harford and Johns

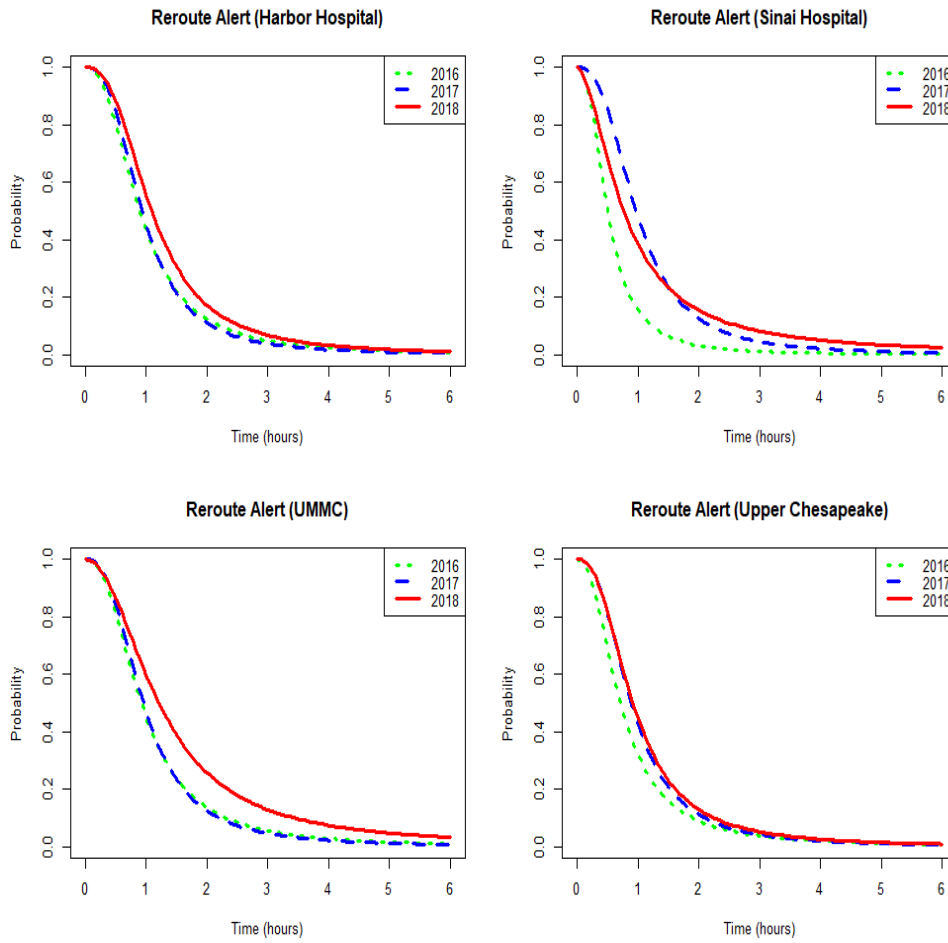


Figure 4.3: Probability of remaining reroute-alert status starting from the initiation of reroute alert.

Hopkins get it improved in 2017, but much worse in 2018. Greater Baltimore also has the worst situation in 2018, but its 2016 and 2017 have similar risk. The other three hospitals, Franklin Square, Howard County, and St. Joseph have the highest risk of remaining to be yellow-alert status once it starts in 2016, and get it improved in 2017 and 2018, which is a good sign of better ED management over years.

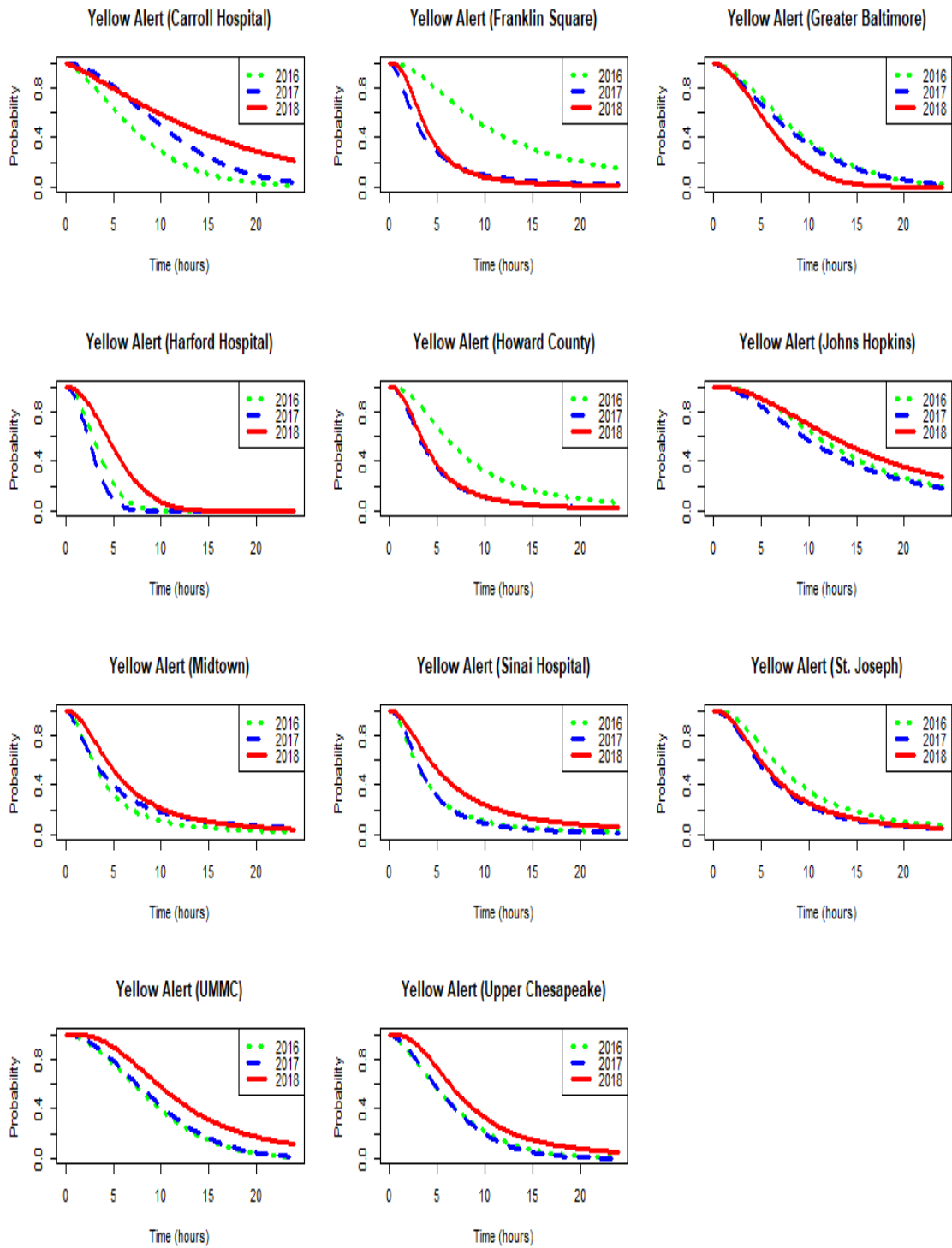


Figure 4.4: Probability of remaining yellow-alert status starting from the initiation of yellow alert.

4.4 Study Limitations

There are several potential limitations of this study and our current investigations. Although we identified a subset of EDs for which the level of access has significantly changed, we are not able to explain the reasons why those changes occurred. While we suspect that the changes occur due to different management plan changes within each individual hospital, our study cannot support or justify such an explanation since we did not collect related data and we did not see broader and consistent changes across the whole region. The study could be extended to address such issues if we had more data on hospital level information.

4.5 Conclusion

Emergency departments (EDs) in the U.S. and across the world are facing increasing levels of overcrowding, which is not only affecting the patients within the crowded ED but also patients requesting access to EDs via emergency medical services (EMS). We investigate three-year trends in the accessibility to ED among 21 hospital EDs in Region III of Maryland using alert-status data provided by the Maryland Institute for Emergency Medical Services Systems (MIEMSS). Specifically, we study the frequency and duration of these alerts (i.e., yellow, red, reroute) as well as alert-free time in EDs to provide evidence of any ongoing trends related to ED accessibility.

We use different metric to evaluate ED accessibilities, including alert-free pe-

riods, durations of red alerts, durations of reroute alerts, and durations of yellow alerts. We employ nonparametric tests to identify significant changes of each metric in each hospital's ED. We find that about half of EDs have statistically significant changes, which show evidence for decreasing ED accessibility in Maryland Region III. In addition, for those hospitals which have significant changes, we fit statistical models on time to alert and duration of each alert types, and we present the probabilities of not getting alerts and of remaining at each alert type over time to visualize the changes of the corresponding accessibility risk for those EDs from 2016 to 2018. There is statistical evidence showing that more than one third of the EDs have higher risk of remaining to be yellow-alert status over time once it starts in 2018 compared to 2016 and 2017, and also almost one third of the EDs have shorter alert-free periods and higher risk of experiencing an alert in 2018 than in the previous two years.

Ten Region III EDs have experienced significant increase in the frequency of alerts over the last three years ($p < 0.01$). The Carroll Hospital ED is the only hospital to observe a significant increase in the frequency of red alerts ($p < 0.01$). For reroute alerts, we observe increase among four hospitals ($p < 0.01$), and for yellow alerts, more than half of the hospitals in Region III observed significant increases. ($p < 0.01$).

All of these signify a concerning trend about the accessibility of ED services and ED crowding in Maryland's most populous region, and improved management need to be done in order to improve the situation.

Chapter 5: Impact of Global Budget Program on Emergency Room Accessibility in Region III of Maryland

5.1 Introduction

There has been increasingly more money spent in the United States (U.S.) related to healthcare than any other comparable countries in the world. It is estimated that about seven percent of its Gross Domestic Product (GDP) was spent on healthcare in the U.S. in 1970 [114]. Until 1980, healthcare expense in the U.S. was still similar to several other developed countries. But this gap between U.S. and others in terms of spending on healthcare has grown significantly since 1980, according to research from Kaiser Family Foundation [114]. In the most recent research, health related spending in the U.S. is projected to grow at an average of 5.5 % per year through 2024 leading to \$5.4 trillion in total or 19.6 % GDP [126]. Therefore, there is an increasing interest in the payment models with purposes to reduce expenditures, improve quality, and eliminate any unnecessary hospitalizations. Moreover, Maryland's unique hospital payment model to control healthcare spending starts to draw a growing attention in recent researches [109, 122].

The state of Maryland sets the same hospital rates for all payers such as Medi-

care, Medicaid, and private insurers since 1970s. This All-Payer Model was revised in 2014 to implement the Global Budget payment system. The revised model requests a specific annual amount for all payers to pay in an effort to limit the growing spending in healthcare and improve service quality. Each hospital understands what revenue they can receive due to the budget specified at the beginning of the year. Therefore, hospitals have to monitor their spending all the time. Reported by CMS, Maryland has been able to limit hospital spending and enhance inpatient and outpatient services since 2014 accordingly [122]. Although the Global Budget payment model aims to control the expenditure growth and improve the quality of services, it may change the accessibility of emergency rooms (ER) in Maryland.

In this Chapter, we evaluate the changes in ER accessibility before and after the Global Budget payment system established in Maryland, using data on ER alert status of each hospital obtained in the County/Hospital Alert Tracking System (CHATS). We analyze the frequency and duration of yellow, red, and reroute alerts, and examine changes of a variety of alerts before and after the new Global Budget payment system was initiated. Moreover, we investigate those changes from 2011 to 2013, in order to verify the significance of changes due to this specific payment model. In this study, we develop appropriate statistical tools and models to present data observations, to evaluate the changing process of ER alert durations from 2011 to 2018, and to explore the impact of the Global Budget Program on accessibilities in ER.

The remaining sections of this chapter are organized as follows. In Section 5.2, we introduce our problem and describe the data we use in this study. We

develop our methods for comparing changes in the duration of ER alerts before and after the Global Budget Program was implemented. In Section 5.3, we present the descriptive statistics for ER alert durations, test for significant changes in adjacent years. In Section 5.4, we discuss several future research directions. and conclude with an impact discussion of our results.

5.2 Statistical Methods

We first calculate descriptive statistics for three types of ER alerts and the duration of each type of alerts among 21 hospitals in Maryland Region III. Then, we use Kruskal-Wallis test to detect statistically significant differences in these measures comparing 2013 and 2015. Since all hospitals initiated the Global Budget program in their system in 2014, we did not use the data immediately collected from 2014 and allow a warm-up period for hospitals to have the program taking effects. For comparison purpose, we also consider alerts data prior to 2014 in order to control for the longitudinal time effect, that is, to control for the fact that the potential significant changes before and after 2014 may be due to purely time changes.

Additionally, we adjust for other variables in our final model. Covariates of interest in our investigation include time, indicator of whether having global budget program implemented or not yet, population size, and area/location. Alert data were acquired longitudinally. Thus, we evaluate potential risk factors using a mixed effect model with a random intercept and first-order autoregressive (AR1) process on log duration of yellow alert. With log transformation, the response variable

becomes more normally distributed than the original measure, so that mixed effect model fits better.

$$\mathbf{Y}_{ij} = \mathbf{X}_{ij}\boldsymbol{\beta} + b_i + e_{ij}$$

where

$$b_i \sim \mathcal{N}(0, \sigma_b^2) \quad \text{and} \quad e_{ij} \sim \mathcal{N}(0, \sigma^2)$$

In this mixed effect model, we assume that the mean response for i th hospital at the j th year differs from the population mean, $\mathbf{X}_{ij}\boldsymbol{\beta}$, by a hospital effect and a within-hospital random error, namely, b_i and e_{ij} respectively [54]. The fixed effects in this model are to evaluate the influence of covariates on mean responses, while the random effects are introduced into the model to accommodate the within-hospital correlations over years. The AR1 correlation structure allows the response measures closer together to be more correlated than those further apart over years within the same hospital. In the mean model, we specify a polynomial regression term to capture the expected nonlinear trend of log responses over years. With the estimated coefficient of our model, we are able to predict hours of yellow alert at a given year adjusted for statistically relevant covariates.

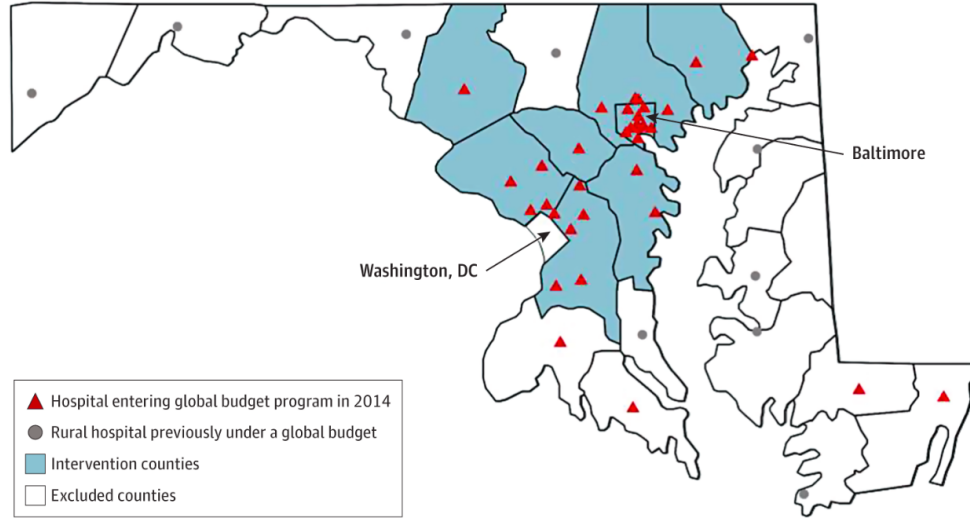


Figure 5.1: Hospitals and Counties in Maryland's Global Budget Program [122].

5.3 Analysis Results and Findings

In Figure 5.1 [122], we notice that most hospitals in Maryland Region III, except for Carroll Hospital, entered the Global Budget program in 2014. In Tables 5.1, 5.2, 5.3, and 5.4, we compare ER's total number of alerts, hours of alert free period, and durations of red alerts, reroute alerts, and yellow Alerts among 21 hospitals in Region III before and after the Global Budget Program was established.

Table 5.1 presents the results for alert-free periods. Almost all hospitals, except for Bon Secours, have increased number of alerts in 2015, compared to 2013. The changes in hours of alerts-free periods are consistent as well. Only Bon Secours, Good Samaritan, Great Baltimore, Harford Hospital, Northwest, Sinai Hospital, UMMC, Union Memorial, and Upper Chesapeake do not observe significant changes in median hours of alert-free periods. All other 12 hospitals in Region III have experienced significantly reduced hours of alert-free periods ($p < 0.05$).

Hospitals	Variables	Year 2013	Year 2015	P-values
Anne Arundel	Total Number of Alerts	37	267	< 0.0001
	Hours of Alert-free Period*	41.05 (167.72)	14.3 (22.78)	
Baltimore Washington	Total Number of Alerts	37	210	0.0002
	Hours of Alert-free Period*	67.93 (148.37)	17.58 (40.09)	
Bon Secours	Total Number of Alerts	36	37	0.9736
	Hours of Alert-free Period*	127.98 (353.4)	111.57 (246.1)	
Carroll Hospital	Total Number of Alerts	3	86	0.0431
	Median (IQR)	596.93 (708.12)	42.31 (110.54)	
Franklin Square	Total Number of Alerts	100	251	< 0.0001
	Hours of Alert-free Period*	32.93 (90.525)	14.43 (18.38)	
Good Samaritan	Total Number of Alerts	130	157	0.2817
	Hours of Alert-free Period*	33.93 (64.23)	24.63 (50.22)	
Great Baltimore	Total Number of Alerts	28	146	0.1216
	Hours of Alert-free Period*	43.72 (186.34)	25.85 (55.09)	
Harbor Hospital	Total Number of Alerts	50	128	< 0.0001
	Hours of Alert-free Period*	85.68 (169.53)	25.12 (67.95)	
Harford Hospital	Total Number of Alerts	39	37	0.9214
	Hours of Alert-free Period*	170 (261.95)	143.37 (377.22)	
Howard County	Total Number of Alerts	88	79	0.0257
	Hours of Alert-free Period*	34.21 (68.28)	57.6 (115.63)	
Johns Hopkins	Total Number of Alerts	103	152	0.0077
	Hours of Alert-free Period*	37.53 (77.59)	22.16 (39.24)	
JH Bayview	Total Number of Alerts	235	361	< 0.0001
	Hours of Alert-free Period*	18.18 (32.57)	11.87 (11.63)	
Mercy Medical	Total Number of Alerts	92	134	0.0339
	Hours of Alert-free Period*	46.21	35.35 (62.5)	
Midtown	Total Number of Alerts	46	130	0.0002
	Hours of Alert-free Period*	95.56 (209.99)	34.88 (71.79)	
Northwest	Total Number of Alerts	143	181	0.1713
	Hours of Alert-free Period*	21.2 (60.13)	16.35 (36.83)	
Sinai Hospital	Total Number of Alerts	141	267	0.5592
	Hours of Alert-free Period*	12.98 (35.63)	14.23 (26.32)	
St. Agnes	Total Number of Alerts	116	191	0.0057
	Hours of Alert-free Period*	38.68 (97.63)	22.7 (40.61)	
St. Joseph	Total Number of Alerts	54	195	0.0088
	Hours of Alert-free Period*	43.22 (98.26)	18.22 (27.42)	
UMMC	Total Number of Alerts	132	133	0.2432
	Hours of Alert-free Period*	25.89 (60.15)	37.63 (50.02)	
Union Memorial	Total Number of Alerts	101	172	0.2943
	Hours of Alert-free Period*	27.85 (49.58)	21.25 (33.93)	
Upper Chesapeake	Total Number of Alerts	107	113	0.3239
	Hours of Alert-free Period*	27.23 (81.53)	33.75 (81.05)	

* reports the corresponding median hours of all alert-free periods, in parentheses are the interquartile ranges (IQRs).

Table 5.1: Descriptive statistics for alerts-free periods.

As to red alerts in Table 5.2, we observe different trends on the change of numbers of alerts from 2013 to 2015 across different hospitals. For example, increased number of red alerts are observed in Johns Hopkins from 2 in 2013 to 49 in 2015, Johns Hopkins Bayview from 28 in 2013 to 52 in 2015. But on the other hand, Northwest, UMMC, and Upper Chesapeake have the number of red alerts decreased in 2015, compared to 2013. We test on the differences between 2013 and 2015, in terms of duration of each alert in hours, and found that the median red alert duration is significantly shorter in 2015 for Anne Arundel, Midtown, and UMMC, but all with more alerts and longer total alert duration in 2015. Only Johns Hopkins hospital has significantly longer red alert durations as well, besides having more red alerts and longer total red alert duration in 2015, which is after the Global Budget program compared to before. Most of the hospitals in Table 5.2 do not have significant differences comparing 2013 with 2015.

In Table 5.3, only one hospital, Baltimore Washington, has significant difference in median duration of each reroute alert comparing 2013 and 2015, but the increase is not big. Two hospitals (Anne Arundel and Baltimore Washington) in Anne Arundel have the number and total time of reroute alert dramatically increased. Hospitals in Carroll (Carroll Hospital), Harford (Upper Chesapeake and Harford Hospital), Howard (Howard County Hospital), and Anne Arundel don't have much changes, while five hospitals (Franklin Square, Good Samaritan, Harbor Hospital, Johns Hopkins, and St. Joseph) in Baltimore city and county experience big changes in number of reroute alert.

Hospitals	Variables	Year 2013	Year 2015	P-values
Anne Arundel	Total Number of Alerts	13	27	0.0102
	Total Alert Duration	218.84	212.24	
	Hours of Each Alert*	16.31 (14.18)	5.34 (6.54)	
Baltimore Washington	Total Number of Alerts	0	1	NA
	Total Alert Duration	0	0.63	
	Hours of Each Alert*	NA	0.63 (0)	
Bon Secours	Total Number of Alerts	13	16	0.6295
	Total Alert Duration	153.15	246.16	
	Hours of Each Alert*	9.76 (10.27)	8.98 (11.18)	
Carrol Hospital	Total Number of Alerts	0	4	NA
	Total Alert Duration	0	136.74	
	Hours of Each Alert*	NA	16.33 (31.3)	
Franklin Square	Total Number of Alerts	0	2	NA
	Total Alert Duration	0	18.15	
	Hours of Each Alert*	NA	9.08 (0.38)	
Good Samaritan	Total Number of Alerts	4	9	0.8167
	Total Alert Duration	31.38	51.41	
	Hours of Each Alert*	5.99 (8.12)	4.99 (5.96)	
Greater Baltimore	Total Number of Alerts	9	36	0.2938
	Total Alert Duration	98.33	569.61	
	Hours of Each Alert*	6.86 (9.84)	12.09 (17.09)	
Harbor Hospital	Total Number of Alerts	0	3	NA
	Total Alert Duration	0	25.78	
	Hours of Each Alert*	NA	5.44 (5.49)	
Harford Hospital	Total Number of Alerts	10	1	0.1138
	Total Alert Duration	61.38	26	
	Hours of Each Alert*	5.61 (5.49)	26 (0)	
Howard County	Total Number of Alerts	0	2	NA
	Total Alert Duration	0	3.92	
	Hours of Each Alert*	NA	1.96 (1.96)	
Johns Hopkins	Total Number of Alerts	2	49	0.0289
	Total Alert Duration	14.93	1313.55	
	Hours of Each Alert*	7.47 (2.23)	21.3 (21.63)	
JH Bayview	Total Number of Alerts	28	52	0.8165
	Total Alert Duration	137.62	257.07	
	Hours of Each Alert*	3.49 (4.47)	3.38 (6.06)	
Mercy Medical	Total Number of Alerts	2	2	0.6831
	Total Alert Duration	0.77	0.84	
	Hours of Each Alert*	0.39 (0.26)	0.42 (0.29)	
Midtown	Total Number of Alerts	9	39	0.011
	Total Alert Duration	118.55	288.23	
	Hours of Each Alert*	14.56 (7.55)	6.16 (5.18)	
Northwest	Total Number of Alerts	26	10	0.1913
	Total Alert Duration	255.47	148.42	
	Hours of Each Alert*	6.68 (7.53)	12.47 (6.54)	
Sinai Hospital	Total Number of Alerts	29	36	0.8328
	Total Alert Duration	346.41	403.06	
	Hours of Each Alert*	8.25 (8.44)	7.8 (8.11)	
St. Agnes	Total Number of Alerts	4	20	0.0528
	Total Alert Duration	9.71	175.8	
	Hours of Each Alert*	2.57 (3.31)	4.82 (8.26)	
St. Joseph	Total Number of Alerts	10	25	0.1653
	Total Alert Duration	45.48	177.64	
	Hours of Each Alert*	3.08 (7.73)	6.79 (7.59)	
UMMC	Total Number of Alerts	43	31	0.0005
	Total Alert Duration	448.53	142.28	
	Hours of Each Alert*	8.18 (7.65)	4.59 (4.94)	
Union Memorial	Total Number of Alerts	47	64	0.417
	Total Alert Duration	505.17	899.39	
	Hours of Each Alert*	7.84 (10.29)	10.23 (11.82)	
Upper Chesapeake	Total Number of Alerts	55	12	0.7068
	Total Alert Duration	1007.37	268.61	
	Hours of Each Alert*	12.7 (12.18)	10.68 (20.12)	

* reports the corresponding median hours of each alert duration, in parentheses are the interquartile ranges (IQRs).

Table 5.2: Descriptive statistics for duration of red alert.

Hospitals	Variables	Year 2013	Year 2015	P-values
Anne Arundel	Total Number of Alerts	12	187	
	Total Alert Duration	14.09	252.32	
	Hours of Each Alert*	1.24 (1.11)	1.25 (1.015)	0.6753
Baltimore Washington	Total Number of Alerts	29	155	
	Total Alert Duration	33.89	235.34	
	Hours of Each Alert*	1.15 (1)	1.46 (1.34)	0.0417
Bon Secours	Total Number of Alerts	15	18	
	Total Alert Duration	14.11	28.44	
	Hours of Each Alert*	0.79 (1)	0.89 (1.89)	0.4263
Carrol Hospital	Total Number of Alerts	1	0	
	Total Alert Duration	0.45	0	
	Hours of Each Alert*	0.45 (0)	NA	NA
Franklin Square	Total Number of Alerts	19	42	
	Total Alert Duration	22.63	51.48	
	Hours of Each Alert*	1.04 (0.52)	1.09 (0.39)	0.6423
Good Samaritan	Total Number of Alerts	47	15	
	Total Alert Duration	61.45	18.24	
	Hours of Each Alert*	0.97 (1.05)	1.09 (0.66)	0.7548
Greater Baltimore	Total Number of Alerts	7	10	
	Total Alert Duration	5.16	9.61	
	Hours of Each Alert*	0.52 (0.7)	0.88 (0.25)	0.1432
Harbor Hospital	Total Number of Alerts	41	97	
	Total Alert Duration	69.09	118.48	
	Hours of Each Alert*	1.02 (0.85)	0.94 (0.91)	0.2644
Harford Hospital	Total Number of Alerts	17	19	
	Total Alert Duration	8.47	12.54	
	Hours of Each Alert*	0.41 (0.54)	0.44 (0.49)	0.2882
Howard County	Total Number of Alerts	23	12	
	Total Alert Duration	51.78	23.76	
	Hours of Each Alert*	1.59 (1.42)	1.02 (1.05)	0.0707
Johns Hopkins	Total Number of Alerts	57	16	
	Total Alert Duration	79.9	36.14	
	Hours of Each Alert*	1.22 (1.18)	1.06 (3.13)	0.831
JH Bayview	Total Number of Alerts	96	111	
	Total Alert Duration	132.39	133.81	
	Hours of Each Alert*	1.07 (1.15)	0.98 (0.55)	0.1146
Mercy Medical	Total Number of Alerts	54	22	
	Total Alert Duration	62.06	38.25	
	Hours of Each Alert*	0.97 (0.67)	0.97 (1.45)	0.7571
Midtown	Total Number of Alerts	20	22	
	Total Alert Duration	35.57	23.54	
	Hours of Each Alert*	1.19 (1.74)	0.77 (1.11)	0.0641
Northwest	Total Number of Alerts	22	35	
	Total Alert Duration	20.83	43.99	
	Hours of Each Alert*	0.91 (0.52)	1.03 (0.89)	0.1736
Sinai Hospital	Total Number of Alerts	35	41	
	Total Alert Duration	43.49	41.16	
	Hours of Each Alert*	0.77 (1.01)	0.79 (0.8)	0.6998
St. Agnes	Total Number of Alerts	82	95	
	Total Alert Duration	114.12	120.45	
	Hours of Each Alert*	1.14 (1.01)	1.04 (0.84)	0.165
St. Joseph	Total Number of Alerts	3	37	
	Total Alert Duration	12.5	51.76	
	Hours of Each Alert*	2.01 (4.43)	1.23 (1.05)	0.2478
UMMC	Total Number of Alerts	43	36	
	Total Alert Duration	55.33	52.76	
	Hours of Each Alert*	1.04 (1.15)	0.92 (0.85)	0.7677
Union Memorial	Total Number of Alerts	11	1	
	Total Alert Duration	13.03	2.45	
	Hours of Each Alert*	1.39 (1.08)	2.45 (0)	0.1924
Upper Chesapeake	Total Number of Alerts	42	83	
	Total Alert Duration	32.61	77.53	
	Hours of Each Alert*	0.71 (0.55)	0.83 (0.64)	0.0893

* reports the corresponding median hours of each alert duration, in parentheses are the interquartile ranges (IQRs).

Table 5.3: Descriptive statistics for duration of reroute alert.

Hospitals	Variables	Year 2013	Year 2015	P-values
Anne Arundel	Total Number of Alerts	24	169	
	Total Alert Duration	307.47	1429.51	
	Hours of Each Alert*	9.08 (8.77)	6.49 (7.37)	0.0211
Baltimore Washington	Total Number of Alerts	17	106	
	Total Alert Duration	103.15	664.2	
	Hours of Each Alert*	5.51 (1.87)	5.69 (3.42)	0.898
Bon Secours	Total Number of Alerts	11	7	
	Total Alert Duration	37.03	17.91	
	Hours of Each Alert*	3.45 (1.65)	1.9 (1.19)	0.1351
Carrol Hospital	Total Number of Alerts	4	87	
	Total Alert Duration	19.16	798.39	
	Hours of Each Alert*	3.99 (4.04)	8.24 (5.08)	0.0604
Franklin Square	Total Number of Alerts	99	242	
	Total Alert Duration	909.82	3088.26	
	Hours of Each Alert*	7.02 (6.73)	10.65 (8.79)	0.0002
Good Samaritan	Total Number of Alerts	101	147	
	Total Alert Duration	636.17	990.01	
	Hours of Each Alert*	5.38 (4.96)	5.78 (4.16)	0.1539
Greater Baltimore	Total Number of Alerts	20	130	
	Total Alert Duration	135.45	994.43	
	Hours of Each Alert*	6.53 (5.54)	7.01 (5.54)	0.556
Harbor Hospital	Total Number of Alerts	22	58	
	Total Alert Duration	68.92	220.64	
	Hours of Each Alert*	2.6 (1.87)	2.93 (2.03)	0.3322
Harford Hospital	Total Number of Alerts	20	23	
	Total Alert Duration	51.73	68.25	
	Hours of Each Alert*	2.56 (1.65)	3.25 (2.03)	0.3807
Howard County	Total Number of Alerts	74	74	
	Total Alert Duration	714.06	752.8	
	Hours of Each Alert*	9.14 (9.03)	7.51 (6.78)	0.3644
Johns Hopkins	Total Number of Alerts	57	153	
	Total Alert Duration	366	2005.71	
	Hours of Each Alert*	5.76 (5.94)	11.09 (7.97)	< 0.0001
JH Bayview	Total Number of Alerts	176	318	
	Total Alert Duration	1115.67	3200.43	
	Hours of Each Alert*	4.59 (6.91)	8.62 (9.59)	< 0.0001
Mercy Medical	Total Number of Alerts	51	123	
	Total Alert Duration	168.13	632.97	
	Hours of Each Alert*	2.67 (2.84)	3.94 (4.38)	0.002
Midtown	Total Number of Alerts	28	91	
	Total Alert Duration	134.23	363.01	
	Hours of Each Alert*	3.75 (3.4)	3.37 (2.95)	0.2035
Northwest	Total Number of Alerts	123	169	
	Total Alert Duration	509.08	987.31	
	Hours of Each Alert*	2.74 (3.59)	4.23 (5.64)	0.0003
Sinai Hospital	Total Number of Alerts	99	228	
	Total Alert Duration	456.28	1508.58	
	Hours of Each Alert*	1.87 (5.07)	3.83 (7.12)	< 0.0001
St. Agnes	Total Number of Alerts	53	130	
	Total Alert Duration	203.58	571.27	
	Hours of Each Alert*	2.52 (3.51)	3.55 (3.46)	0.0618
St. Joseph	Total Number of Alerts	46	164	
	Total Alert Duration	261.43	1682.21	
	Hours of Each Alert*	4.21 (3.94)	8.54 (7.79)	< 0.0001
UMMC	Total Number of Alerts	77	92	
	Total Alert Duration	608.1	586.92	
	Hours of Each Alert*	6.34 (7.2)	5.19 (4.83)	0.2713
Union Memorial	Total Number of Alerts	64	141	
	Total Alert Duration	368.46	832.57	
	Hours of Each Alert*	4.86 (4.2)	4.95 (3.7)	0.9899
Upper Chesapeake	Total Number of Alerts	51	73	
	Total Alert Duration	233.95	432.35	
	Hours of Each Alert*	3.32 (4.01)	4.78 (3.99)	0.0482

* reports the corresponding median hours of each alert duration, in parentheses are the interquartile ranges (IQRs).

Table 5.4: Descriptive statistics for duration of yellow alert.

Table 5.4 presents the comparison between 2015 and 2013, in terms of yellow alert numbers, total alert duration, and hours of each alert. Only Howard County, Harford Hospital, and Bon Secours kept about the same amount of yellow alerts. All other hospitals have the number of yellow alerts greatly increased. The median duration of each yellow alert is marginally significantly increased in Carroll county (Carroll Hospital) and significantly increased in Anne Arundel, Franklin Square hospital, Johns Hopkins, JH Bayview, Mercy Medical, Sinai Hospital, St. Joseph, and Upper Chesapeake.

Summarizing Tables 5.1-5.4, six hospitals, including Anne Arundel, Baltimore Washington, Franklin Square, Harbor Hospital, Johns Hopkins, and JH Bayview hospitals, report dramatical decreases of ER's alert-free period in 2015 after the Global Budget Program was implemented comparing to 2013 before the program. There are also six hospitals (Franklin Square, Johns Hopkins, JH Bayview, Northwest, Sinai Hospital, and St. Joseph in Figure 5.2) showing significant changes in yellow alerts. However, although we observe such significant changes in alert-free period and ER's yellow alert, we are not certain if the changes are due to other potential reasons such as longitudinal time effects or impacted by the Global Budget Program, given that not much impact on reroute alert and red alert has been observed.

Thus, we further look into the previous years, 2012 and 2013 to evaluate if there are similar changes from year to year even before the Global Budget Program. From the test results in Table 5.5, we can see that there are five hospitals (Franklin Square, Howard County, JH Bayview, Sinai, and Union Hospitals) experiencing significant

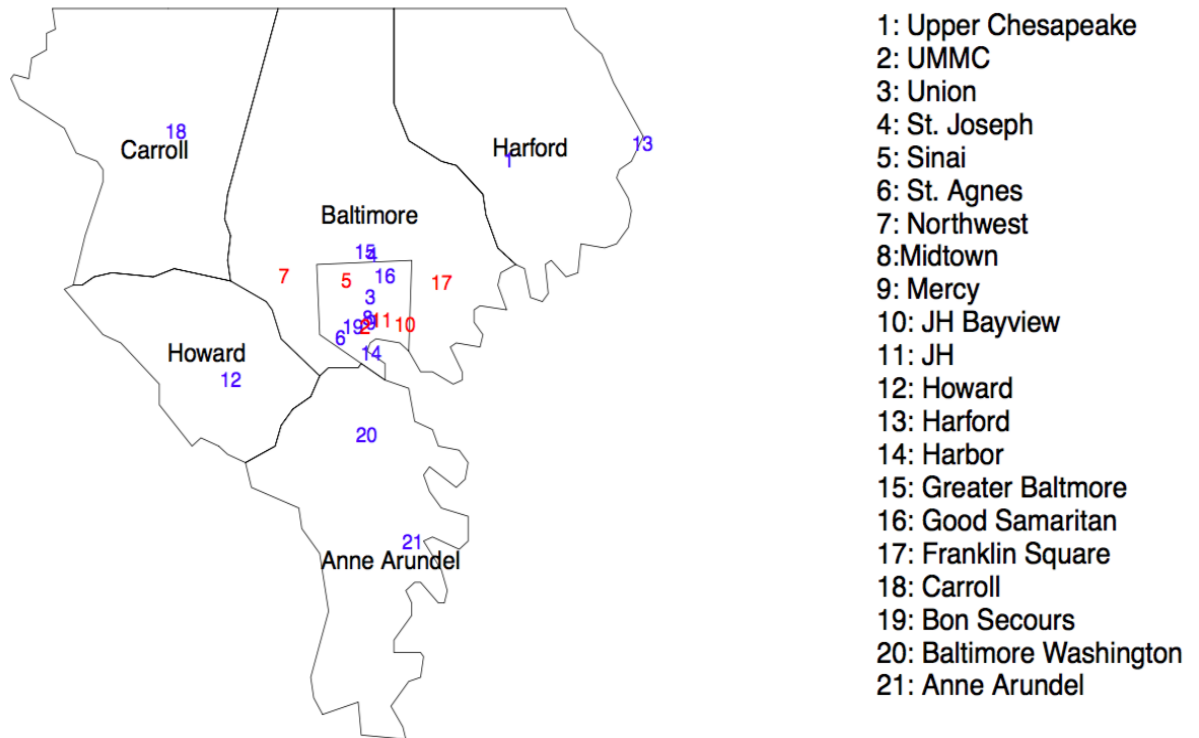


Figure 5.2: Hospitals with significant changes (red) in region III from 2013 to 2015.

changes in ER’s yellow alerts, and three hospitals (Harford, Johns Hopkins, and Upper Chesapeake Hospitals) with significant changes in ER alert-free periods. Most of the 21 hospitals in Maryland Region III do not see significant changes in red and reroute alerts from 2012 to 2013. This is similar to the comparison results of 2013 v.s. 2015, and demonstrate a potential longitudinal time effect.

To control for such a time effect and further investigate the association between Global Budget Program implementation and the ER’s accessibilities, we collect all data from 2011 to 2018 and fit a longitudinal regression model adjusting for time and other potential confounders. We focus on ER’s yellow alerts, given that the average hours of yellow alert is increasing over the time each year regardless of regions. In Figure 5.3, we also notice that the average hours of yellow alert of Baltimore and

Hospitals	Alert-free Period	Red Alert	Reroute Alert	Yellow Alert
Anne Arundel	0.6415	0.1439	0.5375	0.1031
Baltimore Washington	0.3851	NA	0.1819	0.2437
Bon Secours	0.3427	0.1724	0.7072	0.0516
Carrol Hospital	0.0914	NA	0.3173	0.351
Franklin Square	0.0618	NA	0.7349	0.0019
Good Samaritan	0.0632	1	0.5688	0.3363
Greater Baltimore	0.7507	0.8137	0.0946	0.2701
Harbor Hospital	0.5286	NA	0.7471	0.5881
Harford Hospital	0.0026	0.2513	0.136	0.0519
Howard County	0.0421	NA	0.041	0.0059
Johns Hopkins	< 0.0001	0.1109	0.7699	0.9009
JH Bayview	0.0489	0.3604	0.0012	< 0.0001
Mercy Medical	0.1572	1	0.0419	0.0659
Midtown	0.2535	0.0594	0.2301	0.191
Northwest	0.1045	0.0774	0.8395	0.1212
Sinai Hospital	0.9944	0.0757	0.0141	< 0.0001
St. Agnes	0.2459	0.5637	0.3137	0.1326
St. Joseph	0.7502	0.6121	0.1011	0.7388
UMMC	0.6062	0.3326	0.9014	0.8359
Union Memorial	0.1172	0.7708	0.4615	0.0027
Upper Chesapeake	0.0103	0.0964	0.7766	0.78

Table 5.5: Summary of Kruskal-Wallis test p-values for the difference in outcome probability over time for 2012 and 2013.

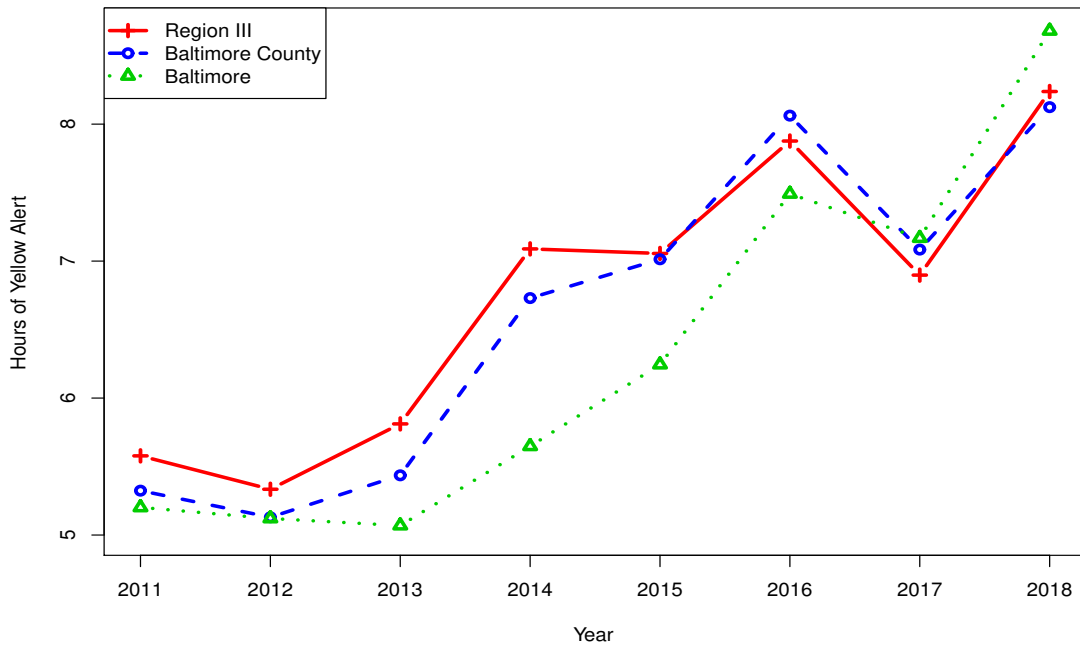


Figure 5.3: Mean duration of yellow alert profile each year by different regions.

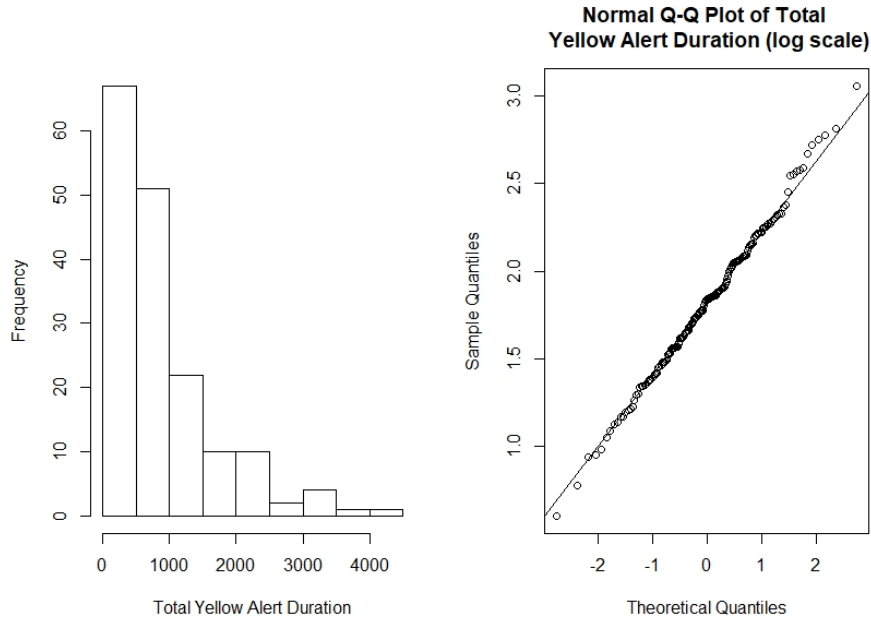


Figure 5.4: Histogram of yellow alert durations (skewed) and Q-Q-plot of the log duration of yellow alerts (more normal with log scale).

Baltimore County are generally lower than the average in Region III before 2016, but become higher after 2016, which shows that location and population size may take an effect as well.

We fit a mixed effect model on the total duration of ER yellow alert to evaluate the impact of the Global Budget Program, with a random intercept and an AR1 correlation structure to account for within-hospital correlations among the repeated alert measures for each hospital. The histogram of total duration of ER yellow alert (Figure 5.4) shows that its distribution is very skewed, and thus we apply a Log transformation in order to get a more normally distributed outcome variable (Q-Q plot in Figure 5.4). Considering the nonlinear change of ER yellow alert durations over time, we fit a polynomial regression with regard to time. We also control for the population size of each hospital's location in the model. Table 5.6 presents the

Effect	Estimate	SE	P-values
Intercept	2.2172	1.3451	0.1015
Time*	5.9852	2.1173	0.0054
Time ² *	-4.27	1.2366	0.0007
Time ³ *	1.2778	0.3204	0.0001
Time ⁴ *	-0.1649	0.0381	< 0.0001
Time ⁵ *	0.0077	0.0017	< 0.0001
Population**	0.0001	< 0.0001	0.1459
Global Budget program***	-0.171	0.2733	0.5325

* reports that year-2010

** reports county/city population

*** reports if enrolled in the Global Budget program

Table 5.6: Estimated coefficients, standard errors (SE), and P-values obtained from mixed model analysis of log total yellow alert duration on covariates of interest.

estimated coefficients, standard errors (SE), and P-values. No statistically significant association is observed between the total hours of yellow alert and population or whether the hospital enroll the Global Budget Program or not. The predicted mean trajectory of yellow alert durations obtained from our model is consistent with the observed mean profile in region III (Figure 5.5), Baltimore County (Figure 5.6), and Baltimore city (Figure 5.7).

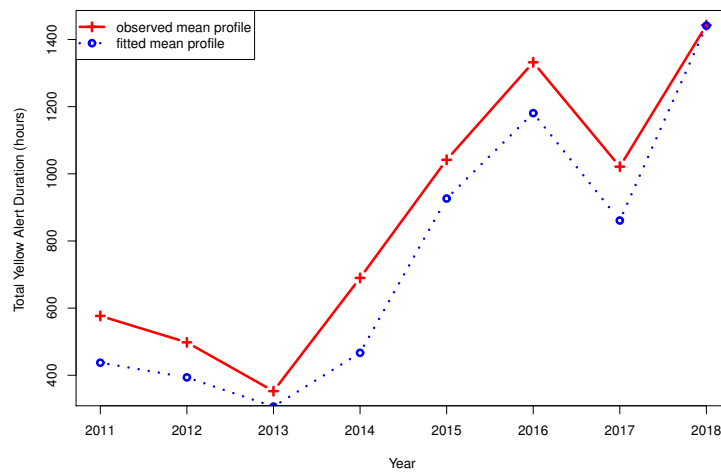


Figure 5.5: Comparison of fitted model with observed data in region III.

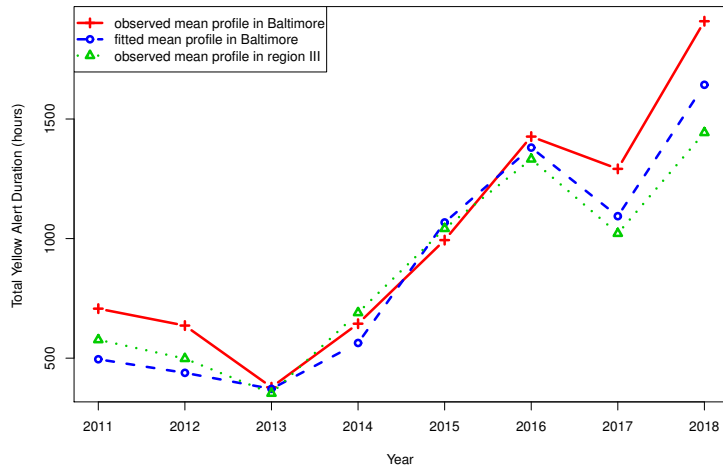


Figure 5.7: Comparison of fitted model with observed data in Baltimore city.

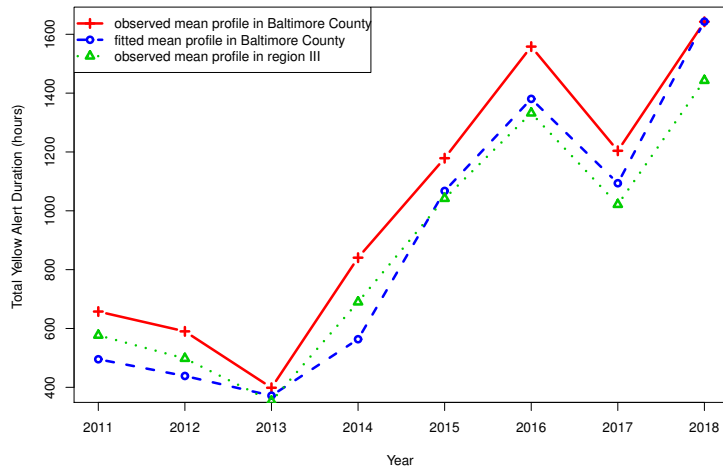


Figure 5.6: Comparison of fitted model with observed data in Baltimore county.

5.4 Discussion and Conclusions

The state of Maryland continues to implement All-Payer model and established the Global Budget program to control the expenditure and improve the quality of

services in 2014. In this study, we focus on investigating the impact of the Global Budget payment model on ER accessibilities among 21 hospitals in Maryland Region III. Particularly, we look into the changes in red, reroute, and yellow ER alerts, as well as alert-free periods from 2012 (the year right before the Global Budget program was implemented) to 2015 (the year right after the Global Budget program was implemented). Although we observe changes in 2015 compared to 2013, and notice that about one third of hospitals had changes in yellow alert and alert-free period, similar patterns have been observed when comparing 2012 with 2013. We further fit a mixed effect model on repeated alert measures to capture within-hospital correlations and adjust for other potential risk factors and confounders. The mean profile of predicted total durations of yellow alerts obtained from the mixed model are consistent with the observed data. In this study, the total duration of yellow alert in each year is increasing from 2011 to 2018. This nonlinear trend is accommodated by fitting a polynomial regression curve in time. From the results of our multivariate mixed effect model, no significant changes are observed for hospitals enrolled in the Global Budget program or not. Thus, we do not have enough evidence to demonstrate that the Global Budget payment program initiated in 2014 influences the ERs accessibilities in Maryland Region III.

The work could be extended in several ways. The first extension would be to apply the investigation to Baltimore City only. The performances in ER's accessibility are similar in rural hospitals, but is very different than that in city. Thus, a separate study on hospitals in Baltimore city may avoid heterogeneity between hospitals in region III. The second future research extension would be to collect more

hospital-specific or region-specific covariates to take into account, such as bed size, median home income, and other social-economical variables. For instance, bed size might have some interaction with the Global Budget program. A study accounting for these potential confounders and effect modifiers may help us understand if the interaction between other covariates and the Global Budget program will impact the accessibility of ERs in Maryland.

Chapter 6: Multi-state Markov Model for Cascading Problems in Emergency Rooms in Maryland

6.1 Introduction

Emergency rooms (ERs) serve as an important part in American's healthcare system and they are significantly critical for providing urgent treatment and acute care to patients without any appointment [65, 74, 107]. Most of the cases seeking for ER services may require immediate attention or even be life-threatening. As noted in the 2006 Institute of Medicine report, ERs have become "the safety net of the safety net". Thus, accessibility to ER services is especially necessary for emergency care such as trauma, stroke, acute coronary syndrome, and burn [5, 86]. While rapid access to ER services is essential given the above special properties of ER services, long waiting time or inaccessibility to ER services is pretty common and frequently occurs everyday [108]. ER crowding has become a widespread problem in hospitals across the United States, particularly severe in urban and teaching hospitals.

We recently focused on investigating the cascading problems in ERs of region III in Maryland, which is the most populous area in Maryland, including five counties (Anne Arundel, Baltimore, Carroll, Harford, and Howard) and Baltimore City. We

studied accessibility to ER services among 21 hospitals in the region: Anne Arundel Medical Center, Baltimore Washington Medical Center, Bon Secours Hospital, Carroll Hospital Center, Franklin Square Hospital, Good Samaritan Hospital, Greater Baltimore Medical Center, Harbor Hospital, Harford Memorial Hospital, Howard County General Hospital, Johns Hopkins Hospital (JH), Johns Hopkins Bayview Hospital (JH Bayview), Mercy Medical Center, Northwest Hospital Center, Sinai Hospital, Saint Agnes Hospital (St. Agnes), Saint Joseph’s Hospital (St. Joseph), Union Memorial Hospital, University of Maryland Medical Center (UMCC), University of Maryland Medical Center Midtown (Midtown), and Upper Chesapeake Medical Center [1]. For each hospital, the County/Hospital Alert Tracking System (CHATS) generates real-time and historical data about the timing (i.e., start and end date and time) of alerts by the Maryland Institute for Emergency Medical Services Systems (MIEMSS) [2]. The event of high ER utilization or inaccessibility to ER may result in a hospital activating an alert status. Specifically, a yellow alert is initiated when the ER is experiencing a high level of crowding such that patients with urgent needs (e.g., emergency severity index level 2 and 3 patients) are not being managed safely. Under such circumstances, the ER will temporarily request that it receives no patients in need of acute medical care.

We present the total hours of the duration of yellow alerts in Maryland in Figure 6.1. The deeper the color is, the longer the total hours of yellow alert durations are. Compared to other regions in Maryland, we observe longer total hours of yellow alert durations in Region III. This observation motivates us to investigate more on the potential issues about ER accessibility in this region and if there are

any statistically significant risk factors related to increased ER crowding to help facilitate future management to improve this issue.

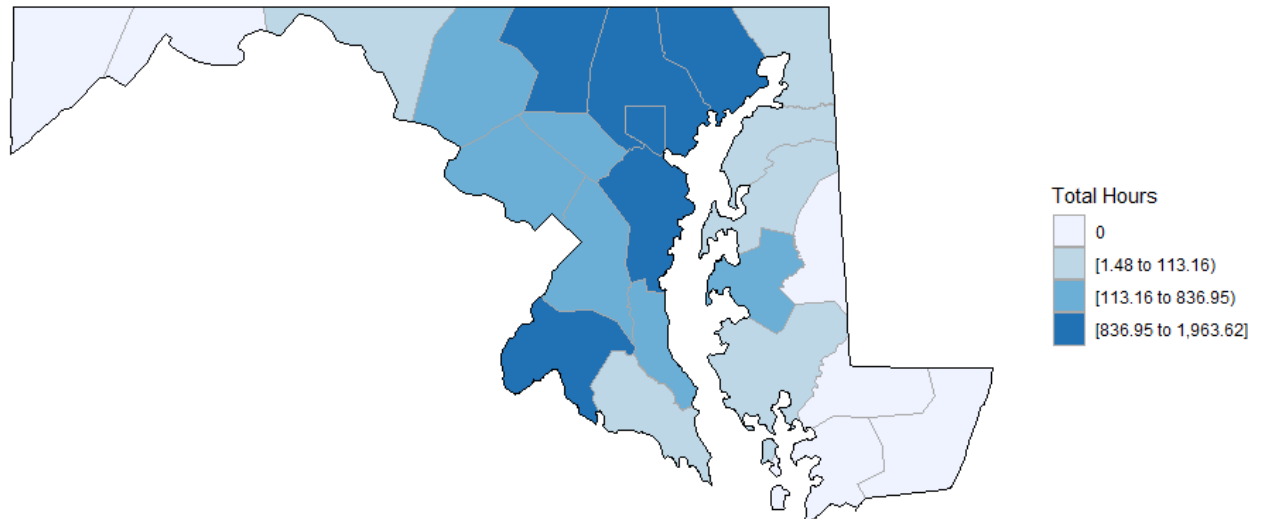


Figure 6.1: Choropleth map for the duration of yellow alerts in Maryland.

In this chapter, we particularly focus on one of the ER accessibility issues: the cascading problem. We illustrate this problem in Figure 6.2, where yellow indicates the occurrence of yellow alert in this hospital's ER. Figure 6.2 shows the yellow alert status for 21 hospitals in Maryland Region III from November 24 to November 29 in 2018. We can see that only a few hospitals have yellow alerts occasionally before November 27 and after. However, more than half of the 21 hospitals have yellow alerts around November 27. We call this scenario as a cascading event.

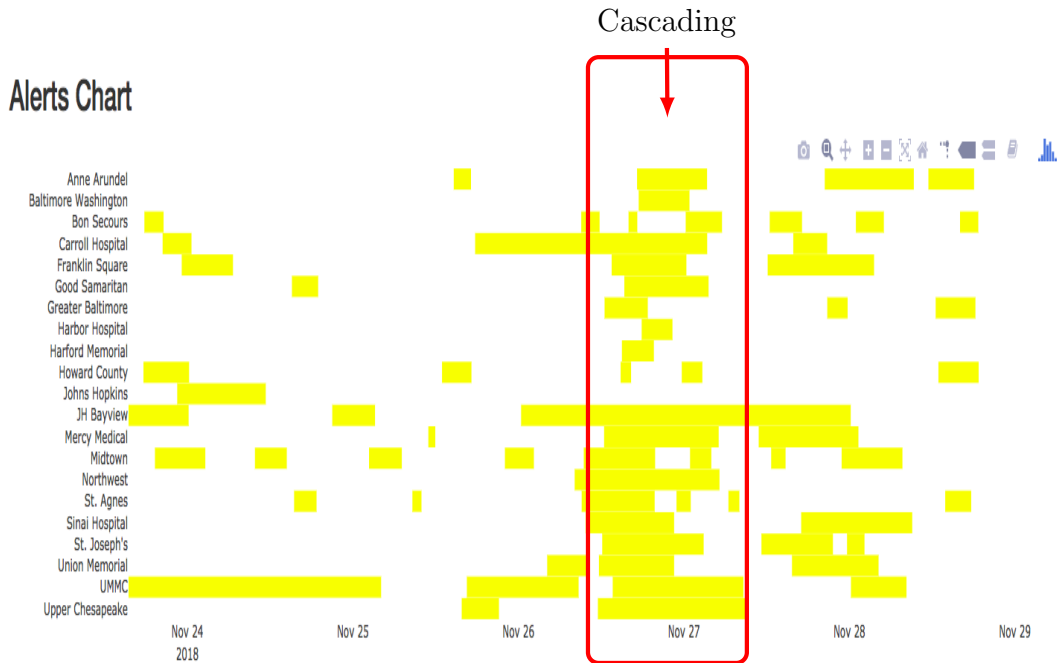


Figure 6.2: Cascading problem observed around November 27, 2018.

In this project, our goal is to model such a cascading problem, understand its evolution, and explore reasons that may cause the issue. We propose a multi-state Markov model to formulate the cascading problem, in which we use polynomial and Fourier series to approximate the general form of baseline intensities. Our proposed method is not limited to the case where the assumption of time-homogeneity holds, and could be used anywhere when intensities is time-sensitive [76, 77]. Furthermore, we develop an adjusted model to modify the hazard ratio in order to explain an cascading event. The cascading problem has several challenging characteristics. First, we need to find an appropriate model in order to translate the cascading problem into a mathematical and statistical model. After setting up this fundamental model, we can use more tools to quantify issues of interest. Unfortunately, we haven't seen any previous work related to this new healthcare issue arising from CHATS. The

second challenge is violation of the time-homogeneity assumption frequently used in multi-state Markov model. When intensities are time-dependent, such homogeneity model assumption becomes unrealistic. To address such limitations and overcome the challenges, we propose to utilize two types of functions of time to estimate the intensities in order to provide more flexibilities and better fit the data. Moreover, we need to develop an appropriate model to reduce time-varying hazard ratios, which explain significant impact to cascading issues from different hospitals.

The remaining sections of this chapter are organized as follows. In Section 6.2, we formulate our problem mathematically and present our proposed method for understanding the cascading transition via a multi-state Markov model. In Section 6.3, we extend the method to more general scenarios, and validate the performance of our proposed estimation method when the assumption of time-homogeneity is violated. In Section 6.4, we apply our proposed method to a dataset collected from CHATS from 2016 to 2018 and illustrate our findings, followed by Section 6.5, where we conclude with a brief discussion on our results and future work.

6.2 The Proposed Method Using Multi-state Markov Models

In this section, we introduce a modified multi-state Markov model to fit data arising from cascading problems in ER crowding. After we formulate the cascading events in this region using a multi-state Markov model, we propose to estimate the parameters of our scientific interest through maximum likelihood estimation (MLE) and derive the asymptotic distributions of our proposed estimators. Finally, we

present the hypothesis testing procedure for the cascading factors.

To start, we introduce two basic concepts in multi-state Markov model before we formally introduce the specific model for the cascading problem: the transition probability and intensity. The transition probability is the probability moving from one state to another state. When using continuous-time Markov models, a common assumption is the time-homogeneity assumption. Under this assumption, the transition probability only relies on the length of the time interval, denoted as s , no matter when it starts. That is, the transition probability is independent of the start time t . With time-homogeneity assumed, we have the following property of the transition probability that the next move of the process is from state i to state j :

$$P_{ij}(t, t + s) = P\{X(t + s) = j | X(t) = i\} = P_{ij}(s) \quad \text{for any states } i \text{ and } j.$$

The intensities describe the instantaneous rate of moving from state i to state j . The movement between states is represented by the transition intensities below.

$$\lambda_{ij}(t) = \lim_{s \rightarrow 0} \frac{P(X(t + s) = j | X(t) = i)}{s}$$

for states $i \neq j$. When the time-homogeneity assumption holds, the intensities remain constant over time. It has an obvious drawback ignoring time-dependent intensities. In the following, we will generalize the multi-state Markov model to accommodate more flexible forms of the intensities and the transition probabilities

when modeling the cascading events.

6.2.1 The Multi-state Markov Model

We use yellow alert as an example for presentation purpose. We model the time varying alert state of each hospital by a binary stochastic process:

$$\zeta_i(t) = \begin{cases} 1 & \text{if having yellow alerts at time } t \\ 0 & \text{otherwise} \end{cases}$$

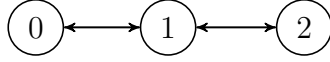
where $i = 1, \dots, 21$. That is, if hospital i has a yellow alert at time t , we define the alert state of hospital i , $\zeta_i(t)$, as 1. Otherwise, we have the state of hospital i at time t as 0. Then based on the alert process from all 21 hospitals, we define the alert status of the whole region III at any time t as $\zeta(t) = \sum_{i=1}^{21} \zeta_i(t)$. It is easy to see that $\zeta(t)$ ranges from 0 to 21.

Then with two pre-specified thresholds τ_1 and τ_2 , we define $X(t)$, the Markov state at time t with three levels of the region, as follows:

$$X(t) = \begin{cases} 0 & \text{if } \zeta(t) \leq \tau_1, \text{ (normal)} \\ 1 & \text{if } \tau_1 < \zeta(t) \leq \tau_2, \text{ (cascading level I)} \\ 2 & \text{if } \zeta(t) > \tau_2, \text{ (cascading level II)} \end{cases}$$

We model the evolution of the region state as a stochastic process using a continuous-time Markov chain. We illustrate the multi-state Markov model in the

diagram below:



where we define 0 as normal, 1 as cascading level I, and 2 as cascading level II, indicating three region states.

Starting from a normal status where the number of hospitals having yellow alerts at time t is less than or equal to τ_1 , the region remains at normal status unless more than τ_1 but less than τ_2 hospitals start to have yellow alerts which lead to less accessibility to emergency rooms. The region becomes very urgent once more than τ_2 hospitals start to have yellow alerts at time t . The region may transit between adjacent states among normal, cascading level I, and level II.

Given such a transition path defined above, we have the following intensity matrix:

$$\mathbf{Q}(t) = \{\lambda_{ij}(t)\} = \begin{pmatrix} \lambda_{00}(t) & \lambda_{01}(t) & 0 \\ \lambda_{10}(t) & \lambda_{11}(t) & \lambda_{12}(t) \\ 0 & \lambda_{21}(t) & \lambda_{22}(t) \end{pmatrix}$$

where each row sums to zero. Thus, the diagonal entries are $\lambda_{ii}(t) = -\sum_{j \neq i} \lambda_{ij}(t)$,

and

$$\lambda_{ij}(t) = \lim_{s \rightarrow 0} \frac{P(X(t+s) = j | X(t) = i)}{s}$$

for states $i \neq j$.

6.2.2 The Proposed Estimators and Asymptotic Distributions

To investigate the effects of covariates, we model the intensity $\lambda_{ij}(t)$ as

$$\lambda_{ij}(t) = \lambda_{ij}^0(t) \exp(\boldsymbol{\beta}\mathbf{x}),$$

where $\lambda_{ij}^0(t)$ represents the baseline intensity process,

$$\boldsymbol{\beta} = (\beta_0, \beta_1, \dots, \beta_n)$$

and

$$\mathbf{x}' = (x_0, x_1, \dots, x_n).$$

Here \mathbf{x} contains the variables of interest, and $\boldsymbol{\beta}$ contains the effect of covariates from state i to j . We generalize the baseline intensities by approximating $\log(\lambda_{ij}^0(t))$ using polynomial and Fourier series. Thus, this yields

$$\begin{aligned}\lambda_{ij}(t) &= \exp[\log\{\lambda_{ij}^0(t)\}] \exp(\boldsymbol{\beta}\mathbf{x}) \\ &= \exp(\boldsymbol{\alpha}_{ij}\mathbf{t}) \exp(\boldsymbol{\beta}\mathbf{x}) \\ &= \exp(\mathbf{b}_{ij}\mathbf{z})\end{aligned}$$

When using polynomial approximation, we define

$$\alpha'_{ij} = \begin{pmatrix} \alpha_0 \\ \alpha_1 \\ \alpha_2 \\ \cdot \\ \cdot \\ \cdot \\ \alpha_m \end{pmatrix}, \quad t = \begin{pmatrix} 1 \\ t \\ t^2 \\ \cdot \\ \cdot \\ \cdot \\ t^m \end{pmatrix}, \quad b'_{ij} = \begin{pmatrix} \alpha_0 \\ \cdot \\ \cdot \\ \alpha_m \\ \beta_0 \\ \cdot \\ \cdot \\ \beta_n \end{pmatrix}, \text{ and } z = \begin{pmatrix} 1 \\ \cdot \\ \cdot \\ t^m \\ x_0 \\ \cdot \\ \cdot \\ x_n \end{pmatrix}.$$

When using Fourier approximation, we define

$$\alpha'_{ij} = \begin{pmatrix} a_0 \\ a_1 \\ b_1 \\ \cdot \\ \cdot \\ \cdot \\ a_m \\ b_m \end{pmatrix}, \quad t = \begin{pmatrix} 1 \\ \cos t \\ \sin t \\ \cdot \\ \cdot \\ \cdot \\ \cos(mt) \\ \sin(mt) \end{pmatrix}, \quad b'_{ij} = \begin{pmatrix} a_0 \\ a_1 \\ b_1 \\ \cdot \\ \cdot \\ a_m \\ b_m \\ \beta_0 \\ \cdot \\ \cdot \\ \beta_n \end{pmatrix}, \text{ and } z = \begin{pmatrix} 1 \\ \cos t \\ \sin t \\ \cdot \\ \cdot \\ \cos(mt) \\ \sin(mt) \\ x_0 \\ \cdot \\ \cdot \\ x_n \end{pmatrix}.$$

The likelihood is then maximized over the corresponding parameter space for $\boldsymbol{\alpha}$ and $\boldsymbol{\beta}$. We suppose that the data consist of a series of transition times $\{t_1, \dots, t_k, \dots, t_{n_{ij}}\}$ and the corresponding transitions from i to j , where states i and $j \in S = \{0, 1, 2\}$. Also let $f_{ij}(t)$ denote the density, $F_{ij}(t)$ denote the cumulative density function, and $S_{ij}(t)$ denote the survival function corresponding to $\lambda_{ij}(t)$. We derive the likelihood function as follows:

$$\begin{aligned} L &= \prod_{(i,j) \in S} \prod_{k=1}^{n_{ij}} f_{ij}(t_k) \\ &= \prod_{(i,j) \in S} \prod_{k=1}^{n_{ij}} \lambda_{ij}(t_k) \exp \left\{ - \int_0^{t_k} \lambda_{ij}(s_k) ds_k \right\}. \end{aligned}$$

Then the log-likelihood function can be written as:

$$\begin{aligned} \log L &= \sum_{(i,j) \in S} \sum_{k=1}^{n_{ij}} \log \left\{ \lambda_{ij}(t_k) \exp \left(- \int_0^{t_k} \lambda_{ij}(s_k) ds_k \right) \right\} \\ &= \sum_{(i,j) \in S} \sum_{k=1}^{n_{ij}} \log \left\{ \exp(\boldsymbol{\alpha}_{ij} \mathbf{t}_k) \exp(\boldsymbol{\beta} \mathbf{x}) \exp \left(- \int_0^{t_k} \exp(\boldsymbol{\alpha}_{ij} \mathbf{s}_k) \exp(\boldsymbol{\beta} \mathbf{x}) ds_k \right) \right\} \\ &= \sum_{(i,j) \in S} \sum_{k=1}^{n_{ij}} \left\{ \boldsymbol{\alpha}_{ij} \mathbf{t}_k + \boldsymbol{\beta} \mathbf{x} - \int_0^{t_k} \exp(\boldsymbol{\alpha}_{ij} \mathbf{s}_k) \exp(\boldsymbol{\beta} \mathbf{x}) ds_k \right\} \end{aligned}$$

Using maximum likelihood estimation (MLE), we propose to estimate the parameters in the above model as:

$$\hat{\mathbf{b}}_{ij} = \operatorname{argmax}_{\mathbf{b}_{ij}} \sum_{(i,j) \in S} \sum_{k=1}^{n_{ij}} \left\{ \boldsymbol{\alpha}_{ij} \mathbf{t}_k + \boldsymbol{\beta} \mathbf{x} - \int_0^{t_k} \exp(\boldsymbol{\alpha}_{ij} \mathbf{s}_k) \exp(\boldsymbol{\beta} \mathbf{x}) ds_k \right\}.$$

Under regularity conditions, our proposed estimators $\hat{\mathbf{b}}_{ij}$ have excellent properties

such as consistency, efficiency, and asymptotic normality. The asymptotic distribution of $\hat{\mathbf{b}}_{ij}$ is

$$\sqrt{n_{ij}}(\hat{\mathbf{b}}_{ij} - \mathbf{b}_{ij}) \xrightarrow{\mathcal{D}} \mathcal{N}(0, I^{-1})$$

where I is the Fisher information for \mathbf{b}_{ij} . After some algebra and regular derivations, we summarize the asymptotic properties of $\hat{\alpha}_{ij}^0$, $\hat{\alpha}_{ij}^1$, and $\hat{\boldsymbol{\beta}}$ with the first order polynomial approximation in the following Theorems.

Theorem 6.1. *Under regularity conditions, the asymptotic distribution of $\hat{\alpha}_{ij}^0$ is*

$$\sqrt{n_{ij}}(\hat{\alpha}_{ij}^0 - \alpha_{ij}^0) \xrightarrow{\mathcal{D}} \mathcal{N}(0, I_{\alpha_{ij}^0}^{-1})$$

where

$$I_{\alpha_{ij}^0} = \frac{e^{\alpha_{ij}^0 + \boldsymbol{\beta}\mathbf{x}}}{\alpha_{ij}^1} \left\{ A e^{A/e_{ij}^1} \frac{1}{b\alpha_{ij}^1} \left(1 + \frac{1}{b}\right) e^{-b} - 1 \right\}, \quad A = e^{\alpha_{ij}^0 + \boldsymbol{\beta}\mathbf{x}}, \quad \text{and} \quad b = \frac{A}{\alpha_{ij}^1}.$$

Proof. We start from the full log likelihood function

$$\log L = \sum_{(i,j) \in S} \sum_{k=1}^{n_{ij}} \left\{ \alpha_{ij}^0 + \alpha_{ij}^1 t_k + \boldsymbol{\beta}\mathbf{x} - \int_0^{t_k} e^{\alpha_{ij}^0 + \alpha_{ij}^1 s_k} e^{\boldsymbol{\beta}\mathbf{x}} ds_k \right\}.$$

Then we calculate the second derivative of the log likelihood function:

$$\frac{\partial \log L}{\partial \alpha_{ij}^0} = n_{ij} - e^{\boldsymbol{\beta}\mathbf{x}} \sum_{k=1}^{n_{ij}} \int_0^{t_k} e^{\alpha_{ij}^0 + \alpha_{ij}^1 s_k} ds_k, \quad \frac{\partial^2 \log L}{\partial (\alpha_{ij}^0)^2} = -e^{\boldsymbol{\beta}\mathbf{x}} e^{\alpha_{ij}^0} \frac{1}{\alpha_{ij}^1} \left\{ \sum_{k=1}^{n_{ij}} e^{\alpha_{ij}^1 t_k} - n_{ij} \right\}.$$

Together with the following fact:

$$\begin{aligned}\mathbb{E} e^{\alpha_{ij}^1 t_k} &= \int_0^{t_k} e^{\alpha_{ij}^1 s_k} f_{ij}(s_k) ds_k \\ &= A e^{A/e_{ij}^1} \frac{1}{b \alpha_{ij}^1} \left(1 + \frac{1}{b}\right) e^{-b}\end{aligned}$$

where

$$A = e^{\alpha_{ij}^0 + \beta \mathbf{x}}, \quad \text{and} \quad b = \frac{A}{\alpha_{ij}^1},$$

we can derive the Fisher information as below:

$$I_{\alpha_{ij}^0} = -\frac{\mathbb{E} \frac{\partial^2 \log L}{\partial (\alpha_{ij}^0)^2}}{n_{ij}} = \frac{e^{\alpha_{ij}^0 + \beta \mathbf{x}}}{\alpha_{ij}^1} \left\{ A e^{A/e_{ij}^1} \frac{1}{b \alpha_{ij}^1} \left(1 + \frac{1}{b}\right) e^{-b} - 1 \right\}.$$

The results now follow. □

Theorem 6.2. *Under regularity conditions, the asymptotic distribution of $\hat{\alpha}_{ij}^1$ is*

$$\sqrt{n_{ij}}(\hat{\alpha}_{ij}^1 - \alpha_{ij}^1) \xrightarrow{\mathcal{D}} \mathcal{N}(0, I_{\alpha_{ij}^1}^{-1})$$

where

$$\begin{aligned}I_{\alpha_{ij}^1} &= \frac{e^{\beta \mathbf{x}}}{(\alpha_{ij}^1)^2} \left\{ e^{\alpha_{ij}^0} \left\{ E_1 - (\alpha_{ij}^1 + 1)E_2 + \alpha_{ij}^1 E_3 \right\} - e^{\alpha_{ij}^0} \right\}, \\ E_1 &= A e^{A/e_{ij}^1} \frac{1}{b \alpha_{ij}^1} \left(1 + \frac{1}{b}\right) e^{-b}, \quad E_2 = A e^{A/e_{ij}^1} \frac{1}{\alpha_{ij}^1} \frac{1}{b^2} \left\{ e^{-b} - E_i(-b) \right\}, \\ E_3 &= \frac{A e^{A/\alpha_{ij}^1}}{(\alpha_{ij}^1)^3 b^2} \left\{ \frac{2}{b} G_{2,3}^{3,0}(b | \begin{smallmatrix} 1,1 \\ 0,0,0 \end{smallmatrix}) + (2 - 2 \log(b)) \left\{ e^{-b} \log(b) + \Gamma(0, b) \right\} + \left\{ [\log(b)]^2 - 2 \log(b) \right\} e^{-b} \right\}\end{aligned}$$

$$A = e^{\alpha_{ij}^0 + \beta \mathbf{x}}, \quad \text{and} \quad b = \frac{A}{\alpha_{ij}^1}.$$

Proof. The proof is similar to that of Theorem 6.1, but the derivatives of the log likelihood function now are

$$\frac{\partial \log L}{\partial \alpha_{ij}^1} = \sum_k^{n_{ij}} t_k - \frac{e^{\beta \mathbf{x}}}{\alpha_{ij}^1} \sum_{k=1}^{n_{ij}} \left\{ (t_k - 1) e^{\alpha_{ij}^0 + \alpha_{ij}^1 t_k} + n_{ij} e^{\alpha_{ij}^0} \right\}$$

$$\frac{\partial^2 \log L}{\partial (\alpha_{ij}^1)^2} = -\frac{e^{\beta \mathbf{x}}}{(\alpha_{ij}^1)^2} \left\{ e^{\alpha_{ij}^0} \sum_{k=1}^{n_{ij}} \left\{ \underbrace{e^{\alpha_{ij}^1 t_k}}_1 - (\alpha_{ij}^1 + 1) \underbrace{t_k e^{\alpha_{ij}^1 t_k}}_2 + \alpha_{ij}^1 \underbrace{(t_k)^2 e^{\alpha_{ij}^1 t_k}}_3 \right\} - n_{ij} e^{\alpha_{ij}^0} \right\}.$$

Hence, we need to calculate the expectations for parts 1, 2, and 3, respectively.

For part 1,

$$\mathbb{E} e^{\alpha_{ij}^1 t_k} = A e^{A/e_{ij}^1} \frac{1}{b \alpha_{ij}^1} \left(1 + \frac{1}{b}\right) e^{-b} = E_1,$$

and for part 2,

$$\mathbb{E} t_k e^{\alpha_{ij}^1 t_k} = A e^{A/e_{ij}^1} \frac{1}{\alpha_{ij}^1} \frac{1}{b^2} \{e^{-b} - E_i(-b)\} = E_2$$

where E_i denotes the exponential integral.

For part 3,

$$\mathbb{E} (t_k)^2 e^{\alpha_{ij}^1 t_k} = \frac{A e^{A/\alpha_{ij}^1}}{(\alpha_{ij}^1)^3 b^2} \left\{ \frac{2}{b} G_{2,3}^{3,0} \left(b \mid \begin{matrix} 1,1 \\ 0,0,0 \end{matrix} \right) + (2 - 2 \log(b)) \{e^{-b} \log(b) + \Gamma(0, b)\} + \{[\log(b)]^2 - 2 \log(b)\} e^{-b} \right\} = E_3,$$

where $G_{p,q}^{m,n} \left(z \mid \begin{matrix} a_1, \dots, a_p \\ b_1, \dots, b_q \end{matrix} \right)$ is the Meijer G-function and $\Gamma(0, x)$ is the incomplete gamma function.

Thus, it yields the Fisher information below

$$I_{\alpha_{ij}^1} = -\frac{\mathbb{E} \frac{\partial^2 \log L}{\partial (\alpha_{ij}^1)^2}}{n_{ij}} = \frac{e^{\beta \mathbf{x}}}{(\alpha_{ij}^1)^2} \left\{ e^{\alpha_{ij}^0} \left\{ E_1 - (\alpha_{ij}^1 + 1)E_2 + \alpha_{ij}^1 E_3 \right\} - e^{\alpha_{ij}^0} \right\},$$

and then Theorem 6.2 follows. \square

Theorem 6.3. *Under regularity conditions, the asymptotic distribution of $\hat{\beta}$ is*

$$\sqrt{n_{ij}}(\hat{\beta} - \beta) \xrightarrow{\mathcal{D}} \mathcal{N}(0, I_{\beta}^{-1}),$$

where

$$I_{\beta} = -e^{\beta \mathbf{x}} \mathbf{x}^2 \sum_{(i,j) \in \mathcal{S}} \left\{ \frac{e^{\alpha_{ij}^0}}{\alpha_{ij}^1} \left\{ A e^{A/e_{ij}^1} \frac{1}{b \alpha_{ij}^1} \left(1 + \frac{1}{b}\right) e^{-b} - 1 \right\} \right\}, \quad A = e^{\alpha_{ij}^0 + \beta \mathbf{x}}, \quad \text{and} \quad b = \frac{A}{\alpha_{ij}^1}.$$

Proof. A similar proof applies. Now the first and second derivatives of the log likelihood function with respect to β are

$$\frac{\partial \log L}{\partial \beta} = \sum_{(i,j) \in \mathcal{S}} \sum_{k=1}^{n_{ij}} \left\{ \mathbf{x} - e^{\beta \mathbf{x}} \mathbf{x} \int_0^{t_k} e^{\alpha_{ij}^0 + \alpha_{ij}^1 s_k} ds_k \right\}$$

and

$$\frac{\partial^2 \log L}{\partial (\beta)^2} = \sum_{(i,j) \in \mathcal{S}} \sum_{k=1}^{n_{ij}} -e^{\beta \mathbf{x}} \mathbf{x}^2 \int_0^{t_k} e^{\alpha_{ij}^0 + \alpha_{ij}^1 s_k} ds_k.$$

Then, we derive the expectation of the second partial derivative as

$$\begin{aligned}\mathbb{E} \frac{\partial^2 \log L}{\partial \beta^2} &= \sum_{(i,j) \in S} \sum_{k=1}^{n_{ij}} -e^{\beta \mathbf{x}} \mathbf{x}^2 \mathbb{E} \int_0^{t_k} e^{\alpha_{ij}^0 + \alpha_{ij}^1 s_k} ds_k \\ &= \sum_{(i,j) \in S} \sum_{k=1}^{n_{ij}} -e^{\beta \mathbf{x}} \mathbf{x}^2 \frac{e^{\alpha_{ij}^0}}{\alpha_{ij}^1} \left\{ A e^{A/e_{ij}^1} \frac{1}{b \alpha_{ij}^1} \left(1 + \frac{1}{b}\right) e^{-b} - 1 \right\}.\end{aligned}$$

Thus, we have

$$I_{\beta} = \frac{-\mathbb{E} \frac{\partial^2 \log L}{\partial \beta^2}}{n_{ij}} = -e^{\beta \mathbf{x}} \mathbf{x}^2 \sum_{(i,j) \in S} \left\{ \frac{e^{\alpha_{ij}^0}}{\alpha_{ij}^1} \left\{ A e^{A/e_{ij}^1} \frac{1}{b \alpha_{ij}^1} \left(1 + \frac{1}{b}\right) e^{-b} - 1 \right\} \right\}$$

where

$$A = e^{\alpha_{ij}^0 + \beta \mathbf{x}}, \quad \text{and} \quad b = \frac{A}{\alpha_{ij}^1}.$$

Therefore, Theorem 6.3 follows. □

6.2.3 Hypothesis Testing

We further investigate the reasons that may cause the cascading problem in this region. It is reasonable to believe that continuous yellow alerts at some big hospitals such as University of Maryland Medical Center (UMMC) or John Hopkins Hospital (JH) makes ERs in the region hardly accessible. Thus, identifying such hospitals is the first step to solve the cascading issue. We name such hospitals as indicator hospitals. To achieve this goal, we need to compare cascading events caused by indicator hospitals and those caused by non-indicator hospitals. In the following multi-state Markov model, we include a binary indicator variable x to

denote whether the cascading event is caused by an indicator hospital or not. Then the hazard ratio can be interpreted as the differences between two cases. We have the model

$$\lambda_{ij}(t) = \lambda_{ij}^0(t)e^{\beta_{ij}x}$$

where $x = 1$ if the cascading event is caused by indicator hospitals, and $x = 0$, otherwise. Thus, $\beta_{ij} = \log(HR_{ij})$ where HR_{ij} is a hazard ratio comparing state i versus state j . Hence, the null and alternative hypotheses for the test of the effect of indicator hospitals are

$$H_0 : \beta_{ij} = 0 \quad \text{for all } i, j \quad \text{vs.} \quad H_1 : \beta_{ij} \neq 0 \quad \text{for some } i, j.$$

Given the natural order as we define the levels of region alert states $X(t)$, we modify the Markov model accordingly to make sure that the state-wise hazard ratio always follows one direction. Here hazard ratios provide group comparisons in terms of inaccessibility of ERs in the region over time:

$$\lambda_{ij}(t) = \lambda_{ij}^0(t)e^{\beta_{ij}x}$$

where $\beta_{ij} = (-1)^{I\{i>j\}}\beta$, i.e.

$$\beta_{ij} = \begin{cases} \beta & i < j \\ -\beta & i > j. \end{cases}$$

Therefore, the hypotheses becomes

$$H_0 : \beta = 0 \quad vs. \quad H_1 : \beta \neq 0,$$

and $\beta = \log(HR)$. The parameter estimation is similar as in Section 6.2.2. Following Wilks' theorem [142], the asymptotic distribution of the likelihood ratio test (LRT) statistic (L_0/L_1) , where L_0 is the maximum value of the likelihood under H_0 and L_1 is the maximum value of the likelihood across the full parameter space, is as follows:

$$-2 \log\left(\frac{L_0}{L_1}\right) \xrightarrow{\mathcal{D}} \chi_1^2$$

where χ_1^2 is a χ^2 random variable with 1 degree of freedom.

6.3 Simulation

In this section, we validate the finite sample performances of our proposed methods via simulation studies. We approximate the intensities by either polynomial and Fourier series. In order to demonstrate the flexibility of our methods, we consider two scenarios: (1) intensities are time-homogeneous in Section 6.3.1 and (2) intensities are time-heterogeneous in Section 6.3.2.

6.3.1 The Time-homogeneous Scenario

When intensities are time-homogeneous, they remain constant over time. Specifically, we generate the transition time between different states from an exponential

distribution. We denote t_{ij} time until transition from state i to j where $i, j \in \{0, 1\}$. In the time-homogeneous scenario, we assume that $t_{01} \sim \text{Exp}(1/7)$, $t_{10} \sim \text{Exp}(1)$, $t_{12} \sim \text{Exp}(1)$, and $t_{21} \sim \text{Exp}(1)$. Here, $\text{Exp}(\lambda)$ denotes an exponential distribution with rate parameter λ , that is, the density function is $f(t) = \lambda e^{-\lambda t}$ and the hazard rate is λ . The intensity matrix is

$$\mathbf{Q}(\mathbf{t}) = \begin{pmatrix} -1/7 & 1/7 & 0 \\ 1 & -2 & 1 \\ 0 & 1 & -1 \end{pmatrix}.$$

We simulate the cascading transition process across a 3-year period to avoid a factor of seasonality. We generate data as follows:

1. The region starts from state 0.
2. If the region starts in state 0, we simulate $t_{00} \sim \exp(-\lambda_{00})$, and then at time t_{00} it jumps to 1.
3. If the region starts in state 1, we simulate $t_{11} \sim \exp(-\lambda_{11})$, and then it jumps to 0 with probability $-\frac{\lambda_{10}}{\lambda_{11}}$. Otherwise, it jumps to 2.
4. If the region starts with state 2, we simulate $t_{22} \sim \exp(-\lambda_{22})$, and then it jumps to 1.
5. We repeat steps 2 to 4 until the total time reaches 3 years.

When the assumption of time-homogeneity for intensities holds, the simulation for cascading transition in the region within a month can be illustrated in Figure

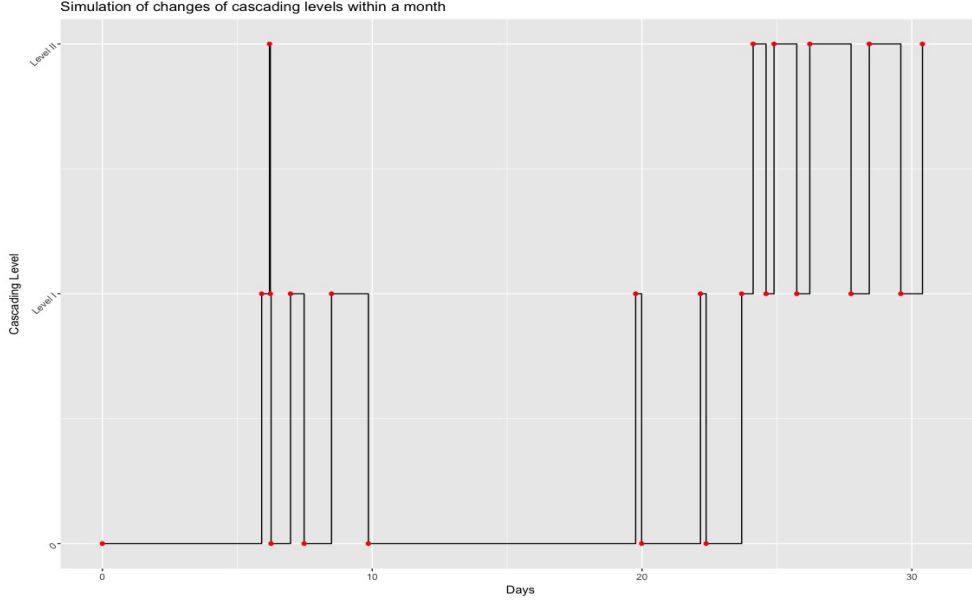


Figure 6.3: A cascading simulation in the region within a month in the time-homogeneous scenario.

6.3.

We validate the goodness of fit by comparing between true and estimated survival curves between transition states in terms of Mean Integrated Squared Error (MISE):

$$MISE = \mathbb{E} \int_0^t (S_{ij}(t) - \widehat{S}_{ij}(t))^2 dt = \frac{1}{K} \sum_{k=1}^K \int_0^t (S_{ij}(t) - \widehat{S}_{ij}^k(t))^2 dt,$$

where K is number of simulated datasets. Due to the complexity of likelihood function when using Polynomial or Fourier approximations, we numerically maximize the likelihood function to estimate the desired parameters. The underline true survival and the estimated survival are shown in Figures 6.4 and 6.5 for using Polynomial and Fourier approximations respectively. In Table 6.1, we summarize the estimated MISEs when using different order-Polynomial or Fourier approximations

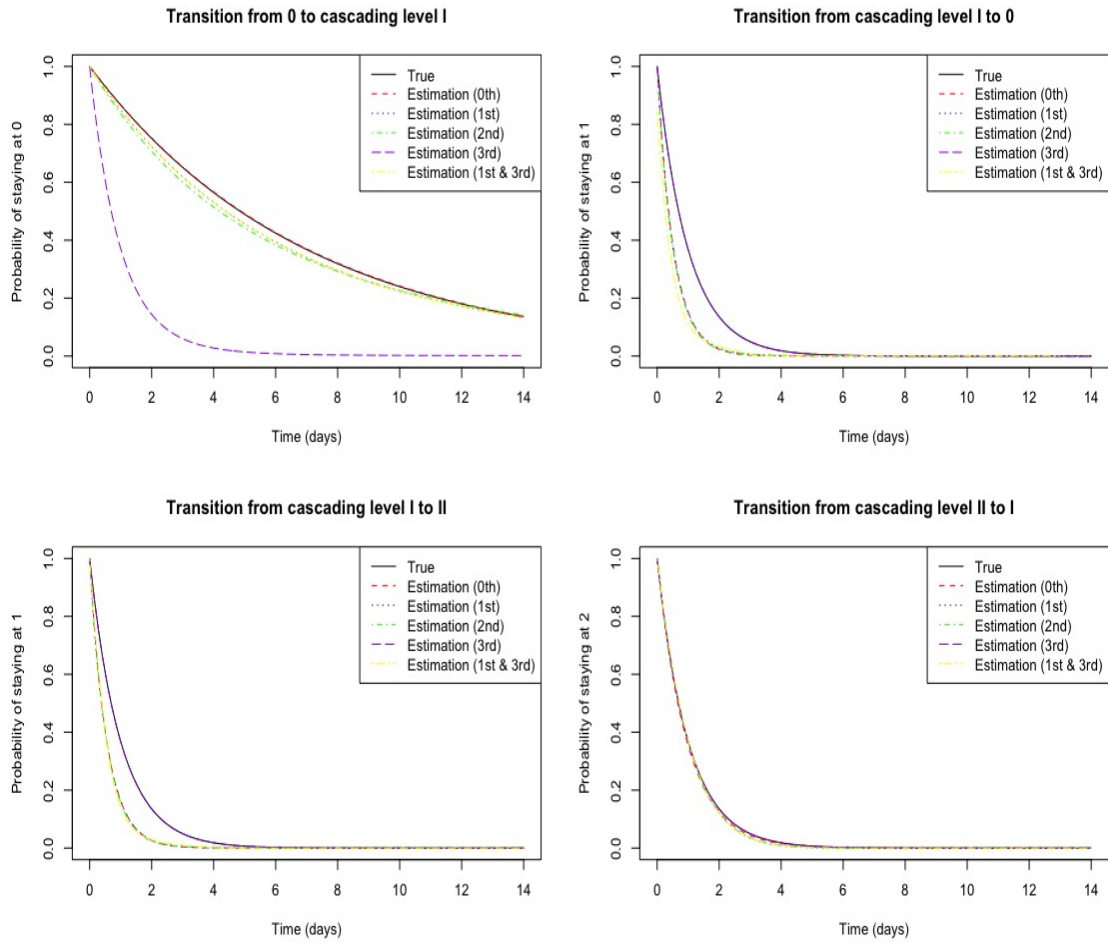


Figure 6.4: The comparison between true and estimated survival curves between states by polynomial approximation in time-homogeneous scenario.

for the time-homogeneous scenario.

More specifically, we employ constant, first, second, third, and combination of first and third order polynomial approximations (Figure 6.4 and Table 6.1). The 3rd order polynomial approximation diverges from the true survival curve when fitting transitions from normal ER level to Cascading level I, while other cases yield an estimated survival curve close to the truth and achieve small MISEs. In transition from Cascading level I to Normal ER level or from Cascading I to II, the 3rd order

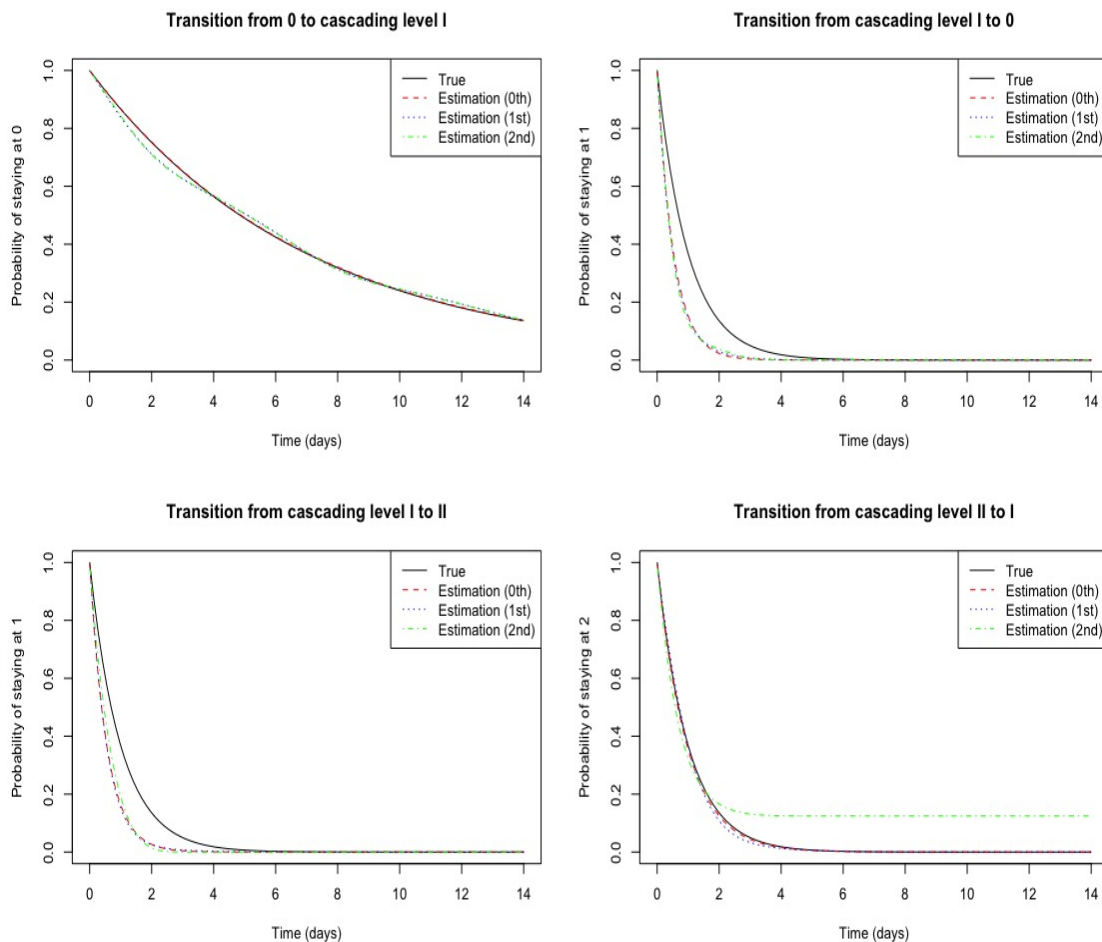


Figure 6.5: The comparison between true and estimated survival curves between states by Fourier approximation in time-homogeneous scenario.

polynomial approximation can estimate the true survival curve better compared to lower orders of approximations. All work well for the transition from Cascading level II to I, and have been validated.

Similarly, we try Fourier approximations with the constant, first and second order Fourier series in Figure 6.5 and Table 6.1. For the transition from normal ER level to Cascading level I, all methods fit the data well and yield good estimates of the true survival curve. They all diverge a little bit from the true survival curves for

transition from ER Cascading level I to Normal ER status and from Cascading level I to level II. Compared to the case using the second order Fourier series, constant or the first order Fourier approximation performs better for the transition from ER Cascading level II to level I.

Survival function	Polynomial				Fourier	
	0th	1st	2nd	3rd	1st	2nd
S_{01}	0.0085	0.0259	0.0164	0.3407	0.0037	0.0004
S_{10}	0.0795	0.0692	0.0967	0.0131	0.093	0.1115
S_{12}	0.0796	0.094	0.0889	0.0151	0.0919	0.0825
S_{21}	0.0019	0.0016	0.0035	0.0001	0.0017	0.0045

Table 6.1: Summary of MISE for time-homogeneous scenario.

6.3.2 The Time-Heterogeneous Scenario

A more common or more general scenario assumes no time-homogeneity for intensities, which means that the intensities rely on time. In such scenarios, we assume the transition time between states follows a Weibull distribution. Let $\text{Weibull}(p, q)$ denote a Weibull distribution with shape and scale parameters, p and q , then its density function is $g(t) = (p/q)(t/q)^{p-1}e^{-(t/q)^p}$ and hazard rate is $h(t) = (p/q^p)t^{p-1}$. We assume that $t_{01} \sim \text{Weibull}(3, 8)$, $t_{10} \sim \text{Weibull}(4,1)$, $t_{12} \sim \text{Weibull}(4, 1)$, and $t_{21} \sim \text{Weibull}(3,1)$. Since each row of the intensity matrix is supposed to sum to zero, we specify the intensity matrix as follows:

$$\mathbf{Q}(t) = \begin{pmatrix} -\frac{3}{8^3}t^2 & \frac{3}{8^3}t^2 & 0 \\ 4t^3 & -8t^3 & 4t^3 \\ 0 & 3t^2 & -3t^2 \end{pmatrix}.$$

The data can be generated in the following manner:

1. The region starts from state 0.
2. If the region starts with state 0, we simulate $t_{00} \sim \text{Weibull}(3, 8)$, then it jumps to 1.
3. If the region starts with state 1, we simulate $t_{11} \sim \text{Weibull}(4, (1/2)^{1/4})$, then it jumps to 0 with probability $-\frac{\lambda_{10}(t)}{\lambda_{11}(t)}$. Otherwise, it jumps to 2.
4. If the region starts with state 2, we simulate $t_{22} \sim \text{Weibull}(3, 1)$, then it jumps to 1.
5. We repeat steps 2 to 4 until the total time reaches 3 years.

The simulated data for cascading transition in a region within the first month assuming time-heterogeneous intensities is illustrated in Figure 6.6.

In Figures 6.7 and 6.8, we compared our estimated survival curves using Polynomial and Fourier approximations with the true survival curve. In Table 6.2, we report the MISEs calculated by using each type of Polynomial and Fourier series. We found that the third order Polynomial dramatically diverge from the underlying true survival curve in the transition from ER normal level to Cascading level I. For the other three transitions, the first and second order Polynomial series perform better than the rest by a smaller MISE. It turns out that there is no statistically significant difference after four weeks for the transition from cascading level I to normal, cascading level I to II, and cascading level II to I. When using either constant,

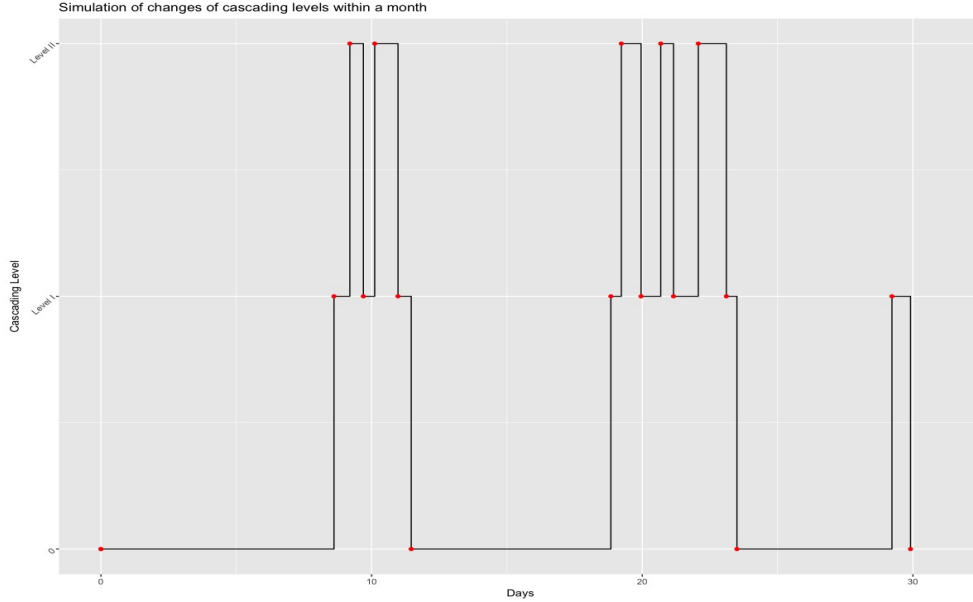


Figure 6.6: A cascading simulation in the region within a month in time-inhomogeneous scenario.

or the first and second order Fourier series for the proposed method, all three models obtain an estimate that diverge from the true survival curves at certain levels when fitting the transition from ER normal status and Cascading level I. For the other three transitions between Markov states, the first and second order Fourier approximation perform relatively better, but it does not demonstrate dramatically better performance after staying at the current states for more than four weeks.

Survival function	Polynomial				Fourier	
	0th	1st	2nd	3rd	1st	2nd
S_{01}	0.4812	0.0259	0.0388	4.19	0.0429	0.3868
S_{10}	0.1098	0.0313	0.032	0.0968	0.0323	0.0362
S_{12}	0.1099	0.0172	0.0175	0.0968	0.0323	0.0362
S_{21}	0.0699	0.0015	0.0031	0.0709	0.0014	0.0011

Table 6.2: Summary of MISE for time-inhomogeneous case.

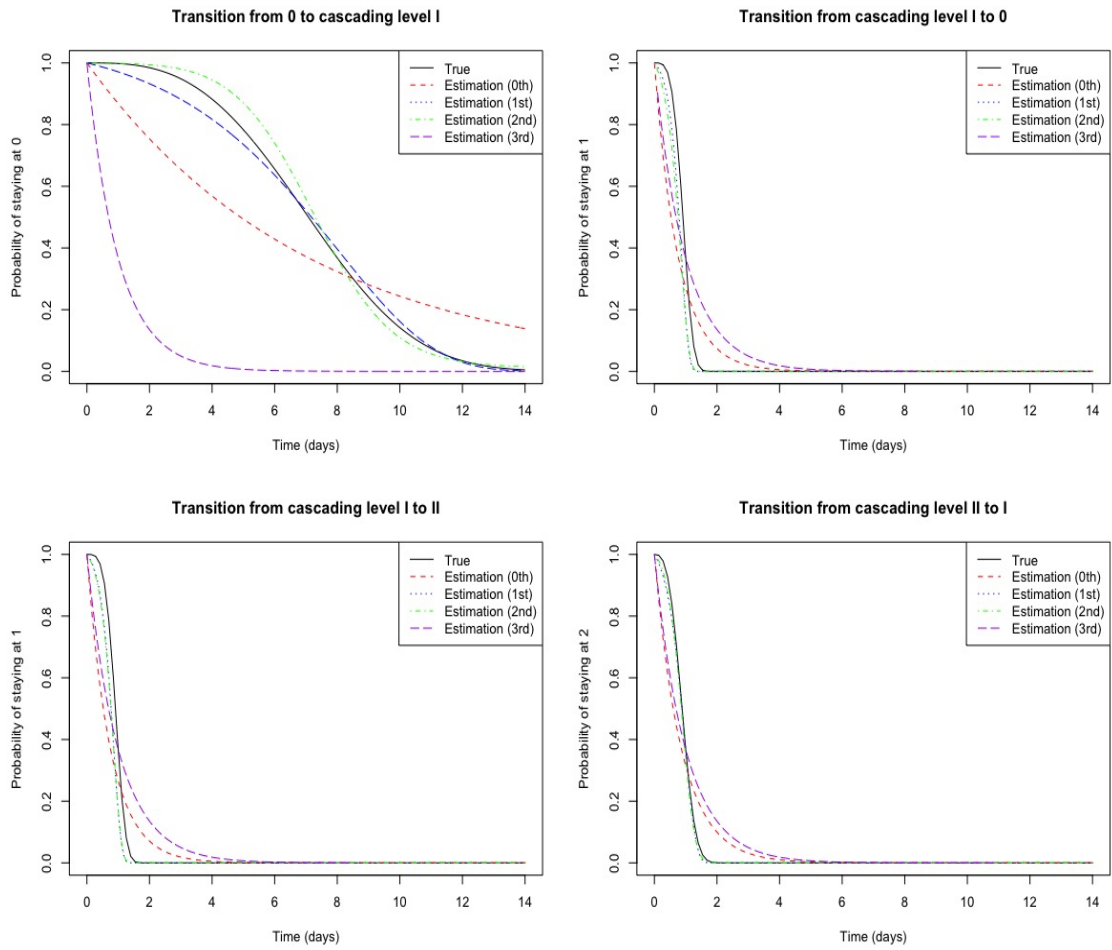


Figure 6.7: The comparison between true and estimated survival curves between states by polynomial approximation in time-inhomogeneous scenario.

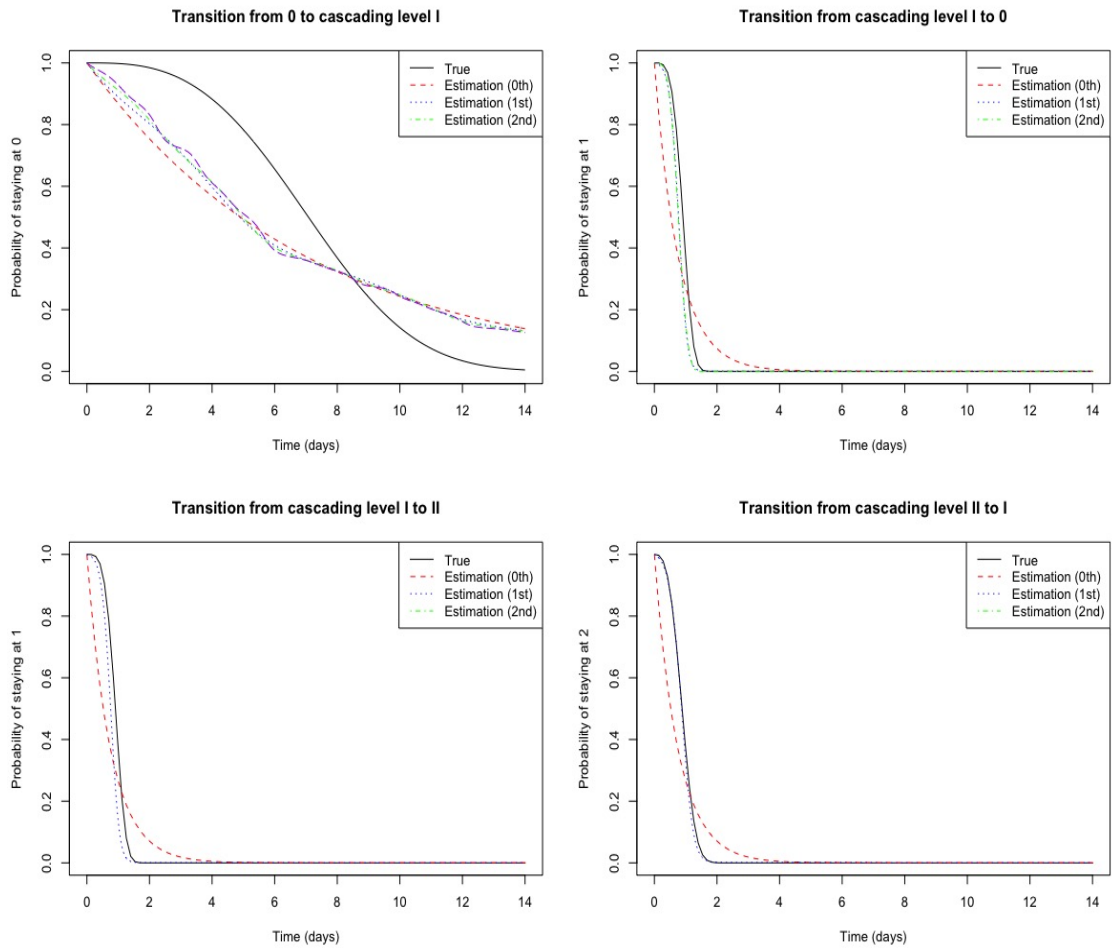
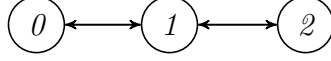


Figure 6.8: The comparison between true and estimated survival curves between states by Fourier approximation in time-inhomogeneous scenario.

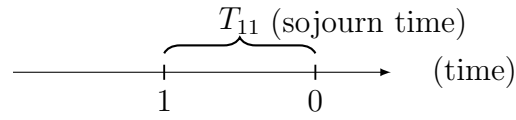
In fact, we have the following Theorem about the jumping probabilities.

Theorem 6.4. *In the multi-state Markov model illustrated by diagram below:*



the jumping probability from 1 to 0 is $-\frac{\lambda_{10}(t)}{\lambda_{11}(t)}$.

Proof. Let T_{ij} denote a random variable for sojourn time from state i to j .



Considering an infinitely small time period Δt , then

$$\begin{aligned}
 & Pr(\text{jump to 0 after staying at 1 for } t_{11}) \\
 &= Pr(T_{10} < T_{12} | T_{11} \in (t_{11}, t_{11} + \Delta t)) \\
 &= \frac{Pr(T_{10} < T_{12}, t_{11} \leq T_{11} \leq t_{11} + \Delta t)}{F_{11}(t_{11} + \Delta t) - F_{11}(t_{11})} \\
 &= \frac{(\int_{t_{11}}^{t_{11} + \Delta t} S_{12}(t) dF_{10}(t)) / \Delta t}{(F_{11}(t_{11} + \Delta t) - F_{11}(t_{11})) / \Delta t} = \frac{S_{12}(t) f_{10}(t)}{f_{11}(t)} \text{ (as } \Delta t \rightarrow 0) \\
 &= \frac{S_{11}(t) f_{10}(t)}{S_{10}(t) f_{11}(t)} = -\frac{\lambda_{10}(t)}{\lambda_{11}(t)}
 \end{aligned}$$

□

6.3.3 Hypothesis Testing

Additionally, we validate the performance in the adjusted model using simulations. In this simulation, we assume constant intensities and constant hazard ratio

(HR). Specifically, we assume HR is 0.5 and the intensity matrix in one group is

$$\mathbf{Q}(\mathbf{t}) = \begin{pmatrix} -1/7 & 1/7 & 0 \\ 1 & -2 & 1 \\ 0 & 1 & -1 \end{pmatrix},$$

and the intensity matrix in another group is

$$\mathbf{Q}(\mathbf{t}) = \begin{pmatrix} -2/7 & 2/7 & 0 \\ 1/2 & -5/2 & 2 \\ 0 & 1/2 & -1/2 \end{pmatrix}.$$

We evaluate each parameter estimation in terms of Mean Squared Error (MSE) and bias in the tables below. Small MSEs and biases in Table 6.3 for the adjusted model and Table 6.4 for the full model indicate that the proposed method work well in both cases.

critierion	λ_{01}	λ_{10}	λ_{12}	λ_{21}	HR
MSE	2.16e-02	6.41e-02	4.78e-02	1.8e-02	2.97e-02
Bias	-0.0144	-0.0024	0.0064	-0.0012	0.0403

Table 6.3: Simulation results for the adjusted model.

critierion	λ_{01}	λ_{10}	λ_{12}	λ_{21}	HR_{01}	HR_{10}	HR_{12}	HR_{21}
MSE	2.1528e-02	8.2348e-03	4.7707e-02	2.1817e-02	8.0841e-03	4.403e-02	2.2601e-01	1.826e-02
Bias	-0.0143	-0.0026	0.0064	-0.0012	0.0045	0.0113	-0.1699	0.0472

Table 6.4: Simulation results for the model with varying HR between states.

6.4 Real Data Analysis

In this section, we analyze the yellow alerts data collected from CHATS for all emergency rooms in 21 hospitals in region III from 2016 to 2018. We first evaluate the transition between different levels of accessibility in emergency rooms. To achieve this goal, we employ a multi-state Markov model using the proposed and generalized methods described above. In addition, we further investigate the underlying reasons that may cause the cascading events in order to support better decision-making for both patients and hospital administrators.

To understand the evolution in the proposed multi-state Markov model, we consider the following transition probabilities and intensities.

- Transition probabilities:

$$P_{ij}(t, t + s) = P(X(t + s) = j | X(t) = i) = P_{ij}(t) \quad \text{for any states } i \text{ and } j.$$

- Intensity matrix $\mathbf{Q}(t) = \{\lambda_{ij}(t)\}$ whose rows sum to zero, diagonal entries are

$$\lambda_{ii} = -\sum_{i \neq j} \lambda_{ij}, \text{ and}$$

$$\lambda_{ij}(t) = \lim_{s \rightarrow 0} \frac{P(X(t + s) = j | X(t) = i)}{s}$$

for states $i \neq j$.

- Transition probabilities and intensities are connected via Kolmogorov equation

$$\mathbf{P}'(\mathbf{t}) = \mathbf{Q}(\mathbf{t})\mathbf{P}(\mathbf{t}) \quad \text{where } \mathbf{P}(\mathbf{t}) = \{P_{ij}(t)\}.$$

Thus, we solve for $P_{01}(t)$, $P_{11}(t)$, and $P_{21}(t)$ via the following system of ODE using the Runge-Kutta method.

$$P'_{01}(t) = \lambda_{00}(t)P_{01}(t) + \lambda_{01}(t)P_{11}(t)$$

$$P'_{21}(t) = \lambda_{21}(t)P_{11}(t) + \lambda_{22}(t)P_{21}(t)$$

$$P'_{11}(t) = \lambda_{10}(t)P_{01}(t) + \lambda_{11}P_{11}(t) + \lambda_{12}(t)P_{22}(t)$$

In the system of ODE, we try different ways to approximate the intensities using Polynomials or Fourier series. Among all approximations, the second order polynomial performs the best and achieves a better goodness of fit to the data, and we have the empirical transition probability calculated as below:

$$\tilde{P}_{ij}(t) = \frac{\# \text{ of transitions to state } j \text{ from } i \text{ at time } t}{\text{total number of transitions starting from state } i}$$

where $i, j = 0, 1, 2$.

In Figure 6.9, we visualize our estimated transition probabilities from normal ER status to Cascading level I compared to the empirical data. As we can see, the estimated curve oscillate around the empirical one within two weeks and it achieves

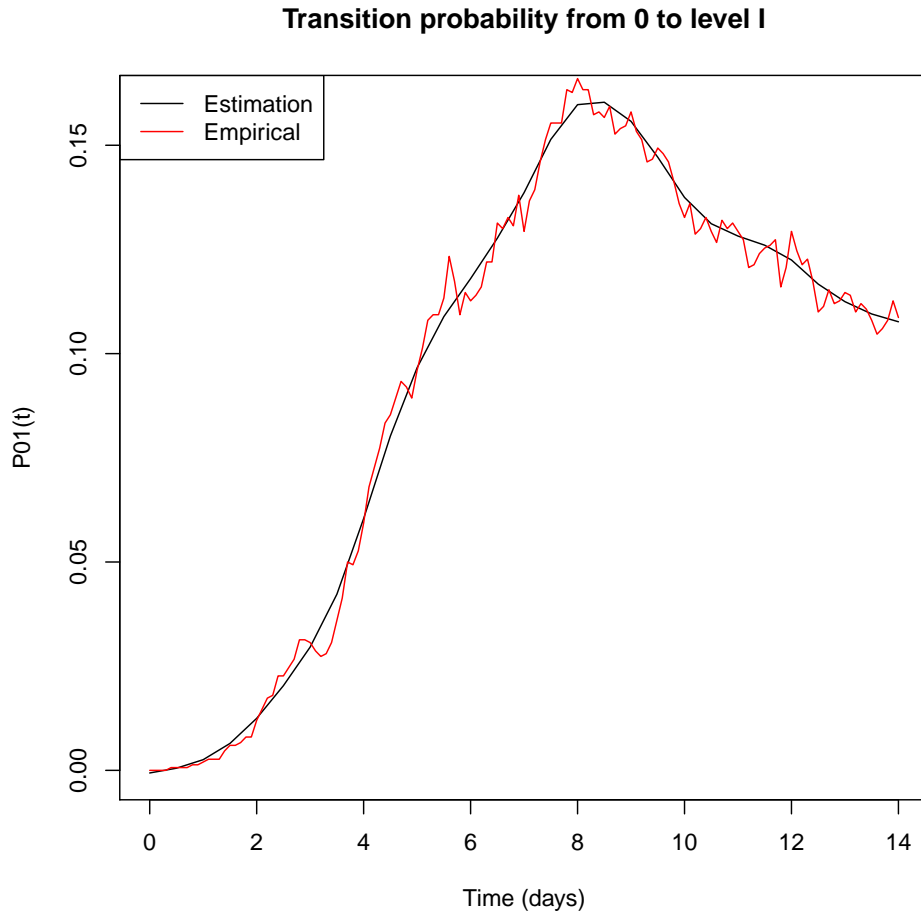


Figure 6.9: Empirical and estimated transition probability from normal to cascading level I within two weeks.

the maximum after one week at around Day 8.

In order to find indicator hospitals that may cause the cascading effects, we conduct analyses to explore the connection between hospitals by calculating the conditional probabilities below:

$$Pr(\text{hospital } j \text{ will have a yellow alert} | \text{hospital } i \text{ is having a yellow alert}) \\ = \frac{\text{total duration of simultaneous yellow alerts at both hospitals } i \text{ and } j}{\text{total duration of yellow alerts in hospital } i}$$

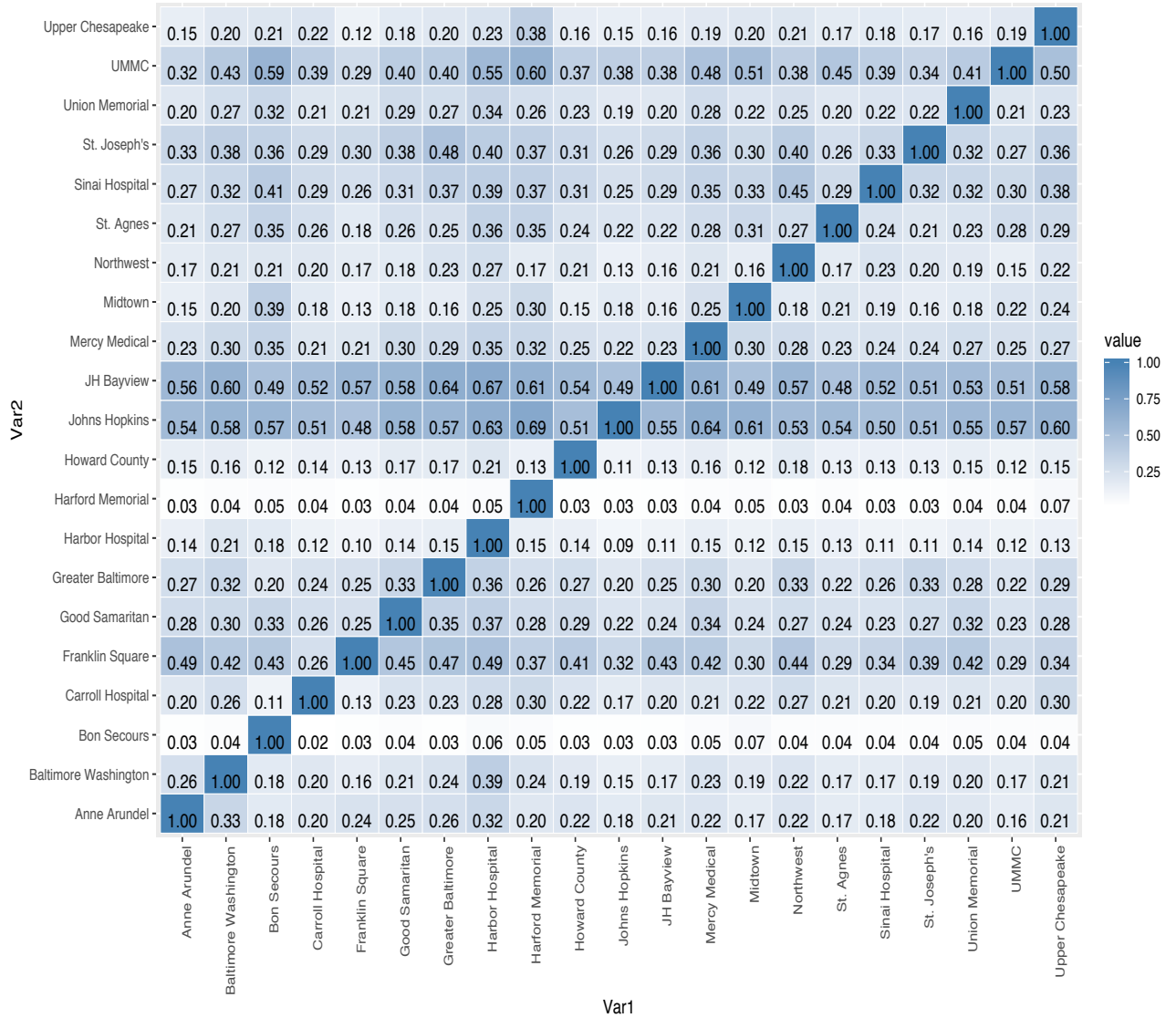
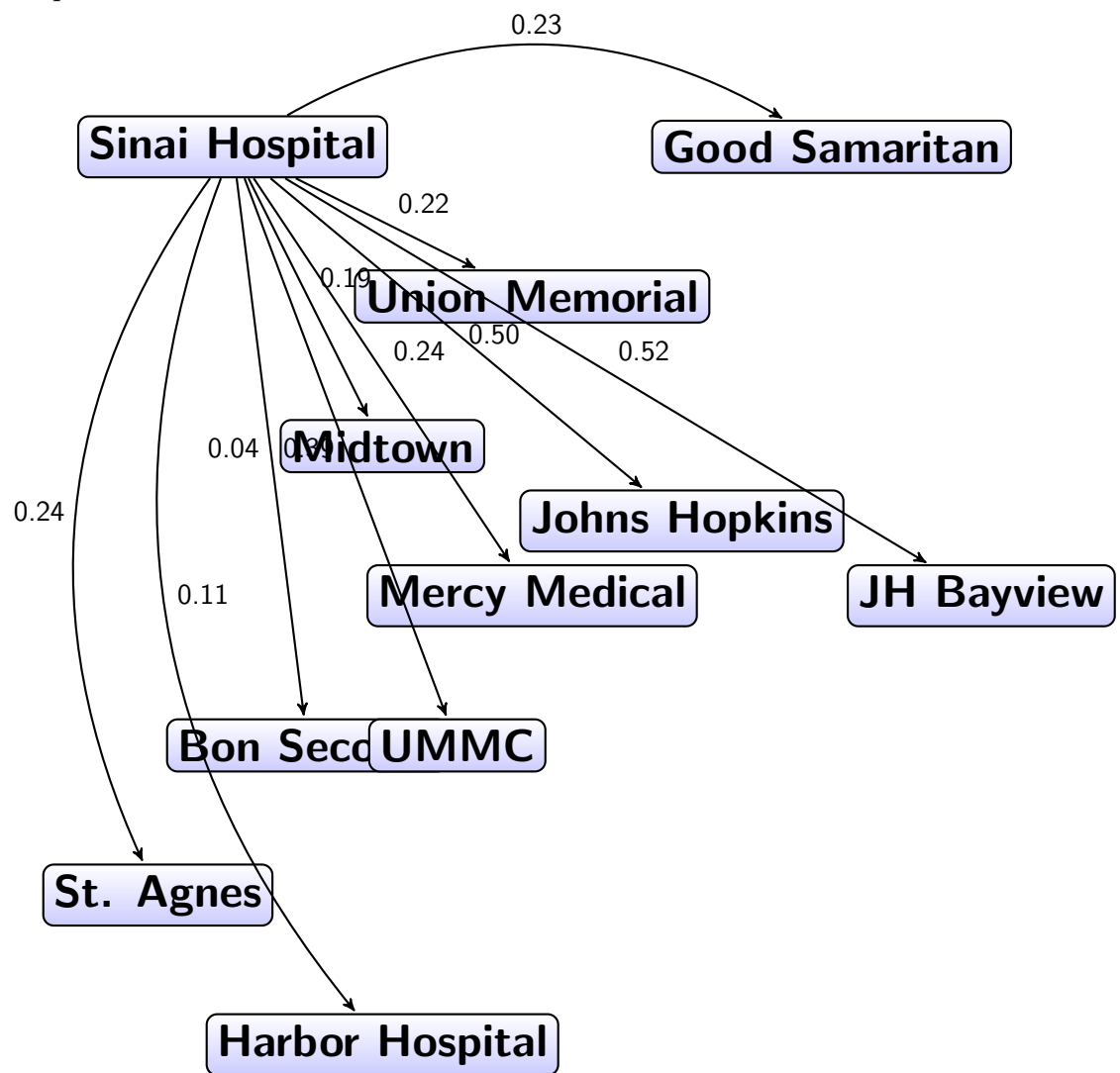


Figure 6.10: Probability of having a yellow alert at hospital i conditional on hospital j having a yellow alert.

To better illustrate the results in Figure 6.10, we demonstrate the connections between hospitals in the following diagram. For instance, we list 11 hospitals in Baltimore area and place them in the diagram according to their location in Baltimore. The number 0.23 above the arrow going from Sinai Hospital to Good Samaritan indicates that if Sinai hospital is having a yellow alert, then the probability that Good Samaritan also has a yellow alert is 0.23. Similar interpretations can be applied to other hospitals.



From the results, we notice that two major hospitals, University of Maryland Medical

Center (UMMC) and John Hopkins Hospital (JH) significantly influence the other hospitals in this region. To further investigate this issue, we use adjusted model to calculate the hazard ratio. We define any cascading level (normal, level I, or level II) caused by JH or UMMC as group A, and all the remainders as group B. We calculate the hazard ratio (HR) using the validated method described before, and get a HR as 0.63 (95%CI=0.58-0.67, $p < 0.01$). That is, group B has the hazard risk reduced by about 37% for the transition to a higher cascading level compared to group A.

6.5 Discussion

A cascading event happening in ER is an important issue, in which case hospitals cannot provide necessary emergency services to the acute care of patients in the region. However, the issue has not obtained enough attention and has not been studied well in the literature. The main reason is that such cascading problems are hard to handle quantitatively. Therefore, the investigation in this Chapter becomes complicated, but important for the emergency service system in Region III of Maryland.

In this chapter, we have developed a multi-state Markov model to address the cascading event. We use a general form of intensities to accommodate potential violations of time-homogeneity assumption and extend the model to handle time-varying hazard ratios appropriately. Our extensive simulation studies illustrate good performances of the proposed method. We demonstrate that polynomial and Fourier

approximation to baseline intensities and the generalized model for handling time-varying hazard ratios perform consistently well. We also apply the new method to yellow alert data in ERs of 21 hospitals in Maryland Region III.

6.5.1 Applications in Emergency Room

The proposed method and this study could help patients and hospital administrators to understand the evolution of cascading events, as well as similarity and heterogeneity among hospitals in terms of accessibility to emergency rooms in Region III. For example, we are able to observe this evolution of accessibility status of emergency rooms in Maryland Region III via transition probabilities between different states in the Markov model.

We also anticipate that this study could help patients, hospital administrators, or emergency service staff to allocate patients' flow or resources in Region III wisely to avoid overload. For instance, Figure 6.10 can help us to understand the correlations of yellow alert status between different ERs. Once a yellow alert is initiated at one ER, we can roughly estimate the probability of starting a yellow alert at another ER. Also, using our proposed method, one can calculate the hazard ratio, which provides guidance on differences in risks to cause a cascading event from different ERs. These results could be used to allocate resources in ERs ahead of time.

In addition, the proposed method can be used to predict the time left at current ER accessibility state. For instance, expected time remaining at current

cascading level can be evaluated given the elapsing time and other covariates at the current time. This is essentially to calculate the Mean Residual Life Time (MRLT), $m(t)$, below

$$m(t) = \mathbb{E}(T_{ij} - t | T_{ij} > t) = \frac{1}{S(t)} \int_t^{\infty} S(u) du.$$

where $S(t)$ can be estimated by the proposed methods in this Chapter. By estimating the remaining time at current cascading level, it helps to reallocate the resources available, for example, reallocating more beds or other facilities or gradually control the numbers of patients in need of care.

Furthermore, by adding some covariates of interest, such as bed size or number of service staff, we would be able to know how those covariates impact the cascading problems in the region, which provide us guidances on how to reduce such risk of cascading events.

6.5.2 Future Research

It would be of interest to extend our current work in several ways. Firstly, it would be helpful to consider reparametrization to reduce the dimension of parameters, since using polynomial and Fourier series would involve a high dimension of parameters and make the computation complex and time-consuming. The second extension would be related to our current data limitations. If more data at hospital-specific level is accessible, such as the number of beds in the 21 emergency rooms, the study may provide more insights on the cascading issues. The last extension could be: applying the method to only eleven hospitals in Baltimore city, where the

hospitals are more closely connected. These problems are beyond the scope of this chapter, but would be interesting topics for future research.

Chapter 7: Conclusions

Numerous healthcare problems consistently attract researchers' attention because these problems are closely related to individual and social well-being and new challenges are always developing over time. While statistical tools are critical and useful in understanding healthcare issues, the emerging healthcare challenges call for the exploration, application, and development of more suitable and appropriate statistical methods.

In this dissertation, we have applied and developed a variety of statistical methods to address different healthcare problems. First, we performed exploratory data analysis to investigate interesting data characteristics using statistical visualization tools such as boxplot, Q-Q plot, histogram and descriptive statistics. Then, we used more complex statistical tools to address each healthcare issue under study. Specifically, we developed mixture models with the EM algorithm to model length of hospital stay in Chapter 2; stochastic processes in Chapter 3 were applied to study patients' readmission risk; nonparametric tests in Chapters 4 and 5 identified significant differences for hospital alert duration over time; survival curves in Chapter 4 visualized changes in alert duration; linear mixed models in Chapter 5 helped us investigate the impact of the global budget payment model on ED accessibil-

ity; and we used survival analysis and Markov chain models in Chapter 6 to study the evolution of and reasons for a cascading event. Finally, our use of innovative statistical techniques obtained some interesting findings and applications, and the research methodology can be extended to other studies in the future. For instance, the distribution model we found for length of stay can be used to simulate patients' stay in other real-world scenarios. Our proposed two-state continuous-time Markov chain can be generalized to monitor the expected number of readmitted patients over time. Among our noteworthy findings, we observed a recent decrease in the level of ED accessibility in Maryland Region III, and we found that the global budget program had no impact on ED accessibility. Both of these findings have significant implications for future healthcare policy making in Maryland. Lastly, we built a multi-state Markov model that calculates the expected time of a current alert state and identifies reasons for cascading events, which can provide guidance for future ED management in Maryland.

Healthcare is undergoing a period of pivotal change. The digital and mobile revolution allows organizations to collect personalized healthcare data from each patient and compare it with other patient data using artificial intelligence-based methods. It also enables us to better quantify characteristics of each patient and distinguish individual patients, thus allowing the creation of more precise and more personalized treatment plans to improve healthcare for every individual. The complexity and volume of personalized healthcare data are staggering. The ongoing development of appropriate statistical methods is therefore necessary in order to resolve the more challenging precision medicine and personalized healthcare issues.

Appendices

Appendix A: The Derivation for LGMM

In this appendix, we present the associated derivations for the EM algorithm for the Lognormal-Gamma Mixture Model.

Assume n independent and identically distributed (i.i.d.) length of stay observations $x_i \in R$, $i = 1, \dots, n$, drawn from a LGMM, our objective is to estimate the parameter set $\theta = \{p, \mu, \sigma, \alpha, \beta\}$ that best fits the observed data. We assume the observations x_i belong to a mixture distribution defined by:

$$X_i = Z_i U_i + (1 - Z_i) V_i$$

where

$$U_i \sim f_1(u_i | \mu, \sigma)$$

$$V_i \sim f_4(v_i | \alpha, \beta)$$

$$Z_i \sim f_3(z_i | p)$$

and Z_i is independent of U_i and V_i . For any v_i , the pdf for the Gamma distribution

is defined as

$$f_4(v_i|\alpha, \beta) = \frac{1}{\Gamma(\alpha)\beta^\alpha} v_i^{\alpha-1} \exp(-v_i/\beta), \quad \alpha, \beta \in R^+.$$

The pdf for the LGMM is then defined as:

$$f(x_i|p, \mu, \sigma, \alpha, \beta) = pf_1(x_i|\mu, \sigma) + (1-p)f_4(x_i|\alpha, \beta).$$

The E-step of the EM algorithm proceeds as follows:

$$\epsilon_i^{(m)} = \frac{p^{(m)} f_1(x_i|\mu^{(m)}, \sigma^{(m)})}{p^{(m)} f_1(x_i|\mu^{(m)}, \sigma^{(m)}) + (1-p^{(m)}) f_4(x_i|\alpha^{(m)}, \beta^{(m)})}.$$

With the assumptions that the samples are i.i.d., we calculate the Q-function below:

$$\begin{aligned} Q(\theta|\theta^{(m)}) &= \sum_{i=1}^n \left\{ \epsilon_i^{(m)} \log[pf_1(x_i|\mu, \sigma)] \right. \\ &\quad \left. + (1 - \epsilon_i^{(m)}) \log[(1-p)f_4(x_i|\alpha, \beta)] \right\} \\ &= \sum_{i=1}^n \left\{ \epsilon_i^{(m)} \left(\log(p) - \log(\sigma) - \log(x_i) - \frac{(\log(x_i) - \mu)^2}{2\sigma^2} \right) \right. \\ &\quad \left. + (1 - \epsilon_i^{(m)}) [\log(1-p) + \log \Gamma(\alpha) - \alpha \log \beta + \right. \\ &\quad \left. (\alpha - 1) \log x_i - \frac{x_i}{\beta}] \right\} + C \end{aligned}$$

where C does not depend on any of the elements of θ .

The M-step determines the next iterate of θ that maximizes the Q-function above:

$$\theta^{(m+1)} = \operatorname{argmax}_{\theta} Q(\theta|\theta^{(m)}).$$

The optimal p , μ , σ^2 , α , β are found by equating the respective partial derivatives to zero, and solving.

For p , μ , and σ^2 , similarly to the LEMM, we have

$$p^{(m+1)} = \frac{1}{n} \sum_{i=1}^n \epsilon_i^{(m)},$$

$$\mu^{(m+1)} = \frac{\sum_{i=1}^n \epsilon_i^{(m)} \log(x_i)}{\sum_{i=1}^n \epsilon_i^{(m)}},$$

and

$$(\sigma^2)^{(m+1)} = \frac{\sum_{i=1}^n \epsilon_i^{(m)} (\log(x_i) - \mu^{(m+1)})^2}{\sum_{i=1}^n \epsilon_i^{(m)}}.$$

For α and β , we have

$$\frac{\partial Q(\theta|\theta^{(m)})}{\partial \alpha} = \sum_{i=1}^n (1 - \epsilon_i^{(m)}) (\psi(\alpha) - \log \beta + \log x_i) = 0$$

and

$$\frac{\partial Q(\theta|\theta^{(m)})}{\partial \beta} = \sum_{i=1}^n (1 - \epsilon_i^{(m)}) \left(-\frac{\alpha}{\beta} + \frac{x_i}{\beta^2}\right) = 0$$

which yields

$$\alpha^{(m+1)} = \psi^{-1} \left\{ \frac{(\log \beta^{(m)}) \sum_{i=1}^n (1 - \epsilon_i^{(m)}) - \sum_{i=1}^n \log x_i (1 - \epsilon_i^{(m)})}{\sum_{i=1}^n (1 - \epsilon_i^{(m)})} \right\}$$

and

$$\beta^{(m+1)} = \frac{\sum_{i=1}^n (1 - \epsilon_i^{(m)}) x_i}{\alpha^{(m+1)} \sum_{i=1}^n (1 - \epsilon_i^{(m)})}$$

where $\Gamma(x) = \int_0^\infty z^{x-1} e^{-z} dz$ denotes the gamma function and $\psi(x) = \Gamma'(x)/\Gamma(x)$

denotes the digamma function.

Appendix B: The Derivation for LLMM

In this appendix, we present the associated derivations for the EM algorithm for the Lognormal-Lognormal Mixture Model.

Assume n independent and identically distributed (i.i.d.) length of stay observations $x_i \in R$, $i = 1, \dots, n$, drawn from a LLMM, our objective is to estimate the parameter set $\theta = \{p, \mu_1, \sigma_1, \mu_2, \sigma_2\}$ that best fits the observed data. We assume the observations x_i belong to a mixture distribution defined by:

$$X_i = Z_i U_i + (1 - Z_i) V_i$$

where

$$U_i \sim f_1(u_i | \mu_1, \sigma_1)$$

$$V_i \sim f_1(v_i | \mu_2, \sigma_2)$$

$$Z_i \sim f_3(z_i | p)$$

and Z_i is independent of U_i and V_i .

The pdf for the LLMM is defined as:

$$f(x_i | p, \mu_1, \sigma_1, \mu_2, \sigma_2) = p f_1(x_i | \mu_1, \sigma_1) + (1 - p) f_1(x_i | \mu_2, \sigma_2).$$

The E-step of the EM algorithm proceeds as follows:

$$\epsilon_i^{(m)} = \frac{p^{(m)} f_1(x_i | \mu_1^{(m)}, \sigma_1^{(m)})}{p^{(m)} f_1(x_i | \mu_1^{(m)}, \sigma_1^{(m)}) + (1 - p^{(m)}) f_1(x_i | \mu_2^{(m)}, \sigma_2^{(m)})}.$$

With the assumptions that the samples are i.i.d., we calculate the Q-function below:

$$\begin{aligned} Q(\theta | \theta^{(m)}) &= \sum_{i=1}^n \left\{ \epsilon_i^{(m)} \log[p f_1(x_i | \mu_1, \sigma_1)] \right. \\ &\quad \left. + (1 - \epsilon_i^{(m)}) \log[(1 - p) f_1(x_i | \mu_2, \sigma_2)] \right\} \\ &= \sum_{i=1}^n \left\{ \epsilon_i^{(m)} \left[\log(p) - \log(\sigma_1) - \log(x_i) - \frac{(\log(x_i) - \mu_1)^2}{2\sigma_1^2} \right] \right. \\ &\quad \left. + (1 - \epsilon_i^{(m)}) \left[\log(1 - p) + \log(\sigma_2) - \log(x_i) \right. \right. \\ &\quad \left. \left. - \frac{(\log(x_i) - \mu_2)^2}{2\sigma_2^2} \right] \right\} + C \end{aligned}$$

where C is a constant that does not depend on θ .

The M-step determines the next iterate of θ that maximizes the Q-function above:

$$\theta^{(m+1)} = \underset{\theta}{\operatorname{argmax}} Q(\theta | \theta^{(m)}).$$

The optimal $p, \mu_1, \sigma_1^2, \mu_2, \sigma_2^2$ are found by equating the respective partial derivatives with zero, and solving. Similarly as two models above, we have

$$p^{(m+1)} = \frac{1}{n} \sum_{i=1}^n \epsilon_i^{(m)},$$

$$\mu_1^{(m+1)} = \frac{\sum_{i=1}^n \epsilon_i^{(m)} \log(x_i)}{\sum_{i=1}^n \epsilon_i^{(m)}},$$

and

$$(\sigma_1^2)^{(m+1)} = \frac{\sum_{i=1}^n \epsilon_i^{(m)} (\log(x_i) - \mu^{(m+1)})^2}{\sum_{i=1}^n \epsilon_i^{(m)}}.$$

For μ_2 and σ_2^2 , we have

$$\frac{\partial Q(\theta|\theta^{(m)})}{\partial \alpha_2} = \sum_{i=1}^n (1 - \epsilon_i^{(m)}) \frac{\log(x_i) - \mu}{\sigma^2} = 0$$

and

$$\frac{\partial Q(\theta|\theta^{(m)})}{\partial \beta} = \sum_{i=1}^n \left(\frac{1 - \epsilon_i^{(m)}}{\sigma} + \frac{(1 - \epsilon_i^{(m)}) (\log(x_i) - \mu)^2}{\sigma^3} \right) = 0$$

which yields

$$\mu_2^{(m+1)} = \frac{\sum_{i=1}^n (1 - \epsilon_i^{(m)}) \log(x_i)}{\sum_{i=1}^n (1 - \epsilon_i^{(m)})}$$

and

$$(\sigma_2^2)^{(m+1)} = \frac{\sum_{i=1}^n (1 - \epsilon_i^{(m)}) [\log(x_i) - \mu^{(m+1)}]^2}{\sum_{i=1}^n (1 - \epsilon_i^{(m)})}.$$

Bibliography

- [1] *Maryland region iii emergency medical services advisory council*, <https://miemss.org/home/Portals/0/Docs/Open-Meetings/RegIII-Council-Agenda-Sep26-2018.pdf?ver=2019-03-19-110247-900>. Accessed: 2019-11-04.
- [2] *Maryland region iii emergency medical services advisory council*, <https://www.miemssalert.com/chats/>. Accessed: 2019-11-04.
- [3] H. Akaike, *A new look at the statistical model identification*, in *Selected Papers of Hirotugu Akaike*, Springer, 1974, pp. 215–222.
- [4] R. Akkerman and M. Knip, *Reallocation of beds to reduce waiting time for cardiac surgery*, *Health Care Manag Sci* 7 (2004), pp. 119–126.
- [5] Z. Alharbi, A. Piatkowski, R. Dembinski, S. Reckort, G. Grieb, J. Kauczok, and N. Pallua, *Treatment of burns in the first 24 hours: simple and practi-*

- cal guide by answering 10 questions in a step-by-step form*, World journal of emergency surgery 7 (2012), p. 13.
- [6] V. Allareddy, S. Rampa, M.K. Lee, V. Allareddy, and R.P. Nalliah, *Hospital-based emergency department visits involving dental conditions: profile and predictors of poor outcomes and resource utilization*, The Journal of the American Dental Association 145 (2014), pp. 331–337.
- [7] D. Anderson, B. Golden, W. Jank, and E. Wasil, *The impact of hospital utilization on patient readmission rate*, Health Care Management Science 15 (2012), pp. 29–36.
- [8] G.F. Anderson and E.P. Steinberg, *Predicting hospital readmissions in the medicare population*, Inquiry 22 (1985), pp. 251–258.
- [9] C.M. Ashton, D.J. Del Junco, J. Soucek, N.P. Wray, and C.L. Mansyur, *The association between the quality of inpatient care and early readmission: a meta-analysis of the evidence*, Medical Care 35 (1997), pp. 1044–1059.
- [10] C.M. Ashton and N.P. Wray, *A conceptual framework for the study of early readmission as an indicator of quality of care*, Social Science & Medicine 43 (1996), pp. 1533–1541.
- [11] N. Atienza, J. García-Heras, J. Muñoz-Pichardo, and R. Villa, *An application of mixture distributions in modelization of length of hospital stay*, Statistics in medicine 27 (2008), pp. 1403–1420.

- [12] N. Atienza, J. García-Heras, J. Muñoz-Pichardo, and R. Villa, *An application of mixture distributions in modelization of length of hospital stay*, Stat Med 27 (2008), pp. 1403–1420.
- [13] P.C. Austin, W.A. Ghali, and J.V. Tu, *A comparison of several regression models for analysing cost of cabg surgery*, Statistics in medicine 22 (2003), pp. 2799–2815.
- [14] T. Bardell, J. Legare, K. Buth, G. Hirsch, and I. Ali, *Icu readmission after cardiac surgery*, European journal of cardio-thoracic surgery 23 (2003), pp. 354–359.
- [15] S. Barnes, B. Golden, and S. Price, *Applications of agent-based modeling and simulation to healthcare operations management*, in *Handbook of Healthcare Operations Management*, Springer, 2013, pp. 45–74.
- [16] N. Bartolomeo, P. Trerotoli, A. Moretti, and G. Serio, *A markov model to evaluate hospital readmission*, BMC Medical Research Methodology 8 (2008), p. 23.
- [17] A. Basu, *Extended generalized linear models: simultaneous estimation of flexible link and variance functions*, The Stata Journal 5 (2005), pp. 501–516.
- [18] A. Basu, W.G. Manning, and J. Mullahy, *Comparing alternative models: log vs cox proportional hazard?*, Health economics 13 (2004), pp. 749–765.
- [19] J. Benbassat and M. Taragin, *Hospital readmissions as a measure of quality*

- of health care: advantages and limitations*, Archives of Internal Medicine 160 (2000), pp. 1074–1081.
- [20] D. Berwick and A. Hackbarth, *Eliminating waste in US health care*, JAMA 307 (2012), pp. 1513–1516.
- [21] G. Bignardi, *Risk factors for clostridium difficile infection*, J Hosp Infect 40 (1998), pp. 1–15.
- [22] D. Black and M. Pearson, *Average length of stay, delayed discharge, and hospital congestion: A combination of medical and managerial skills is needed to solve the problem*, BMJ: British Medical Journal 325 (2002), pp. 610–611.
- [23] D.K. Blough, C.W. Madden, and M.C. Hornbrook, *Modeling risk using generalized linear models*, Journal of health economics 18 (1999), pp. 153–171.
- [24] D.K. Blough and S.D. Ramsey, *Using generalized linear models to assess medical care costs*, Health Services and Outcomes Research Methodology 1 (2000), pp. 185–202.
- [25] A. Briggs and A. Gray, *The distribution of health care costs and their statistical analysis for economic evaluation*, Journal of health services research & policy 3 (1998), pp. 233–245.
- [26] A. Briggs, R. Nixon, S. Dixon, and S. Thompson, *Parametric modelling of cost data: some simulation evidence*, Health economics 14 (2005), pp. 421–428.

- [27] J. Broder and D.M. Warshauer, *Increasing utilization of computed tomography in the adult emergency department, 2000–2005*, *Emergency radiology* 13 (2006), pp. 25–30.
- [28] C.W. Burt and L.F. McCaig, *Trends in hospital emergency department utilization; united states, 1992-99* (2001).
- [29] K. Cardiff, G. Anderson, and S. Sheps, *Evaluation of a hospital-based utilization management program*, *Healthcare Management Forum* 8 (1995), pp. 38–45.
- [30] K. Carey and T. Stefos, *The cost of hospital readmissions: evidence from the va*, *Health Care Management Science* 19 (2016), pp. 241–248.
- [31] R. Caruana, Y. Lou, J. Gehrke, P. Koch, M. Sturm, and N. Elhadad, *Intelligible models for healthcare: Predicting pneumonia risk and hospital 30-day readmission*, *ACM*, 2015, pp. 1721–1730.
- [32] G. Casella and R. Berger, *Statistical Inference*, 2nd ed., Duxbury Pacific Grove, 2002.
- [33] H. Chakraborty, A. Hossain, and M.A. Latif, *A three-state continuous time markov chain model for HIV disease burden*, *Journal of Applied Statistics* (2018), pp. 1–18.
- [34] M. Chambers and A. Clarke, *Measuring readmission rates.*, *BMJ: British Medical Journal* 301 (1990), pp. 1134–1136.

- [35] J. Chang, G. Freed, L. Prosser, I. Patel, S. Erickson, R. Bagozzi, and R. Balkrishnan, *Comparisons of health care utilization outcomes in children with asthma enrolled in private insurance plans versus medicaid*, *J Pediatr Health Care* 28 (2014), pp. 71–79.
- [36] C. Conigliani and A. Tancredi, *Semi-parametric modelling for costs of health care technologies*, *Statistics in medicine* 24 (2005), pp. 3171–3184.
- [37] N.J. Cooper, A.J. Sutton, M. Mugford, and K.R. Abrams, *Use of bayesian markov chain monte carlo methods to model cost-of-illness data*, *Medical Decision Making* 23 (2003), pp. 38–53.
- [38] J. Corrigan and V. Kazandjian, *Characteristics of multiple admissions.*, *Journal American Medical Record Association* 62 (1991), pp. 37–47.
- [39] A. Costa, S. Ridley, A. Shahani, P.R. Harper, V. De Senna, and M. Nielsen, *Mathematical modelling and simulation for planning critical care capacity*, *Anaesthesia* 58 (2003), pp. 320–327.
- [40] S. Csorgo and J. Faraway, *The exact and asymptotic distributions of cramér-von mises statistics*, *J R Statist Soc B* 58 (1996), pp. 221–234.
- [41] K. Daly, R. Beale, and R. Chang, *Reduction in mortality after inappropriate early discharge from intensive care unit: logistic regression triage model*, *BMJ: British Medical Journal* 322 (2001), p. 1274.
- [42] P. Deb and P.K. Trivedi, *Demand for medical care by the elderly: a finite mixture approach*, *Journal of applied Econometrics* 12 (1997), pp. 313–336.

- [43] E. Demir and T. Chausalet, *Capturing the re-admission process: focus on time window*, Journal of Applied Statistics 38 (2011), pp. 951–960.
- [44] E. Demir, T.J. Chausalet, H. Xie, and P.H. Millard, *Emergency readmission criterion: a technique for determining the emergency readmission time window*, IEEE Transactions on Information Technology in Biomedicine 12 (2008), pp. 644–649.
- [45] A. Dempster, N. Laird, and D. Rubin, *Maximum likelihood from incomplete data via the em algorithm*, J R Statist Soc B 39 (1977), pp. 1–38.
- [46] P. Dinh and X.H. Zhou, *Nonparametric statistical methods for cost-effectiveness analyses*, Biometrics 62 (2006), pp. 576–588.
- [47] E.D. Dommasch, C.J. Joyce, and A. Mostaghimi, *Trends in nationwide herpes zoster emergency department utilization from 2006 to 2013*, JAMA dermatology 153 (2017), pp. 874–881.
- [48] R.A. Dudley, F.E. Harrell, L.R. Smith, D.B. Mark, R.M. Califf, D.B. Pryor, D. Glower, J. Lipscomb, and M. Hlatky, *Comparison of analytic models for estimating the effect of clinical factors on the cost of coronary artery bypass graft surgery*, Journal of clinical epidemiology 46 (1993), pp. 261–271.
- [49] S. Dulay, S. Weston, J. Illian, M. Bell, A. Jaffe, and V. Roger, *Thirty day hospital readmissions following acute myocardial infarction: a community study*, Ann Intern Med 157 (2012), pp. 11–18.

- [50] E. El-Darzi, C. Vasilakis, T. Chausalet, and P. Millard, *A simulation modelling approach to evaluating length of stay, occupancy, emptiness and bed blocking in a hospital geriatric department*, Health Care Manag Sci 1 (1998), p. 143.
- [51] J.E. Everett, *A decision support simulation model for the management of an elective surgery waiting system*, Health care management science 5 (2002), pp. 89–95.
- [52] M. Fackrell, *Modelling healthcare systems with phase-type distributions*, Health care management science 12 (2009), p. 11.
- [53] R. Farmer and J. Emami, *Models for forecasting hospital bed requirements in the acute sector.*, Journal of Epidemiology & Community Health 44 (1990), pp. 307–312.
- [54] G.M. Fitzmaurice, N.M. Laird, and J.H. Ware, *Applied longitudinal analysis*, Vol. 998, John Wiley & Sons, 2012.
- [55] D. Fone, S. Hollinghurst, M. Temple, A. Round, N. Lester, A. Weightman, K. Roberts, E. Coyle, G. Bevan, and S. Palmer, *Systematic review of the use and value of computer simulation modelling in population health and health care delivery*, Journal of Public Health 25 (2003), pp. 325–335.
- [56] S.E. Frankl, J.L. Breeling, and L. Goldman, *Preventability of emergent hospital readmission*, The American Journal of Medicine 90 (1991), pp. 667–674.

- [57] P. Fuhs, J. Martin, and W. Hancock, *The use of length of stay distributions to predict hospital discharges*, *Medical care* (1979), pp. 355–368.
- [58] J. Gardiner, Z. Luo, X. Tang, and R. Ramamoorthi, *Fitting heavy-tailed distributions to health care data by parametric and bayesian methods*, *J Stat Theory Pract* 10 (2016), pp. 574–587.
- [59] M. Gul and A.F. Guneri, *A computer simulation model to reduce patient length of stay and to improve resource utilization rate in an emergency department service system*, *International Journal of Industrial Engineering* 19 (2012), pp. 221–231.
- [60] S. Gurmu, *Semi-parametric estimation of hurdle regression models with an application to medicaid utilization*, *Journal of applied econometrics* 12 (1997), pp. 225–242.
- [61] P.R. Harper and A. Shahani, *Modelling for the planning and management of bed capacities in hospitals*, *Journal of the Operational research Society* 53 (2002), pp. 11–18.
- [62] A. Harris, L. Pineles, B. Belton, J. Johnson, M. Shardell, M. Loeb, R. Newhouse, L. Dembry, B. Braun, E. Perencevich, *et al.*, *Universal glove and gown use and acquisition of antibiotic-resistant bacteria in the icu: a randomized trial*, *JAMA* 310 (2013), pp. 1571–1580.
- [63] G. Harrison, *Implications of mixed exponential occupancy distributions and*

- patient flow models for health care planning*, Health Care Manag Sci 4 (2001), pp. 37–45.
- [64] U. Hatipoğlu, B.J. Wells, K. Chagin, D. Joshi, A. Milinovich, and M.B. Rothberg, *Predicting 30-day all-cause readmission risk for subjects admitted with pneumonia at the point of care*, Respiratory Care 63 (2018), pp. 43–49.
- [65] J. He, X.y. Hou, S. Toloo, J.R. Patrick, and G.F. Gerald, *Demand for hospital emergency departments: a conceptual understanding*, World journal of emergency medicine 2 (2011), p. 253.
- [66] T. Heggstad and S.E. Lilleeng, *Measuring readmissions: focus on the time factor*, International Journal for Quality in Health Care 15 (2003), pp. 147–154.
- [67] J. Henderson, M.J. Graveney, and M.J. Goldacre, *Should emergency readmissions be used as health service indicators and in medical audit?*, Health Services Management Research 6 (1993), pp. 109–116.
- [68] S.C. Hill and G.E. Miller, *Health expenditure estimation and functional form: applications of the generalized gamma and extended estimating equations models*, Health economics 19 (2010), pp. 608–627.
- [69] C.S. Hollenbeak, *Functional form and risk adjustment of hospital costs: Bayesian analysis of a box-cox random coefficients model*, Statistics in medicine 24 (2005), pp. 3005–3018.

- [70] N.R. Hoot, L.J. LeBlanc, I. Jones, S.R. Levin, C. Zhou, C.S. Gadd, and D. Aronsky, *Forecasting emergency department crowding: a discrete event simulation*, *Annals of emergency medicine* 52 (2008), pp. 116–125.
- [71] X. Hu, S. Barnes, and B. Golden, *Applying queueing theory to the study of emergency department operations: a survey and a discussion of comparable simulation studies*, *International Transactions in Operational Research* 25 (2018), pp. 7–49.
- [72] A.K. Huber, L. Wang, P. Han, X. Zhang, S. Ekholm, A. Srinivasan, D.N. Irani, and B.M. Segal, *Dysregulation of the *il-23/il-17* axis and myeloid factors in secondary progressive ms*, *Neurology* 83 (2014), pp. 1500–1507.
- [73] A. Ickowicz and R. Sparks, *Modelling hospital length of stay using convolutive mixtures distributions*, *Stat Med* 36 (2017), pp. 122–135.
- [74] D. Ingram, D. Clarke, and R. Murdie, *Distance and the decision to visit an emergency department*, *Social Science & Medicine. Part D: Medical Geography* 12 (1978), pp. 55–62.
- [75] B.W. Jack, V.K. Chetty, D. Anthony, J.L. Greenwald, G.M. Sanchez, A.E. Johnson, S.R. Forsythe, J.K. O’Donnell, M.K. Paasche-Orlow, C. Manasseh, *et al.*, *A reengineered hospital discharge program to decrease rehospitalization: a randomized trial*, *Annals of Internal Medicine* 150 (2009), pp. 178–187.
- [76] C. Jackson, *Multi-state modelling with r: the msm package*, Cambridge, UK (2007).

- [77] C.H. Jackson, *et al.*, *Multi-state models for panel data: the msm package for r*, Journal of statistical software 38 (2011), pp. 1–29.
- [78] M. Jamei, A. Nisnevich, E. Wetchler, S. Sudat, and E. Liu, *Predicting all-cause risk of 30-day hospital readmission using artificial neural networks*, PLOS One 12 (2017), p. e0181173.
- [79] S. Jiang, K.S. Chin, G. Qu, and K.L. Tsui, *An integrated machine learning framework for hospital readmission prediction*, Knowledge-Based Systems 146 (2018), pp. 73–90.
- [80] J. Jun, S.H. Jacobson, and J.R. Swisher, *Application of discrete-event simulation in health care clinics: A survey*, Journal of the operational research society 50 (1999), pp. 109–123.
- [81] D. Kansagara, H. Englander, A. Salanitro, D. Kagen, C. Theobald, M. Freeman, and S. Kripalani, *Risk prediction models for hospital readmission: a systematic review*, JAMA 306 (2011), pp. 1688–1698.
- [82] A.M. Kelly, M. Bryant, L. Cox, and D. Jolley, *Improving emergency department efficiency by patient streaming to outcomes-based teams*, Australian Health Review 31 (2007), pp. 16–21.
- [83] J. Kelly, H. McDowell, V. Crawford, and R. Stout, *Readmissions to a geriatric medical unit: is prevention possible?*, Aging Clinical and Experimental Research 4 (1992), pp. 61–67.

- [84] T.H. Koskela, O.P. Ryyanen, and E.J. Soini, *Risk factors for persistent frequent use of the primary health care services among frequent attenders: a bayesian approach*, Scandinavian journal of primary health care 28 (2010), pp. 55–61.
- [85] W.H. Kruskal and W.A. Wallis, *Use of ranks in one-criterion variance analysis*, Journal of the American statistical Association 47 (1952), pp. 583–621.
- [86] J. Kuhlman, D. Moorhead, J. Kerpchar, D.J. Peach, S. Ahmad, and P.B. O'Brien, *Clinical transformation through change management case study: Chest pain in the emergency department*, EClinicalMedicine 10 (2019), pp. 78–83.
- [87] P. Kulkarni, L.D. Smith, and K.F. Woeltje, *Assessing risk of hospital readmissions for improving medical practice*, Health Care Management Science 19 (2016), pp. 291–299.
- [88] D.N. Kyriacou, V. Ricketts, P.L. Dyne, M.D. McCollough, and D.A. Talan, *A 5-year time study analysis of emergency department patient care efficiency*, Annals of emergency medicine 34 (1999), pp. 326–335.
- [89] A. Lee, A. Ng, and K. Yau, *Determinants of maternity length of stay: a gamma mixture risk-adjusted model*, Health Care Manag Sci 4 (2001), pp. 249–255.
- [90] M. Lefebvre, *Applied Stochastic Processes*, Springer Science & Business Media, 2007.

- [91] J.H. Lichtman, E.C. Leifheit-Limson, S.B. Jones, Y. Wang, and L.B. Goldstein, *Preventable readmissions within 30 days of ischemic stroke among medicare beneficiaries*, *Stroke* 44 (2013), pp. 3429–3435.
- [92] Y.K. Lin, H. Chen, R.A. Brown, S.H. Li, and H.J. Yang, *Healthcare predictive analytics for risk profiling in chronic care: A bayesian multitask learning approach.*, *Mis Quarterly* 41 (2017).
- [93] J. Lisiecki, D.C. Wan, L. Wang, P. Zhang, B. Enchakalody, X. Zhang, S.J. Kasten, S.C. Wang, S.R. Buchman, and B. Levi, *Novel application of human morphomics to quantify temporal soft tissues in pierre robin and treacher collins*, *Journal of Craniofacial Surgery* 24 (2013), pp. 158–162.
- [94] M. Lopreite and M. Mauro, *The effects of population ageing on health care expenditure: a bayesian var analysis using data from italy*, *Health Policy* 121 (2017), pp. 663–674.
- [95] J.D. Malkin, S. Garber, M.S. Broder, and E. Keeler, *Infant mortality and early postpartum discharge*, *Obstetrics & Gynecology* 96 (2000), pp. 183–188.
- [96] A. Marazzi, F. Paccaud, C. Ruffieux, and C. Beguin, *Fitting the distributions of length of stay by parametric models*, *Med Care* 36 (1998), pp. 915–927.
- [97] A. Marazzi, F. Paccaud, C. Ruffieux, and C. Beguin, *Fitting the distributions of length of stay by parametric models*, *Medical care* 36 (1998), pp. 915–927.
- [98] W. Marder, J.S. Knight, M.J. Kaplan, E.C. Somers, X. Zhang, A.A. O’Dell, V. Padmanabhan, and R.W. Lieberman, *Placental histology and neutrophil*

- extracellular traps in lupus and pre-eclampsia pregnancies*, *Lupus science & medicine* 3 (2016), p. e000134.
- [99] A. Marshall and S. McClean, *Conditional phase-type distributions for modelling patient length of stay in hospital*, *International Transactions in Operational Research* 10 (2003), pp. 565–576.
- [100] S. McClean, L. Garg, M. Barton, and K. Fullerton, *Using mixed phase-type distributions to model patient pathways*, in *Computer-Based Medical Systems (CBMS), 2010 IEEE 23rd International Symposium on*. IEEE, 2010, pp. 172–177.
- [101] M. McGrady and K. Hommel, *Medication adherence and health care utilization in pediatric chronic illness: a systematic review*, *Pediatrics* 132 (2013), pp. 730–740.
- [102] F. McGuire, *Using simulation to reduce length of stay in emergency departments*, in *Simulation Conference Proceedings, 1994. Winter*. IEEE, 1994, pp. 861–867.
- [103] N. McKay and M. Deily, *Cost inefficiency and hospital health outcomes*, *Health Econ* 17 (2008), pp. 833–848.
- [104] B. Mihaylova, A. Briggs, A. O’Hagan, and S.G. Thompson, *Review of statistical methods for analysing healthcare resources and costs*, *Health economics* 20 (2011), pp. 897–916.

- [105] P. Millard, *Geriatric medicine: a new method of measuring bed usage and a theory for planning*, Ph.D. diss., University of London, 1988.
- [106] P. Millard, P. Higgs, and P. Rochon, *Occupancy plotting: a method of estimating bed usage in departments of geriatric medicine* (1989).
- [107] K.G. Morganti, S. Bauhoff, J.C. Blanchard, M. Abir, N. Iyer, A. Smith, J.V. Vesely, E.N. Okeke, and A.L. Kellermann, *The evolving role of emergency departments in the united states*, *Rand health quarterly* 3 (2013).
- [108] J.C. Mowen, J.W. Licata, and J. McPhail, *Waiting in the emergency room: how to improve patient satisfaction*, *Marketing Health Services* 13 (1993), p. 26.
- [109] R. Murray, *Setting hospital rates to control costs and boost quality: the maryland experience*, *Health Affairs* 28 (2009), pp. 1395–1405.
- [110] P. New, F. Racp, K. Stockman, P. Cameron, J. Olver, and J. Stoelwinder, *Computer simulation of improvements in hospital length of stay for rehabilitation patients*, *Journal of rehabilitation medicine* 47 (2015), pp. 403–411.
- [111] R.M. Nixon, D. Wonderling, and R.D. Grieve, *Non-parametric methods for cost-effectiveness analysis: the central limit theorem and the bootstrap compared*, *Health economics* 19 (2010), pp. 316–333.
- [112] R. Nixon and S. Thompson, *Parametric modelling of cost data in medical studies*, *Statistics in medicine* 23 (2004), pp. 1311–1331.

- [113] E. Pagano, M. Petrinco, A. Desideri, R. Bigi, F. Merletti, and D. Gregori, *Survival models for cost data: the forgotten additive approach*, *Statistics in medicine* 27 (2008), pp. 3585–3597.
- [114] I. Papanicolas, L.R. Woskie, and A.K. Jha, *Health care spending in the united states and other high-income countries*, *Jama* 319 (2018), pp. 1024–1039.
- [115] M. Papi, L. Pontecorvi, and R. Setola, *A new model for the length of stay of hospital patients*, *Health Care Manag Sci* 19 (2016), pp. 58–65.
- [116] L. Piecoro, M. Potoski, J. Talbert, and D. Doherty, *Asthma prevalence, cost, and adherence with expert guidelines on the utilization of health care services and costs in a state medicaid population*, *Health Serv Res* 36 (2001), pp. 357–371.
- [117] M. Pinsky and S. Karlin, *An introduction to stochastic modeling*, Academic press, 2010.
- [118] M.A. Probst, H.K. Kanzaria, M. Gbedemah, L.D. Richardson, and B.C. Sun, *National trends in resource utilization associated with ed visits for syncope*, *The American journal of emergency medicine* 33 (2015), pp. 998–1001.
- [119] C. Quantin, E. Sauleau, P. Bolard, C. Mousson, M. Kerkri, P. Lecomte, T. Moreau, and L. Dusserre, *Modeling of high-cost patient distribution within renal failure diagnosis related group*, *J Clin Epidemiol* 52 (1999), pp. 251–258.
- [120] F. Reyes-Santías, C. Cadarso-Suárez, and A. Martínez-Calvo, *Applying a simulation model in order to manage waiting lists for hospital inpatient activity*

- in an EU region*, *Mathematical and Computer Modelling* 57 (2013), pp. 1840–1846.
- [121] D.R. Rivera, L. Gallicchio, J. Brown, B. Liu, D.N. Kyriacou, and N. Shelburne, *Trends in adult cancer-related emergency department utilization: an analysis of data from the nationwide emergency department sample*, *JAMA oncology* 3 (2017), pp. e172450–e172450.
- [122] E.T. Roberts, J.M. McWilliams, L.A. Hatfield, S. Gerovich, M.E. Chernen, L.G. Gilstrap, and A. Mehrotra, *Changes in health care use associated with the introduction of hospital global budgets in maryland*, *JAMA internal medicine* 178 (2018), pp. 260–268.
- [123] J.M. Rumble, A.K. Huber, G. Krishnamoorthy, A. Srinivasan, D.A. Giles, X. Zhang, L. Wang, and B.M. Segal, *Neutrophil-related factors as biomarkers in eae and ms*, *Journal of Experimental Medicine* 212 (2015), pp. 23–35.
- [124] G. Schwarz, *et al.*, *Estimating the dimension of a model*, *The annals of statistics* 6 (1978), pp. 461–464.
- [125] R. Shachtman, S. Snapinn, D. Quade, D. Freund, and A. Kronhaus, *A method for constructing case-mix indexes, with application to hospital length of stay*, *Health Serv Res* 20 (1986), pp. 737–762.
- [126] J.M. Sharfstein, E.A. Stuart, and J. Antos, *Global budgets in maryland: assessing results to date*, *Jama* 319 (2018), pp. 2475–2476.

- [127] M. Shulan, K. Gao, and C.D. Moore, *Predicting 30-day all-cause hospital readmissions*, Health Care Management Science 16 (2013), pp. 167–175.
- [128] D. Sibbritt, *Validation of a 28 day interval between discharge and readmission for emergency readmission rates.*, Journal of Quality in Clinical Practice 15 (1995), pp. 211–220.
- [129] R. Sundberg, *Maximum likelihood theory and applications for distributions generated when observing a function an exponential family variable*, Institute of Mathematical Statics, Stockholm University, 1972.
- [130] R. Sundberg, *Maximum likelihood theory for incomplete data from an exponential family*, Scand J Statist 1 (1974), pp. 49–58.
- [131] R. Sundberg, *An iterative method for solution of the likelihood equations for incomplete data from exponential families*, Comm Statist 5 (1976), pp. 55–64.
- [132] X. Tang, Z. Luo, and J.C. Gardiner, *Modeling hospital length of stay by coxian phase-type regression with heterogeneity*, Statistics in medicine 31 (2012), pp. 1502–1516.
- [133] G. Taylor, S. McClean, and P. Millard, *Using a continuous-time markov model with poisson arrivals to describe the movements of geriatric patients*, Applied stochastic models and data analysis 14 (1998), pp. 165–174.
- [134] A. Torabipour, H. Zeraati, A. Mohammad, A. Rashidian, A.A. Sari, and M.R. Sarzaiem, *Bed capacity planning using stochastic simulation approach in*

- cardiac-surgery department of teaching hospitals, tehran, iran*, Iranian journal of public health 45 (2016), p. 1208.
- [135] T.C. Tsai, K.E. Joynt, E.J. Orav, A.A. Gawande, and A.K. Jha, *Variation in surgical-readmission rates and quality of hospital care*, New England Journal of Medicine 369 (2013), pp. 1134–1142.
- [136] L. Turgeman, J. May, A. Ketterer, R. Sciulli, and D. Vargas, *Identification of readmission risk factors by analyzing the hospital-related state transitions of congestive heart failure (chf) patients*, IIE Transactions on Healthcare Systems Engineering 5 (2015), pp. 255–267.
- [137] S. Utzolino, M. Kaffarnik, T. Keck, M. Berlet, and U.T. Hopt, *Unplanned discharges from a surgical intensive care unit: readmissions and mortality*, Journal of critical care 25 (2010), pp. 375–381.
- [138] F. Wei, D. Mark, A. Hartz, and C. Campbell, *Are pro discharge screens associated with postdischarge adverse outcomes?*, Health Services Research 30 (1995), p. 489.
- [139] C. Weissman, *Analyzing intensive care unit length of stay data: problems and possible solutions*, Crit Care Med 25 (1997), pp. 1594–1600.
- [140] E.C. Wick, A.D. Shore, K. Hirose, A.M. Ibrahim, S.L. Gearhart, J. Efron, J.P. Weiner, and M.A. Makary, *Readmission rates and cost following colorectal surgery*, Diseases of the Colon & Rectum 54 (2011), pp. 1475–1479.

- [141] P. Wilkins and M. Beckett, *Audit of unexpected return visits to an accident and emergency department.*, Emergency Medicine Journal 9 (1992), pp. 352–356.
- [142] S.S. Wilks, *The large-sample distribution of the likelihood ratio for testing composite hypotheses*, The Annals of Mathematical Statistics 9 (1938), pp. 60–62.
- [143] C.F. Wu, *On the convergence properties of the EM algorithm*, Ann Statist 11 (1983), pp. 95–103.
- [144] J. Xie, B. Zhang, J. Ma, D.D. Zeng, and J. Lo Ciganic, *Readmission prediction for patients with heterogeneous hazard: A trajectory-based deep learning approach* (2018).
- [145] S. Yu, F. Farooq, A. Van Esbroeck, G. Fung, V. Anand, and B. Krishnapuram, *Predicting readmission risk with institution-specific prediction models*, Artificial Intelligence in Medicine 65 (2015), pp. 89–96.
- [146] X. Zhang, S. Barnes, B. Golden, M. Myers, and P. Smith, *Lognormal-based mixture models for robust fitting of hospital length of stay distributions*, Operations Research for Health Care (2019), p. 100184.
- [147] X. Zhong, S. Lee, C. Zhao, H.K. Lee, P.A. Bain, T. Kundinger, C. Sommers, C. Baker, and J. Li, *Reducing copd readmissions through predictive modeling and incentive-based interventions*, Health Care Management Science 22 (2019), pp. 121–139.

- [148] Z. Zhu, B. Hoon Hen, and K. Liang Teow, *Estimating ICU bed capacity using discrete event simulation*, International Journal of health care quality assurance 25 (2012), pp. 134–144.
- [149] C.J. Zook and F.D. Moore, *High-cost users of medical care*, New England Journal of Medicine 302 (1980), pp. 996–1002.